

## CHAPTER 4

### ***Fine-Grained Sediment Transport***

*Ashish J. Mehta and  
William H. McAnally*

#### **4.1 INTRODUCTION**

The origin of fine-grained sediment transport engineering as a component of hydraulics in the United States must be credited to the work of Hans Albert Einstein and his students at the University of California, Berkeley. Berkeley became a center of sediment transport research with Carl Gustav Gilbert of the U.S. Geological Survey, who, during the early part of the twentieth century, carried out sediment transport studies in a flume located within the Berkeley campus. These studies were conducted in response to a major sedimentation problem in the Sacramento-San Joaquin River delta and the San Francisco Bay due to the significant hydraulic mining activity in the Sierra Nevada mountains starting around the mid-nineteenth century. The bottom of the San Francisco Bay is dominated by fine sediment that is highly cohesive, and much of the early experimental work and its phenomenological interpretation for the development of transport formulas is derived from studies on that sediment.

Fine-grained sediment is generally characterized by size, composition, and plasticity. For fine-grained sediment transport, the first two are especially important and are briefly described here. For definitions related to plasticity, including the Atterberg limits see, for example, Lambe and Whitman (1969). With regard to size, Table 4-1 identifies coarse-grained versus fine-grained sediment and the degree of cohesion. Cohesion is due to electrochemical forces acting on the particle surface. Hence the degree of cohesion depends on the ratio of particle surface area to particle weight, that is, the specific surface area. Clay mineral particles, which occur in sizes less than 2  $\mu\text{m}$ , and many of which are platelike, have a high specific surface area and are cohesive. In contrast, small but less platy particles with comparatively low specific surface areas do not exhibit significant cohesion. Mantz (1977), for example, showed that, with respect to incipient motion, sediment consisting of crushed silica particles in the coarse silt range showed little cohesion and behaved like sand.

In Table 4-1, observe that cohesion increases as particle size decreases (and the associated specific surface area increases). As a result, the tendency for particles to cohere and form aggregates or flocs also increases with decreasing size. An indirect and very approximate measure of the relationship between particle size and cohesion was demonstrated by Migniot (1968), who tested several natural muds and clays in a settling column and plotted the ratio of floc settling velocity to (individual) particle settling velocity against particle size (in micro-meters). He showed that this ratio increased from a little over unity at 40  $\mu\text{m}$  to 300–400 at 1  $\mu\text{m}$ , because with decreasing particle size and increasing cohesion the floc size increased.

With regard to fine-grained sediment composition, two properties are important to transport, namely, the inorganic mineral content and the organic content, including biochemicals. The inorganic constituent can be a clay mineral or a nonclay mineral. Clays are crystalline chemicals composed of silica ( $\text{SiO}_2$ ), alumina ( $\text{Al}_2\text{O}_3$ ), and water, frequently along with appreciable quantities of iron, alkalis ( $\text{Na}^+$ ,  $\text{K}^+$ ), and alkaline earths ( $\text{Ca}^{++}$ ,  $\text{Mg}^{++}$ ). Clay minerals have the property of sorbing certain anions (e.g.,  $\text{NO}_3^-$ ) and cations (e.g.,  $\text{K}^+$ ), and retaining them in an exchangeable state; i.e., these anions and cations can be removed by other anions and cations by treatment with such ions in water solution (Grim 1968).

A characteristic gauge of clay mineral cohesion is the cation exchange capacity (CEC), expressed as milliequivalents of exchangeable ion (e.g.,  $\text{Na}^+$  in terms of  $\text{Na}_2\text{O}$ , whose equivalent weight is 31 g) per 100 g of clay (Grim 1968). The higher the CEC the greater the cohesion, which causes micro-meter-sized individual clay particles to coagulate, or flocculate, in water to form much larger aggregates, or flocs, when water salinity exceeds a critical value, which depends on the clay mineral. Even though flocs are particle-formed units, they contain mostly water. For example, a floc having a density of 1,090  $\text{kg}/\text{m}^3$  and composed of clay particles

**Table 4-1** Sediment Size and its Relation to Cohesion

Size range ( $\mu\text{m}$ )	Classification	Degree of cohesion
>62	Coarse-grained	Cohesionless
40–62	Fine-grained: coarse silt	Practically cohesionless
20–40	Fine-grained: coarse silt	Cohesion increasingly important with decreasing size
2–20	Fine-grained: medium and fine silt	Cohesion important
<2	Fine-grained: coarse, medium, and fine clay	Cohesion very important

of density  $2,650 \text{ kg/m}^3$  will contain nearly 95% water by volume, locked within the interstitial particulate fabric. For descriptions of floc properties, including size, density, and strength, see for example Krone (1963), Dyer (1989), Lick and Huang (1993), and Partheniades (1993).

The (individual) particle size in terms of nominal particle diameter, CEC, and critical salinity for the three most commonly found clays—kaolinite, illite, and smectite (or montmorillonite)—are given in Table 4-2. Also given is information on chlorite, which is rarer but is found in some large estuaries, e.g., San Francisco Bay (Krone 1962). Kaolinite has the lowest CEC and exhibits the lowest degree of cohesion, whereas smectite has the highest CEC and is the most cohesive of the four, with illite and chlorite in between. As salinity increases above the critical value, floc size, density, and strength vary. However, above a salinity of about 10 ppt, its effect on floc properties is comparatively minor (Krone 1962; 1986).

Two commonly found nonclay minerals in coastal and estuarine sediments are quartz and calcium carbonate, the latter being the dominant bottom material in many biogenically active temperate waters (Bentley and Nittrouer 1997). Numerous other nonclay materials can occur; for

example, sediment in San Francisco Bay contains iron flocs and organic matter (Krone 1962). Organic matter can measurably influence the electrochemical flocculation process and the composition of flocs (Dennett et al. 1998). This influence depends on the type of organic matter. Thus, for example, biopolymers can modulate floc properties through adhesive bridge formations (Wells and Goldberg 1993). Mucous filaments formed by bacteria can coat flocs and also reinforce the physicochemical bonds holding particles together (Kranck 1986; Luettich et al. 1993). McCave (1984) showed that active contributions to marine flocculation by zooplankton filtering can be significant compared to those by inorganic processes alone, and Kranck and Milligan (1980) reported that a mixture of 50% organic and 50% inorganic sediments settled an order of magnitude faster than an equivalent concentration of 100% inorganic sediment. In areas of high biodeposition, large suspended aggregates have been recorded *in situ* using a focused-beam laser (Law and Bale 1998).

Several measures of the influence of biochemicals on the erodibility of fine-grained sediment have been examined. Examples include the effects of chlorophyll-*a* (Montague et al. 1993) and colloidal carbohydrate (Amos et al. 1998; Sutherland et al. 1998) on the critical shear stress for erosion. Brief overviews of the interaction between physical and biological parameters in governing erodibility have been provided by, among others, Dade and Nowell (1991), Patterson (1997), and Black et al. (1998). Such interaction has also been examined in Couette flocculators (Drapeau and Dam 1994).

## 4.2 SEDIMENT CHARACTERIZATION

### 4.2.1 Characterization Tests

To make possible intercomparisons of transport-related data from different sites or studies, it is helpful to report values of basic sedimentary parameters that influence floc properties. Table 4-3 lists selected parameters, all of which can be determined through relatively simple and mostly

**Table 4-2** Clay Minerals, CEC, and Critical Salinity for Flocculation

Clay mineral	Nominal diameter <sup>a</sup> ( $\mu\text{m}$ )	Cation exchange capacity (meq/100 g)	Critical salinity (ppt)
Kaolinite	0.36	3–15	0.6
Illite	0.062	10–40	1.1
Chlorite	0.062	24–35	— <sup>b</sup>
Smectite (or montmorillonite)	0.011	80–150	2.4

<sup>a</sup>Defined here as the diameter of a circle with the same surface area as platelike clay particles.

<sup>b</sup>Not reported.

Sources: Ariathurai et al. (1977); McAnally (1999).

documented laboratory test procedures. They include particle size, fall or settling velocity, sediment mineral composition, organic content, clay cation exchange capacity, and fluid salinity. These parameters are considered to be minimally essential; a much larger list has been compiled by Berlamont et al. (1993). There are, however, practical reasons for limiting the number of parameters used to identify a sediment sample. First, the actual number of parameters that determine the behavior of fine sediment in water is so large that it is currently unrealistic to come up with accurate predictive correlations between such parameters and transport-related quantities, e.g., the critical shear stress for erosion (Lee and Mehta 1994). Second, the cost of evaluating a large number of parameters is usually prohibitive for most technical studies. Finally, the six parameters chosen in Table 4-3 are considered to be adequate for a gross characterization of sediment for situations in which the transport is not overwhelmingly influenced by biochemical factors.

An early summary of work related to the erodibility of irrigation channels and agricultural lands is based on a different set of erosion-governing soil parameters including the dispersion ratio, plasticity index, and moisture content (TCECM 1968).

**Table 4-3 Parameters for Characterization of Fine-Grained Sediment Transport**

Parameters	Comments
Particle size	Use standard procedure, e.g., the hydrometer test (ASTM 1993d) or the settling column bottom withdrawal test, preferably using sediment in native water. The exception to the standard procedure is that naturally wet samples should not be air-dried initially, i.e., before the test, because of the difficulty that may occur in completely dispersing the rewetted dry sample (Krone 1962). In this case, to obtain the total weight of the sample necessary for calculations, sediment accumulated at the bottom in the cylinder or column should be collected after the test by filtration and then air-dried. If the sample contains material larger than 75 mm, use the wet-sieving method to separate the coarse fraction (ASTM 1993d). If the organic content is greater than about 10%, this test should not be performed, because, as the organic matter will not deflocculate on addition of floc dispersing agent, the resulting size distribution will not correlate with transport behavior. Instead measure the settling velocity of the untreated, i.e., nondispersed sample.
Fall or settling velocity	Obtain the characteristic relationship between settling velocity and sediment concentration or dry density of the untreated, i.e., nondispersed, sample from measurements in a multiport settling column. See McLaughlin (1959) for test procedure.
Mineral composition	Obtain types and relative quantities of the principal clay and non-clay minerals using standard X-ray diffraction tests (Whittig and Allardice 1986; Rich and Barnhisel 1977).
Organic content	Loss of sample mass on ignition is often measured for this purpose through a standard test (ASTM 1993b). Sometimes this method yields an approximate value due to the loss of structural water from the sample. An alternative is to measure total organic carbon (Walkley and Black 1934).
Cation exchange capacity	Follow standard procedure for clay minerals (ASTM 1993c; SCS 1992). If the organic content is greater than about 10%, the CEC may be excessively high, not representative of the clay constituent.
Salinity	Report salinity if less than about 10 ppt. At higher salinities the influence of salinity on floc structure is comparatively minor (Krone 1962).

#### 4.2.2 Mud Definition and Rheology

Interpretation of the information contained in Table 4-1, according to which the degree of cohesion increases with decreasing particle size, becomes complex in the natural environment, in which mixtures of sizes commonly occur. Such mixtures, or muds, are typically (although not always) cohesive due to the presence of clay minerals. Several definitions of mud are found in the literature. Most are based on the *state* of mud. However, since the *transport* of mud is of present interest, mud is best characterized by its response to an applied stress, based on its rheology. Accordingly, the following definition of mud can be useful (Mehta 2002):

Mud is a sediment-water mixture of grains that are predominantly less than 63 µm in size, exhibits a rheological behavior that is poroelastic or viscoelastic when the mixture is particle-supported, and is highly viscous and non-Newtonian when it is in a fluid-like state.

Other noteworthy parameters are fluid temperature and pH. Temperature affects floc behavior; however, over the normal range of temperature in temperate coastal and estuarine waters

the effect is usually considered small and can instead be dominated by biogenic effects. Slightly acidic waters likewise appear to increase aggregation (Tsai and Hu 1997), but pH is not highly variable in estuarine waters and thus is usually ignored (CTH 1960; Partheniades 1971). On the other hand changing soil pH can alter bed stability to a significant extent (Ravisagar et al. 2001).

Inasmuch as the above definition of mud does not depend on whether the sediment is inorganic or organic, or on such factors as the degree of cohesion or biochemical binding, it encompasses most natural muds. Muds largely composed of silt-sized material have been found to be poroelastic; that is, the internal loss of energy is characterized by Coulomb damping arising from friction between grains. For such muds Darcy's equation for water seepage through the pores is used to determine the pore pressure (Yamamoto and Takahashi 1985; Foda 1987). Most muds also include significant clay-sized fractions, and these are usually considered to be viscoelastic; in such muds internal loss is due to grain-fluid contact (Dade and Nowell 1991).

Figure 4-1 compares four rheological models of materials (continua) in terms of the rate of strain,  $\dot{\gamma}$ , as a function of applied shear,  $\tau$ . Curve A is the Newtonian model, in which the dynamic viscosity,  $\mu = \tau / \dot{\gamma}$ , is independent of  $\dot{\gamma}$ . Curve B represents a pseudoplastic, which shows a shear-thinning behavior; i.e.,  $\mu$  decreases with increasing  $\dot{\gamma}$ . Curve C is the Bingham model, which represents a viscoplastic material that shows a purely Newtonian response, once  $\tau$  exceeds the Bingham yield strength,  $\tau_B$ . Otherwise it remains a solid. A pseudoplastic can be approximated as a Bingham plastic by extrapolation as shown, which defines what can be called the apparent Bingham yield strength,  $\tau_y$ . Last, curve D represents a dilatant or shear-thickening response, in which  $\mu$  increases with  $\dot{\gamma}$ . Most natural, soft muds are shear-thinning, although some seemingly show shear-thickening behavior over certain ranges of shear rate specific to the material (Faas 1995). True Bingham plastic sediments are rare in the coastal and estuarine environment, inasmuch as most soft muds creep even at very low rates of strain. However, many muds have been approximated as Bingham plastics for simplicity of treatment of their flow behavior (Krone 1963; Williams 1986; Mei and Liu 1987; Toorman 1995; Huang and Garcia 1996; 1998; 1999). On a slope over which gravity-induced bottom stress exceeds yield stress, fluid mud can creep and accumulate in downstream depressions in navigation channels and reservoirs (Ali and Georgiadis 1991; Einstein 1941).

A simple model representing the shear-thinning or shear-thickening behavior of mud is the Sisko (1958) power-law relation for the dynamic viscosity,

$$\mu = c_r \dot{\gamma}^{n_r - 1} + \mu_\infty \quad (4-1)$$

in which

$c_r$  = consistency of the non-Newtonian fluid, and  
 $n_r$  = coefficient characterizing flow behavior.

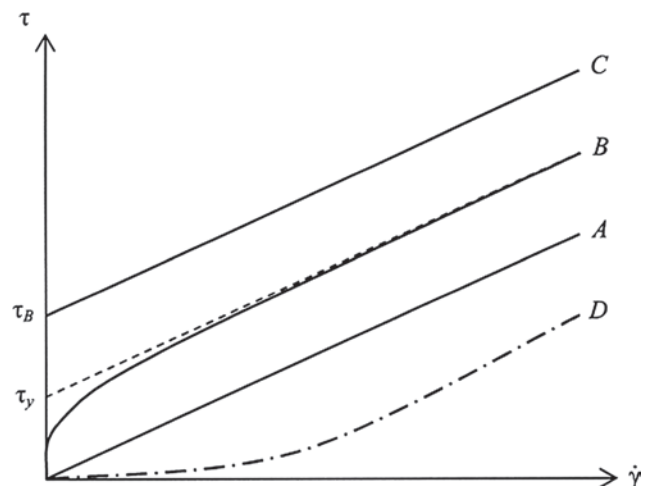


Fig. 4-1. Schematic drawing of models for the relationship between applied stress and rate of strain.

In (4-1),  $n_r < 1$  corresponds to shear-thinning flow behavior, and  $n_r > 1$  represents shear-thickening flow. When  $n_r = 1$  the flow is Newtonian with a constant viscosity  $\mu_\infty$ , since in that case the consistency,  $c_r$ , is nil. At high, theoretically infinite shear rate a shear-thinning material also becomes Newtonian with a viscosity  $\mu_\infty$ .

Ross (1988) summarized a few studies in which  $\mu_\infty$  was, empirically related to the suspension concentration,  $C$  (dry sediment mass divided by volume of sediment plus water), according to

$$\mu_\infty = \mu_w \left( 1 + \alpha_r C^{\beta_r} \right) \quad (4-2)$$

where

$\mu_w$  = viscosity of water.

For example, for a kaolinite in fresh water, the rheometric data of Engelund and Zhaohui (1984) are commensurate with values of the coefficients  $\alpha_r = 1.68$  and  $\beta_r = 0.346$ , when  $C$  is measured in  $\text{kg/m}^3$ . In general, the range of  $C$  over which (4-2) applies varies with the sediment, from a low  $5\text{--}10 \text{ kg/m}^3$  to a high  $400\text{--}500 \text{ kg/m}^3$ .

Following Odd et al. (1993) and based on sediment from the Amazon and (4-1), Vinzon (1998) explicitly included the effect of concentration,  $C$  ( $\text{kg/m}^3$ ), and the shear rate,  $\dot{\gamma}$  (Hz), in the following Sisko-type relations for the kinematic viscosity,  $v = \mu/\rho$  ( $\text{m}^2/\text{s}$ ), where  $\rho$  is the fluid (nominally water) density:

$$v = C \exp(-0.78\dot{\gamma} - 10.24) \text{ for } \dot{\gamma} < 3.9 \text{ Hz} \quad (4-3a)$$

$$v = C \exp(-0.017\dot{\gamma} - 12.95) \text{ for } \dot{\gamma} \geq 3.9 \text{ Hz} \quad (4-3b)$$

Jinchai (1998) conducted rheometric tests on clayey mixtures of a kaolinite ( $K$ ), an attapulgite ( $A$ ), and a bentonite (which is a montmorillonite) ( $B$ ) in fresh water and found the following relations applicable to (4-1):  $\mu_\infty = 0.05CEC_s + 0.001$ ,  $n_r = -0.033CEC_s + 0.28$ ,

and  $\log c_r = 0.13 CEC_s + 0.22$ . The mixture cation exchange capacity,  $CEC_s$ , was defined as

$$CEC_s = f_K CEC_K + f_A CEC_A + f_B CEC_B \quad (4-4)$$

where

$f$  = weight fraction of subscripted sediment, and  
 $CEC$  = cation exchange capacity corresponding to subscript

Note that given the water content (weight of water divided by weight of sediment)  $f_w$ , we have  $f_K + f_A + f_B + f_w = 1$ . The selected cation exchange capacities (in milliequivalents per 100 g of sediment) were 6 for  $K$ , 28 for  $A$ , and 105 for  $B$ . The water content (in percent) in the tests ranged from 86 to 423, and the range of  $CEC_s$  was 1.9 to 10.4 meq/100 g.

Mud viscosity typically decreases with increasing temperature. A simple rheological model can be used to explain this trend based on the theory of momentum exchange between molecules (Krone 1983). According to this theory and data on fluids, the logarithm of  $\mu$  varies linearly with the inverse of the absolute temperature.

At this point it is useful to introduce the relationship between (dry mass) concentration,  $C$ , and (wet) bulk density of mud,  $\rho$ . From mass balance,

$$C = \frac{\rho - \rho_w}{\rho_s - \rho_w} \rho_s \quad (4-5)$$

where

$\rho_w$  = water density,  
 $\rho_s$  = grain or particle density, and  
 $\phi = C/\rho_s$  = solids volume fraction (volume of solids divided by sum of the volumes of solids and water).

The three measures of sediment concentration in water, namely  $C$ ,  $\rho$ , and  $\phi$ , are frequently used in this chapter.

Starting with pure water, with increasing mud density,  $\rho$ , the state of a sediment-water mixture changes from fluid to soft solid to solid with rigidity increasing with increasing density. The transition from a fluid (mud) to a solid (bed)

with an interconnected particulate matrix depends on mud composition and stress history. As a rule of thumb, the transition density ranges from about 1,150 to 1,250 kg/m<sup>3</sup>. Since bed rigidity increases rapidly beyond about 1,250 kg/m<sup>3</sup>, it must be included explicitly in the rheological description of mud, especially because flow curves such as those shown in Fig. 4-1 are not easily obtained for dense muds, e.g., with density exceeding, say, 1,300 to 1,400 kg/m<sup>3</sup> (James et al. 1988). Thus, while for a fluid mud (4-1) is a reasonable descriptor of rheology, for dense muds linear viscoelastic models are used as simplified indicators of a characteristically very complex mud rheology. Two noteworthy constitutive models are the standard solid model in Fig. 4-2a and the Kelvin or Voigt model in Fig. 4-2b (Keedwell 1984). The respective constitutive equations are as follows:

*Standard solid:*

$$\tau + \frac{\mu}{G_1 + G_2} \dot{\tau} = \frac{G_1 G_2}{G_1 + G_2} \gamma + \frac{\mu G_1}{G_1 + G_2} \dot{\gamma} \quad (4-6)$$

*Voigt:*

$$\tau = G\gamma + \mu\dot{\gamma} \quad (4-7)$$

where

$\mu$  = viscosity,  
 $G_1$ ,  $G_2$ , and  $G$  = shear moduli of elasticity,  
 $\tau$  = shear stress,  
 $\gamma$  = strain, and the dot over  $\gamma$  signifies the time derivative.

Thus we note that the standard solid model is a combination of a Hookean solid element (i.e., an elastic spring of rigidity, or storage modulus,  $G_2$ ) and a Newtonian fluid element in parallel, with an additional Hookean element of rigidity  $G_1$  in series. Setting  $G_1 \rightarrow \infty$  and  $G_2 = G$  results in the Voigt model, a special case of the standard solid. If now  $G$  is set equal to zero, a Newtonian fluid element ensues. For fluid

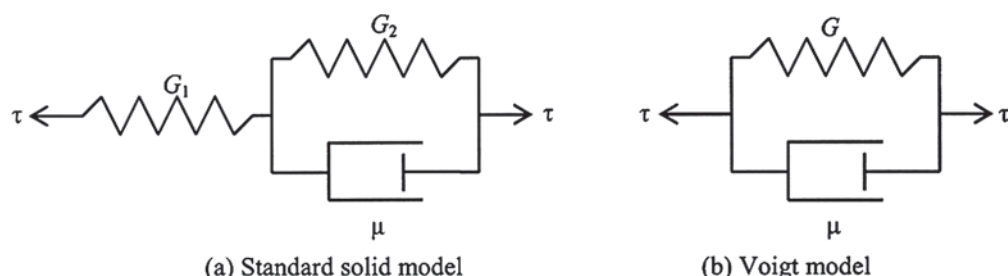


Fig. 4-2. Two linear viscoelastic models: (a) standard solid model; (b) Voigt model.

muds, viscoelasticity has been represented by the Maxwell (fluid) element, which includes a Hookean element and a Newtonian element in series (Li 1996).

Cyclic loading by the action of water waves on mud beds is a means by which loss of structure and rigidity occur, which in turn can lead to the generation of fluid mud. By embedding a miniature rheometer capable of measuring the speed of a high-frequency shear wave through the material, the change in rigidity with time following the inception of water wave motion can be determined. Thus, for example, for a Voigt solid it can be shown that  $G$  is approximately equal to  $\rho V^2$  where  $\rho$  is the material density and  $V$  is the shear-wave velocity (Mehta et al. 1995). Hence, by tracking the change in  $V$  in a constant density mud, the corresponding change in  $G$  can be estimated. In Fig. 4-3, the ratio  $V(t)/V(0)$  is plotted against time,  $t$ ;  $V(0)$  being the initial value of the shear-wave velocity  $V(t)$  at the onset of wave action. This laboratory result is for a clayey bed composed of an aqueous mixture of a kaolinite and an attapulgite of equal weight (AK in Table 4-4). The bed density was 1,170 kg / m, the mean water depth over the bed was 19 cm, and the monochromatic water wave amplitude was 2 cm at a frequency of 1 Hz. The initial rigidity  $G(0)$  was 4,680 Pa; however, in association with a drop in  $V$ , within the first half hour the rigidity decreased by 44%.

Determination of the coefficients in viscoelastic models, e.g., (4-6) and (4-7), requires a combination of creep and dynamic shear tests, ideally in a controlled-stress rheometer, in which mud response to stress can be measured directly (James et al. 1987, 1988; Jones 1997). Thus, for example, Jiang and Mehta (1995) found that all the muds they tested in this way and fit to (4-6) showed the coefficients  $\mu$ ,  $G_1$  and  $G_2$  to vary with the frequency of the forcing (small-amplitude) stress wave. This dependence suggests that (4-6) did not truly represent the rheology, since in that case the coef-

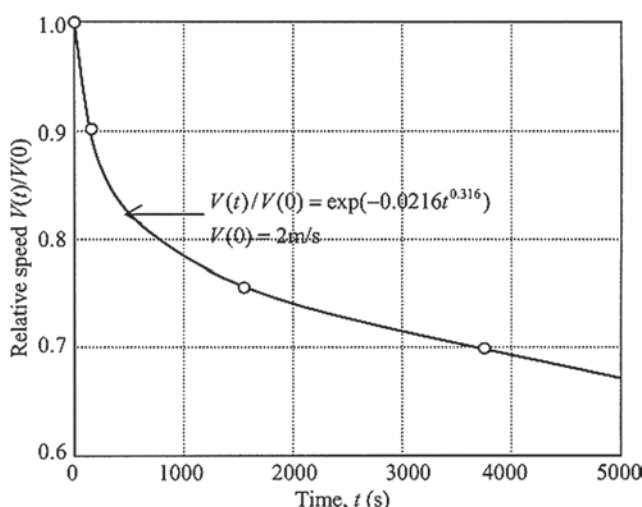


Fig. 4-3. Time variation of relative shearwave velocity (adapted from Mehta et al. 1995).

Table 4-4 Properties of Mud used in Rheometry

Mud type	Median size(μm)	Principal constituents
Kerala, India (KI)	2	Montmorillonite, kaolinite, illite, gibbsite, organic matter (5%)
Okeechobee, Florida (OK)	9	Kaolinite, sepiolite, montmorillonite, 40% organic matter
Mobile Bay, Alabama (MB)	15	Clayey silt of undetermined composition, sand
Attapulgite + kaolinite (AK)	1	Attapulgite (50%) + kaolinite (50%)

Source of data: Jiang (1993); Jiang and Mehta (1993).

ficients would be independent of frequency. Equation (4-6) therefore must be treated as an operational (rather than theoretically correct) model. The coefficients were found to be related to frequency  $f$  (Hz) according to

$$G_1, G_2, \mu = \exp(\alpha_{rh}f^{\beta_{rh}}) \quad (4-8)$$

For muds characterized by particle size and constituents in Table 4-4, values of coefficients  $\alpha_{rh}$  and  $\beta_{rh}$  are given in Table 4-5. The range of frequency,  $f$ , was 0.02 to 40 Hz. Over such a wide frequency range mud response to dynamic loading may be further complicated by thermodynamic effects, inasmuch as while at low frequency the energy dissipation process is thought to occur isothermally, with increasing frequency the process becomes increasingly adiabatic (Krizek 1971).

In general, given the inherent limitations of the standard solid model and its application through (4-6) and (4-8), it has been found reasonable to simplify the rheological description of mud by treating it as a Voigt solid. In this case, characterization of the coefficients in rheometric tests is less cumbersome (Chou 1989; Maa and Mehta 1988).

In Tables 4-4 and 4-5, the effect of sediment composition on the viscoelastic parameters can be qualitatively gauged from the observed variability in the coefficients values. Also, for the Mobile Bay mud (MB), the effect of density can be evaluated. This is shown in Table 4-6, in which  $\mu$  and  $G_2$  are calculated for a representative frequency,  $f = 0.1$  Hz. For comparative purposes, the additional contribution from  $G_1$  to the constitutive behavior may be ignored. Observe the rapid increase in the values of  $\mu$  and  $G_2$  with an increase in  $\phi$  from 0.07 to 0.17.

The description of rheology provided thus far is limited to the effect of shearing the material by the application of a tangential stress. Under wave action, mud also undergoes cycles of compression and tension, for which models representing what is called extensional or elongational rheology are essential (Barnes et al. 1989). In simple dynamical systems, e.g., a viscoelastic element undergoing forcing by

**Table 4-5** Values of Coefficients in (4-8) for Muds of Table 4-4

Mud	Solids weight fraction, $\phi$	$G_1$ (Pa)		$G_2$ (Pa)		$\mu$ (Pa.s)	
		$\alpha_{rh}$	$\beta_{rh}$	$\alpha_{rh}$	$\beta_{rh}$	$\alpha_{rh}$	$\beta_{rh}$
KI	0.12	9.160	0.257	3.843	-0.405	9.292	-0.405
OK	0.11	5.548	0.127	0.318	-0.687	5.290	-0.687
MB	0.07	3.659	0.030	-1.439	-0.975	3.165	-0.975
MB	0.11	6.352	0.075	2.139	-0.745	6.695	-0.745
MB	0.17	8.274	0.108	3.864	-0.696	8.374	-0.696
AK	0.12	8.049	0.114	2.604	-0.490	8.222	-0.490

Source of data: Jiang (1993); Jiang and Mehta (1993).

**Table 4-6** Parameters  $\mu$  and  $G_2$  for Muds of Table 4-4 at Frequency  $f = 0.1$  Hz

Mud	$\phi$	$\mu$ (Pa s)	$G_2$ (Pa)
KI	0.12	$2.76 \times 10^4$	$1.19 \times 10^2$
OK	0.11	$9.65 \times 10^2$	$6.68 \times 10^0$
MB	0.07	$2.24 \times 10^2$	$2.24 \times 10^0$
MB	0.11	$4.49 \times 10^3$	$4.72 \times 10^1$
MB	0.17	$2.15 \times 10^4$	$2.37 \times 10^2$
AK	0.12	$1.15 \times 10^4$	$4.18 \times 10^1$

Source of data: Jiang (1993); Jiang and Mehta (1993).

normal stress with strain assumed to be important only in the direction of applied stress, it can be shown that the extensional viscosity and elastic modulus are related to their shear counterparts defined by (4-7). Given such relations, shear rheometry can be used to determine the extensional coefficients. Such a model has for example been used to calculate the thickness of the fluid mud layer generated by water waves (Li and Mehta 2001).

## 4.3 SEDIMENT TRANSPORT PROCESSES

### 4.3.1 Concentration Profile

The classification of fine-grained sediment transport processes is facilitated by a qualitative description of the vertical profile of the sediment-water mixture concentration or density, as shown in Fig. 4-4. In this description, the term "mobile" means moving horizontally. In contrast, "stationary" implies not moving horizontally. Starting from the water surface, in the top layer the sediment is well-mixed and mobile. In this layer the concentration is so low that fluid rheology is practically Newtonian; i.e., the viscosity is independent of the concentration and the rate of flow shear. The flocs settle independent of each other in the *free settling* mode, with a fall or settling velocity that is independent of concentration,

because the frequency of interparticle collisions is so low that collision outcomes leading to agglomeration or aggregation of particles and flocs are sparse (Krone 1962). The concentration profile is relatively smooth, and turbulent mass diffusion is practically neutral; i.e., upward diffusion of sediment is not significantly influenced by buoyancy stabilization due to the concentration gradient.

Below the mixed layer the suspension is initially nearly Newtonian and has been called concentrated benthic suspension (CBS) (Toorman 2001). With increasing depth the suspension becomes increasingly non-Newtonian as the concentration increases, and concurrently the frequency of interparticle collisions increases. The settling velocity usually increases with increasing concentration as the flocs become larger in the *flocculation settling* mode. Upward mass diffusion due to turbulence is retarded by the concentration gradient due to the negative buoyancy of the suspension. Coupling between concentration-dependent settling velocity and concentration-gradient-dependent diffusion leads to the formation of a stratified structure of the concentration

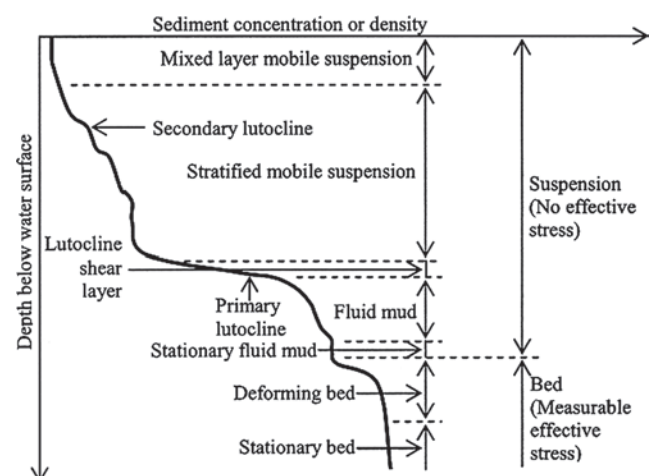


Fig. 4-4. Classification of the vertical profile of sediment concentration (or density).

profile with vertical gradients called secondary lutoclines, which occur above what is called the primary lutocline. A lutocline is a sediment-induced pycnocline (Kirby and Parker 1977; Parker 1987). Its occurrence manifests as a steplike structure of the concentration profile. The primary lutocline occurs near the base of the stratified mobile suspension. This concentration gradient encompasses a shear layer that resembles the boundary layer above a rigid bed, with high shear production and energy dissipation. However, unlike a rigid bed, the “bottom” below the primary lutocline tends to have fluidlike consistency and is dragged by the flow above. Thus the flow velocity does not become zero at the lutocline, but at some depth below it. An important feature of the primary lutocline, in contrast to the usually less stable secondary lutoclines, is that it can persist even under significant flow-induced forcing. This persistence is due to the inability of the turbulent flow to dissipate the lutocline easily by mixing, as a result of the high degree of buoyancy stabilization from the sharp concentration gradient and the inability of the material below the lutocline to fall rapidly due to *hindered settling*. In this mode the settling flux decreases as the concentration increases with depth. Hindered settling is due to the low permeability coupled with increased buoyancy and viscosity of the sediment-water mixture, hence the inability of the interstitial water to easily escape upward.

The layer below the lutocline shear layer is commonly called fluid mud, which is mobile because it tends to move horizontally due to forcing by the flow above. Within fluid mud turbulence is heavily damped and may even collapse completely when a certain threshold concentration is exceeded (Winterwerp 1999), and the base of this layer is defined by the zero mean velocity plane. Below this plane, mud, having a low permeability, may still occur in a fluidlike state but remains stationary; i.e., within it there is practically no horizontal movement. The thickness of the fluid mud layer depends on the type, magnitude, and duration of forcing by tides and waves, on the availability of sediment, and to some extent on its composition. Whereas in low-suspended-sediment-concentration (e.g., a few tens of milligrams per liter at the most) and low-energy (e.g., microtidal sea and calm weather) environments fluid mud is often absent or forms thin layers, in highly energetic environments such as the Amazon estuary it can be several meters thick. In low-energy areas it is often generated episodically when storm waves and surges occur.

A fine-grained sediment bed, which has a very low permeability in comparison with that of a silty or sandy bed, can be differentiated from the suspension above by the effective normal stress, which is practically nil above the bed surface and increases below it with increasing concentration. This stress is the result of interparticle contact within the structured matrix of the bed. The upper part of the bed may undergo time-dependent deformations due to

oscillatory water motion by waves for example, whereas the bed below remains stationary.

#### 4.3.2 Unit Transport Processes

The description presented in Fig. 4-4 is an instantaneous one, because the concentration profile, along with the elevations and thicknesses of the various layers, changes continuously as the forcing changes. Thus, for example, due to continued deformation the bed particulate matrix can break up and generate fluid mud. Fluid mud can entrain sediment and raise the turbidity of the upper water column. Upon cessation of forcing by a current or waves, the water column will be clarified, and if the system remains disturbed, clear water and a hardened bed will eventually result. Such changes can be predicted provided we specify all relevant vertical and horizontal sediment transport fluxes. Since the horizontal transport load strongly depends on the vertical sediment transport mechanisms, we will identify the vertical *unit transport processes* (in qualitative analogy with the terminology once coined at MIT for chemical engineering processes) and fluxes that must be modeled to calculate the horizontal sediment load.

Consider the simplified concentration (or density) profile description shown in Fig. 4-5. Also shown is the horizontal velocity profile. At the boundary between (mobile) fluid mud and (mobile) suspension, sediment entrainment and settling fluxes must be specified. Entrainment of fluid mud depends on turbulent energy resulting from eddy generation in the boundary layer. In this process, the lutocline interface becomes destabilized, interfacial wave generation and breaking occur, and the lower fluid, with its higher sediment content, is ejected into the upper fluid, where sediment concentration increases. The entrained material is then carried above the lutocline by turbulent diffusion. At the bed surface marking the lower level of the fluid mud layer, the bed can undergo erosion, its rate depending on the magnitude of the flow-induced bed shear stress. Bed erosion occurs either by a gradual dislodgement and entrainment of the flocs at the bed surface, or by a more traumatic Mohr-Coulomb type failure of a sizeable thickness of the bed (Lambe and Whitman 1969) and subsequent, relatively rapid entrainment of the failed material. The former process is called surface erosion and the latter mass erosion. Once the material is entrained it can fall by gravitational settling, the settling flux depending on the settling velocity and sediment concentration. For a given settling velocity and concentration, the sediment deposition flux onto the lutocline or the bed is the highest when there is no flow, and decreases as the flow-induced bed shear stress increases. Deposition involves a sorting process by which heavier and stickier particles/flocs that arrive close to the bed by settling become attached to the bed, whereas the remaining material stays in suspension, or elastically rebounds upward from the bed surface (McAnally 1999). The fraction of depositable material decreases with increasing bed

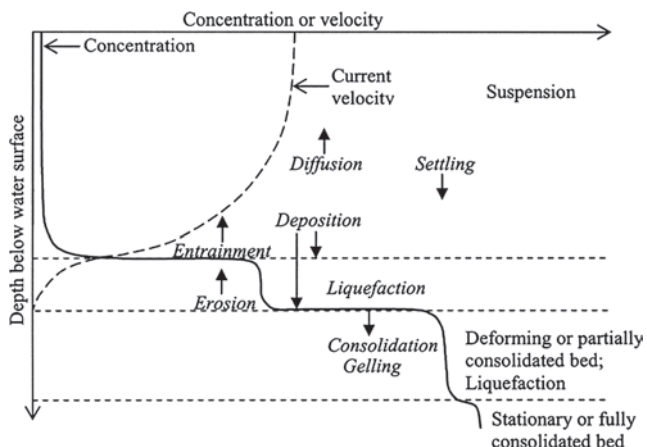


**Fig. 4-5.** Unit transport processes governing sediment concentration (or density) profile dynamics.

shear stress, and above a certain shear stress practically no deposition occurs. When the rate of deposition is high, fluid mud can form because settling is hindered. At low rates of deposition, in case no fluid mud initially exists between the water column and the bed, the settling sediment may deposit to form a bed without generating fluid mud inasmuch as the rate of consolidation is greater than the rate of deposition.

Waves can loosen the bed and generate fluid mud. Technically, liquefaction is considered to occur due to breakup of the soil matrix by shear stresses, while the process of breakup due to excess pore pressure buildup is called fluidization (Toorman 2001). For simplicity, the term liquefaction will be used here, and will be considered to occur by stresses due to pore pressure gradients and associated flows within the bed, which weaken and eventually disrupt the soil matrix. This process manifests itself as a gradual disappearance of the effective normal stress, which becomes practically nil when fluid mud is generated. Once wave action ceases, fluid mud starts to dewater and reform as bed. Dewatering of fluid mud or a partially consolidated bed is described by hindered settling and consolidation. Consolidation is also accompanied by gelling due to rearrangement of water molecules within the pores.

In the above description, the identifiable unit transport processes include settling and deposition, consolidation and gelling, erosion and entrainment, and upward diffusion of eroded/entrained sediment. These processes are considered further in this chapter following a brief description of the particle and floc aggregation processes that govern particle/floc size, density, and strength.

## 4.4 AGGREGATION

### 4.4.1 Floc Transport

Figure 4-6 illustrates the concept of a fine sediment particle or a floc undergoing the process of aggregation, defined as the set of mechanisms by which floc size, density, and

strength change due to flow-particle (or flow-floc) and particle-particle (or floc-floc) interactions. A particle, either an individual grain or a floc of many grains, may originate in the water column or in the bed. Once in suspension, it is subjected to forces due to gravity, inertia, mean flow, turbulent fluctuations, and collisions with other particles in suspension. It may undergo aggregation in the water column, bonding with other particles and breaking apart from them. If the floc grows large enough, it settles toward the bed and can be considered to enter a notional "stirred layer" of high sediment concentration and high shear (Mehta 1991). There it may be deposited on the soft mud layer and eventually become part of the bed, or it may be broken into smaller particulate units and be picked up by the flow and begin the process anew (McDowell and O'Connor 1977).

Aggregation of individual grains into larger, multiple particle units occurs when a collision brings two particles close enough together for mutually attractive forces to overcome repulsive forces, and the two particles bond as a result of those attractive forces. Similarly, fluid forces and collisions exceeding floc strength will break flocs apart. The forces acting on waterborne fine particles include the following fluid and particle forces (Krishnappan 1990; McAnally 1999).

#### Fluid forces:

1. Brownian motion: Thermal motion of fluid molecules causes collisions between the molecules and individual particles, imparting "kicks" that move the particles in random directions.
2. Normal stresses: Small-scale turbulent eddies cause pressure forces that, like Brownian motion, impart random motion to particles of size similar to the eddies.
3. Shear stresses: Both laminar and turbulent shear flows impose tangential stresses on particles that are of the

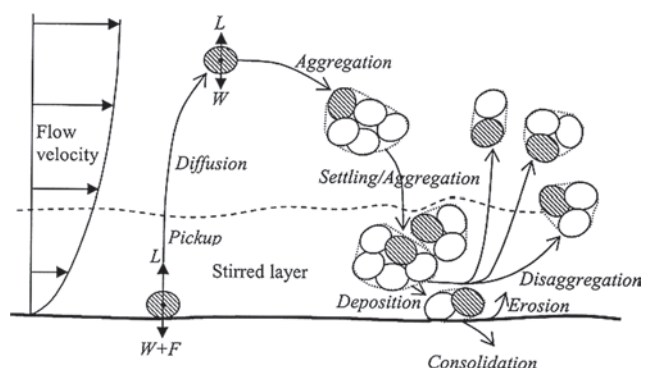


**Fig. 4-6.** Schematic drawing showing transport and aggregation of cohesive sediment particles or flocs.  $L$  = lift force,  $W$  = particle submerged weight, and  $F$  = cohesion (adapted from McAnally 1999).

same size order as the distance over which the velocity changes significantly.

4. Mean flow drag: Any difference between the mean flow velocity and the particle mean velocity will result in a drag force due to pressure and frictional forces.

#### **Particle forces:**

5. Van der Waals attraction: Generated by mutual influence of electron motion within the particles, van der Waals forces act between all matter and are extremely strong, but decay very rapidly (from the 3rd to the 7th power) with distance, so particles must be very close together before the forces exert a significant influence.
6. Electric surface attractions and repulsions; The surface electrical charges of fine particles induce both attractive and repulsive forces between two similar particles.
7. Collisions; Colliding particles impart forces and torques on one another.

#### **Other forces:**

Once two or more sediment particles bond together, additional forces may act on them, including chemical and biochemical cementation and biopolymeric binding, and forces due to pore fluid motion at extremely small scales. Such forces require explicit consideration in theories meant to simulate natural aggregation (Hill 1992; Hill et al. 1992; Hill and Nowell 1995).

The electrical forces include predominantly negative surface charges of most fine sediment grains (exceptions are some metal hydroxides that have positive face charges and negative edge charges), which give most fine sediment grains a net negative charge. This charge induces a repulsive force between two similar grains. If the overall repulsive force is reduced and the positive edge of one grain approaches the negative face of another, the two grains may bond in a T-formation. The overall charge of a grain attracts a cloud of opposite-charge ions if they are available in the surrounding fluid. The cloud of ions, called the Gouy double layer, balances the grain's net charge and represents an equilibrium in the ion field between electrical attraction toward the grain and diffusion away from it. The double layer exerts a repulsive force on other like-charged grains and their double layer, just as the net charge does, and also extends outward some distance to keep grains farther apart. These electrical forces are weaker than the van der Waals force, but decay more slowly with distance, so they dominate the net force between grains unless other processes come into play as discussed below. In a fluid with abundant free ions the double-layer thickness is suppressed, reducing the distance over which

the repulsive forces act and permitting grains to approach more closely. The electrically neutral unit consisting of a mineral grain and its double layer is called a clay micelle (van Olphen 1977).

In nearly ion-free water the net grain charge keeps the clay micelles, and hence the cohesive grains, apart, and only those collisions bringing an edge (typically positive) directly to an oppositely charged face can bring the two close enough together to allow the van der Waals forces to bind them in an edge-to-face configuration. Adding only a few free ions (for example, by dissolving salt in the fluid) creates large ionic double layers and retards aggregation by repelling grains at larger spacings, but at some higher ionic concentration the double layer's diffusion is suppressed and it shrinks, permitting closer approach between grains and collisions that overcome the faces' electrical repulsion so that the short-range van der Waals forces can bind them face-to-face.

Under low ionic concentrations, floc structures can be likened to houses of playing cards with large pore spaces, low density, and low strength, because the edge-to-face connection puts only a few molecules within the range of the attractive forces. Such flocs commonly occur in freshwater lakes. At the higher dissolved-ion concentrations of upper estuaries and some rivers, the orientation of aggregated grains tends toward face-to-face contacts and most often resembles a deck of cards that has been messily stacked. With larger contact areas and shorter moment arms, such structures are significantly stronger than those formed by edge-to-face orientation (Burban et al. 1989; Parchure 1984).

#### **4.4.2 Order of Aggregation**

Based on tests on estuarine sediments, Krone (1963) inferred a conceptual model of floc structure. In this model, initial aggregation creates small, compact flocs of primary grains with strong bonds, referred to as "zero order aggregates," designated  $p0a$  in Fig. 4-7. Subsequent collisions between zero order aggregates create slightly weaker bonds between two or more of these aggregates, leading to an assemblage of  $p0a$ 's, a particle aggregate-aggregate, or first order aggregate,  $p1a$ .



**Fig. 4-7** Idealized floc structure depicting orders of aggregation.

Successive levels (orders) of aggregation lead to particle aggregate-aggregate-aggregates  $p2a$ , then  $p3a$ , and so on.

Based on rheometric experiments with sediments from five locations covering the U.S. Atlantic, Gulf of Mexico, and Pacific coasts, plus one inland river, Krone (1963) calculated up to 6 orders of aggregation with corresponding densities and strengths for each. As an example, results for San Francisco Bay sediment are given in Table 4-7. These properties refer to sediment in suspension. When the material deposits, overburden, gelling, and consolidation alter floc properties. As a result, there is only a remote connection between the density and strength of the suspended flocs and the erodibility of flocs at the bed surface, especially after the bed has aged following its formation by sediment deposition.

#### 4.4.3 Fractal Description

The floc model of Krone (1963), which assigns discrete structures to flocs, is notionally compatible with models of floc structure based on the fractal principle (e.g., Meakin 1988; Kranenburg 1994a; Winterwerp 1998; 1999). The basic model, which has long been used in wastewater treatment research, assumes that floc structure approximately conforms to the fractal property of geometric self-similarity. Self-similar structure leads to a power-law relationship between floc size and properties such as density and surface area. Thus, for example, the relationship between diameter and density for a three-dimensional floc can be expressed as

$$d_f = \sigma_f \rho_f^{1/(n_f - 3)} \quad (4-9)$$

where

$d_f$  = floc diameter,  
 $\rho_f$  = floc density, and  
 $n_f$  = fractal dimension.

**Table 4-7 Characteristics of Aggregate Orders of San Francisco Bay Sediment**

Order of aggregation	Floc density <sup>a</sup> (kg/m <sup>3</sup> )	Floc strength (Pa)
0	1,269	2.2
1	1,179	0.39
2	1,137	0.14
3	1,113	0.14
4	1,098	0.082
5	1,087	0.036
6	1,079	0.020

<sup>a</sup>In sea water of density 1,025 kg/m<sup>3</sup>.

Source: Krone (1963).

The proportionality constant  $\sigma_f$  depends on the sediment and fluid properties. For example, Tambo and Watanabe (1979) report a range of 0.0002 to 0.0012, when  $d_f$  is measured in cm and  $\rho_f$  in g/cm<sup>3</sup>.

For bodies in three-dimensional (Cartesian) space,  $1 \leq n_f \leq 3$ . For a nonfractal solid sphere,  $n_f$  has a value of 3. Wiesner (1992) showed that for aggregation due to Brownian motion, an irreversible process,  $n_f$  should be about 1.78. For reversible processes such as flow shear-induced collisions, it should be about 1.9 to 2.1. He noted, however, that for distinct scales of structure, such as Krone's order-of-aggregation model, each scale may be characterized by a different fractal dimension and the overall apparent dimension will be larger, perhaps 2.1 to 2.6 for a second order aggregate ( $p2a$ ) structure. Kranenburg (1994a) noted that it would be inappropriate to assume that the complex, multi-component structure of real muds possesses completely self-similar geometry. He concluded that muds are probably only approximately self-similar, but that the concept seems useful in interpreting experimental results. These observations have been supported by experimental evidence (Winterwerp 1999); however, from field data Manning and Dyer (1999) reported that there was more variation in floc density for the same floc size than suggested by the fractal model.

#### 4.4.4 Floc Strength

Floc strength, i.e., resistance to breakup or disaggregation, is a function of cohesion, size, and orientation of particles within the floc and organic content (Partheniades 1971; Wolanski and Gibbs 1995), and to a lesser extent depends on salinity and pH (Raveendran and Amirtharajah 1995). Experimental results (e.g., Krone 1963; Hunt 1986; Mehta and Parchure 2000) show that as floc size and organic content increase, floc density and strength decrease. Partheniades (1993) reported that Krone's (1963) data for floc strength fit the expression

$$\tau_f = \alpha_c \Delta \rho_f^{\beta_c} \quad (4-10)$$

where

$\tau_f$  = floc strength (in Pa),  
 $\Delta \rho_f = \rho_f - \rho_w$  (in kg/m<sup>3</sup>),  
 $\rho_w$  = water density, and  
 $\alpha_c, \beta_c$  = empirical coefficients, e.g.,  $1.524 \times 10^{-7}$  and 3, respectively, for San Francisco Bay sediment.

The fractal model of Kranenburg (1994a) results in a floc strength that follows Eq. (4-10), with  $\beta_c = 2/(3-n_f)$ . Kranenburg noted that his expression brackets Krone's (1963) data for  $n_f = 2.1$  and 2.3.

Logically, for given sediment, floc density should be a function of the shearing intensity, sediment concentration and salinity. In practice, it is usually inferred from measured floc size and settling velocity, assuming free settling

and Stokes' law. Empirically, the relation  $\Delta\rho_f = \alpha_{cd} d_f^{-\beta_{cd}}$  is found to hold on a very approximate basis. For San Francisco Bay sediment, Kranck and Milligan (1992) and Kranck et al. (1993) reported  $\alpha_{cd} = 35,000$  and  $\beta_{cd} = 1.09$ , when  $d_f$  is measured in  $\mu\text{m}$ . These coefficients hold in the range of  $d_f$  approximately between 100 and 1,000  $\mu\text{m}$ . For Chesapeake Bay sediment Gibbs (1985) found  $\beta_{cd} = 0.97$ , which is close to the value of Kranck et al.

#### 4.4.5 Floc Size, Concentration, Turbulence, and Shear Stress

In Eq. (4-9),  $d_f$  may be considered to be the mean floc diameter. In addition, other statistical measures of size and their relationships with other parameters have been proposed. For example, Kranck (1986) and Kranck and Milligan (1992) noted that despite the dramatic shift in the particle size spectra due to coagulation of individual (i.e., dispersed) particles into flocs, a relationship was found between the modal floc size and the corresponding modal (individual) grain size. This was the case because the following equation could be fit to both individual particle spectra and floc spectra, with suitable adjustments of the coefficients:

$$C_v = C_{v0} d_f^{\xi} \exp(-\kappa_f \zeta d_f^2) \quad (4-11)$$

where

$C_v$  = volume concentration of sediment in any one size class, i.e., volume of sediment divided by volume of suspension,

$C_{v0}$ ,  $\xi$ ,  $\kappa_f$  = sediment-specific coefficients,

$\zeta = g(\rho_f - \rho_w)/8\nu\rho_w$ ,

$g$  = acceleration due to gravity, and

$\nu$  = kinematic viscosity of fluid.

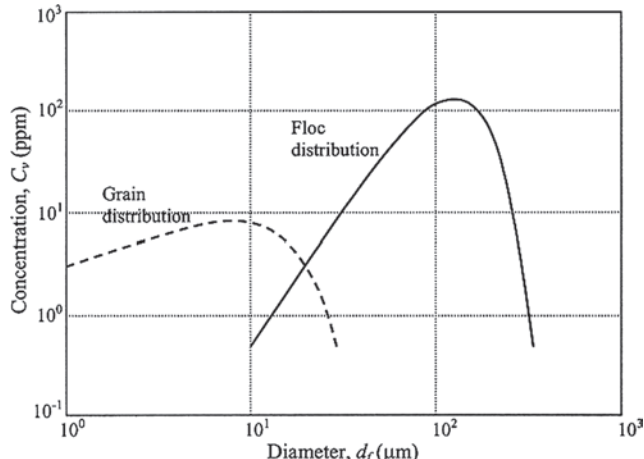


Fig. 4-8. Examples of Eq. (4-11). Dashed curve shows dispersed grain size distribution and continuous curve is for flocs (based on (Kranck 1986; Kranck and Milligan 1992).

Note that  $\zeta d_f^2$  is the Stokes settling velocity. Examples of the fit of (4-11) are shown in Fig. 4-8 for (dispersed) grain size distribution and floc size distribution. Values of  $C_{v0}$ ,  $\xi$ ,  $\kappa_f$ ,  $\nu$ ,  $\rho_f$ , and  $\rho_w$  are based on the work of Kranck (1986) and Kranck and Milligan (1992). The respective set of values are 3.123 ppm, 0.608, 0.0055 s/ $\mu\text{m}$ ,  $10^{-6}$   $\text{m}^2/\text{s}$ , 2,650  $\text{kg}/\text{m}^3$ , and 1,000  $\text{kg}/\text{m}^3$  for dispersed grain distribution, and 0.001 ppm, 2.72, 0.00081 s/ $\mu\text{m}$ ,  $10^{-6}$   $\text{m}^2/\text{s}$ , 1,200  $\text{kg}/\text{m}^3$ , and 1,000  $\text{kg}/\text{m}^3$  for floc distribution. From settling tests using a flocculated marine glacial mud, Kranck (1986) reported wide-ranging values of  $C_{v0}$ ,  $\xi_f$ , and  $\kappa_f$ .

It is feasible to obtain a simple formula relating the median floc size to sediment concentration and turbulence (Galani et al. 1991; Lick et al. 1992): Winterwerp (1998) derived expressions for the equilibrium floc size resulting from a balance between floc formation and breakup, and also the maximum or limiting floc size in a given flow-sediment field. In the latter context, Krone (1963) proposed the following relation for the limiting size:

$$d_{flim} = \frac{2\tau_f \Delta R}{\mu_w \dot{\gamma}} \quad (4-12)$$

where

$\tau_f$  = floc strength,

$\mu_w$  = viscosity of water,

$\dot{\gamma}$  = local flow shear rate, and

$\Delta R$  = interpenetration distance for two colliding flocs.

Assume a moderate flow shearing rate (i.e., the vertical gradient of the horizontal flow velocity) of 10 Hz and a first order aggregate of San Francisco Bay sediment with a strength of 0.39 Pa (Table 4-7). Krone (1962) suggested 2  $\mu\text{m}$  to be a

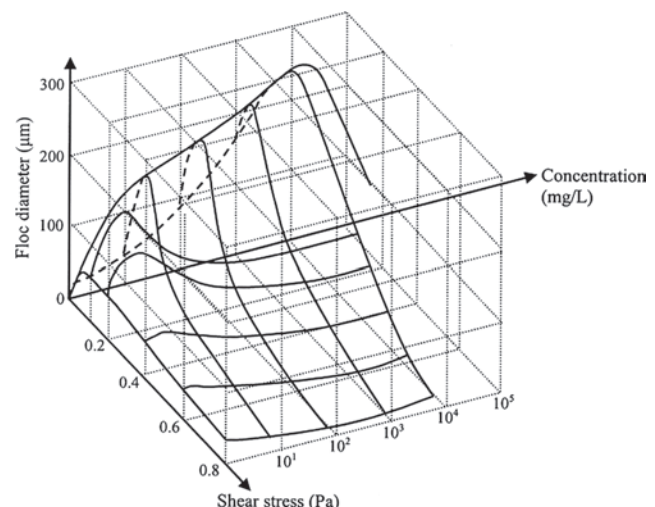


Fig. 4-9. Diagram showing the relationship between floc diameter, suspended sediment concentration and shear stress (after Dyer 1989).

reasonable value of  $\Delta R$ . Substituting these values into Eq. (4-12) along with  $\mu = 0.001 \text{ Pa s}$  gives  $d_{fim} = 156 \mu\text{m}$ .

On a graphical basis, from an analysis of data on modal floc sizes from a variety of experiments Dyer (1989) developed the plot of Fig. 4-9 relating the modal (equilibrium) floc size to suspended sediment concentration and shear stress. From a statistical mechanical representation of two- and three-body collision mechanisms between particles and flocs sorted out by size classes for sediment from the San Francisco Bay, McAnalley (1999) developed a plot relating the equilibrium diameter (actually diameter at time equal to the 99.9% of the time required to reach full equilibrium), the suspended sediment concentration, and the local rate of energy dissipation in the fluid. The plot showed a qualitative resemblance to Fig. 4-9.

#### 4.4.6 Modes of Transport

Referring to Fig. 4-6 we note that the pickup and deposition of particles or flocs must inherently follow a transport regime somewhat different from that for cohesionless grains. Let us represent cohesion simply by a representative force  $F$ , which binds the cohesive particle to the bed. Also, let us assume that the entraining force is represented solely by the hydrodynamic lift  $L$ , i.e., excluding any contribution from drag. Accordingly, the condition for incipient entrainment will be  $L / (W + F) \geq 1$ , where  $W$  is the buoyant weight of the particle. On the other hand, the condition for deposition of a suspended particle will be  $L / W < 1$ .

Following the classical derivation of the bed load function by Einstein (1950), in which bed load is obtained under the condition of equality of number flux (i.e., number of particles per unit bed area per unit time) of entraining and depositing cohesionless particles, Partheniades (1977) examined the transport of cohesive particles. He showed that, under the assumption of  $L$  fluctuating (due to turbulence) between an upper and a lower bound (as opposed to Einstein's boundless Gaussian distribution), cohesion ( $F$ ) precludes, in general, the development of a bed load function, and hence bed load transport. This is so because under this scenario, for instance, deposition can occur exclusively, i.e., without corresponding erosion of bed. In other words, he showed that cohesive sediment is characteristically transported in suspension, rather than as bed load. This transport can occur either as bed material load or as wash load. As for the latter mode, lightweight organic detritus is often transported as wash load through rivers and tidal waters where currents are strong. In quiescent basins where currents become weak this material may be deposited and if so, would be reclassified as bed material load. It is essential to point out, however, that cohesive materials often form balls or pebbles (e.g., Jacinto and Le Hir 2001), and these comparatively hard particles have distinct and durable forms that can be transported as bed load; i.e., their transport can be represented in a large measure by a bed load function derived for coarse

sediment transport, when such "particles" occur in sufficiently large numbers per unit bed area.

To support his argument regarding the mode of transport of cohesive sediment, Partheniades (1977) used evidence from steady flow experiments on the deposition of initially suspended kaolinite in a flume. He showed that the variation of suspension concentration with time during deposition could be explained only if it was assumed that no erosion of the deposited material occurred during the depositional process. The main observation that supported this inference was that up to a fairly high suspension concentration, on the order of  $25 \text{ kg/m}^3$ , the sediment-carrying capacity of the flow was found to be independent of flow velocity; being dependent, instead, on how much sediment was externally introduced into the suspension. Later, Parchure (1984) showed that his steady-flow experimental results on the erosion of a variety of cohesive beds could be explained provided it was assumed that no deposition of the eroded sediment occurred. This inference was mainly based on the observation that at steady state, if the suspension was replaced by clear water without stopping the flow, no significant erosion subsequently occurred. Lick (1982), however, based his erosion rate expression on the assumption of continuous exchange, citing his own experimental evidence for simultaneous deposition and erosion.

Notwithstanding the analysis of Partheniades (1977), which relies on the single grain size analysis of Einstein (1950), the issue of whether erosion and deposition are "mutually exclusive" does not appear to have been fully resolved. The difficulty seems to be due largely to the nature of the experiments that have been conducted thus far; almost all based on relatively simple laboratory setups in which it has not been possible to "observe" particle transport close to the bed. In every case the behavior of particles with regard to near-bed entrainment and deposition has had to be inferred from essentially indirect evidence. For example, by tagging part of the initially suspended sediment with radioactive gold and comparing the rate of deposition of tagged sediment with that of untagged sediment sampled at mid-depth (rather than close to the bed surface, which is typically ill-defined and unidentifiable during deposition), Krone (1962) indirectly inferred that some of the deposited material had seemingly reentrained during the predominantly depositional process.

The question of bed sediment exchange becomes especially important in modeling sediment transport under oscillatory flows, due both to tides and to waves. Whereas in his modeling of tide-induced transport Hayter (1983) assumed mutually exclusive erosion and deposition, Jiang (1999) considered continuous exchange. Similarly, in wave-induced transport modeling, Maa (1986) assumed continuous exchange. Sanford and Halka (1993) showed that in situ measurement of resuspension of fine sediment in the Chesapeake Bay could be better modeled by assuming continuous exchange than by assuming nonsimultaneous erosion/deposition. On the other hand, Teeter (2001b) argued for nonsimultaneous exchange, citing the need to model sediment sorting

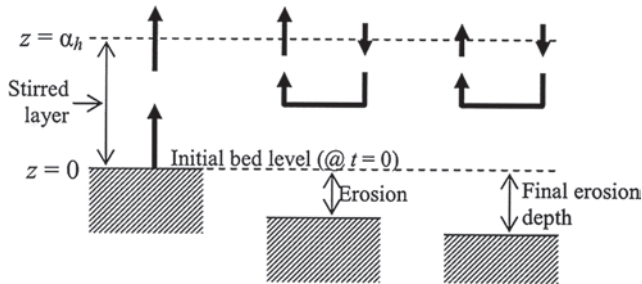


**Fig. 4-10.** Schematic description of vertical sediment fluxes (arrows) in the stirred layer actuated by bed erosion (adapted from Cervantes et al. 1995). Reproduced with permission of PIANC-COPEDEC.

during erosion/deposition, rather than continuous exchange, for an explanation of bed response to unsteady forcing in the prototype environment.

In order to conceptually bridge the knowledge gap between laboratory observed mutually exclusive erosion/deposition and the commonly encountered need to render these processes simultaneous in modeling resuspension in field applications, the schematic drawing of near-bed sediment exchange shown in Fig. 4-10 can be helpful (Cervantes et al. 1995; Mehta 1991). The layer extending from the bed (at  $z = 0$ ) to some suitable notional height  $\alpha_h$  may be idealized as a stirred layer mentioned earlier, within which entrainment of sediment from the bed starting at  $t = 0$  sets up a convective cell of upward diffusive flux of sediment and, as a result, gravity-induced settling flux. Under constant fluid stress-induced forcing at the bed these fluxes will eventually approach equality, erosion of the stratified bed will practically cease at some final depth where the applied shear stress equals the erosion shear strength, and a steady-state concentration of sediment in the water column will occur. Thus, by applying, at  $z = \alpha_h$ , laboratory expressions for erosion and deposition evaluated at  $z = 0$ , formulas compatible with mutually exclusive erosion/deposition can be used in simulating resuspension on a simultaneous basis. Even though this is merely a "convenient" interpretation of two unresolved concepts, it appears that the "insertion" of the stirred layer may be useful in explaining some flume experimental results meant to study deposition, but in which two-way exchange between bed and suspended sediment may actually have occurred (McAnally 1999).

## 4.5 SETTLING VELOCITY

### 4.5.1 Aggregation and Settling

The rate at which suspended flocs settle depends on their weight, diameter, and shape, which in turn are related to their order of aggregation, the latter being governed by the frequency of interparticle collisions. Three mechanisms that have been explicitly shown to influence aggregation in estuarine and coastal waters are Brownian motion, flow-induced shear, and differential settling (Krone 1962). By way of the last mechanism, particles/flocs of different settling velocities collide as they fall. For these three mechanisms, the

frequency functions of collision between two particles of sizes  $i$  and  $j$   $\beta_c$  are given as (McAnally 1999; Burban et al. 1989; Delichatsios and Probstein 1975; Saffman and Turner 1956)

$$\beta_c = \begin{cases} \frac{2}{3} \frac{\kappa T F_c}{\mu} \frac{(d_i + d_j)^2}{d_i d_j} & \text{Brownian motion} \\ \left[ \frac{\pi F_c^2}{4} \sqrt{\frac{2}{15 \pi}} \right] G_s (d_i + d_j)^3 & \text{fluid shear} \\ \left[ \frac{\pi F_c^2}{4} \right] (d_i + d_j)^2 |w_{si} - w_{sj}| & \text{differential settling} \end{cases} \quad (4-13)$$

where

- $\kappa$  = Boltzmann constant;
- $T$  = absolute temperature;
- $\mu$  = dynamic viscosity of fluid;
- $F_c$  = collision diameter correction factor (which varies between 0 and 1);
- $d_i, d_j$  = sizes of colliding particles from  $i$  and  $j$  size classes, respectively;
- $w_{si}, w_{sj}$  = corresponding settling velocities;
- $G_s$  = measure of flow shear given by  $G_s = (\epsilon/v)^{1/2} = v/\lambda$ ;
- $\epsilon$  = flow energy dissipation per unit mass of fluid per unit time;
- $v = \mu/\rho_w$  = kinematic viscosity of fluid (nominally water) and
- $\lambda$  = Kolmogorov turbulence microscale.

The settling velocities can be simply related to the corresponding diameters through Stokes' law:  $w_{si} = \Delta\rho_i d_i^2 / 18\mu$  and  $w_{sj} = \Delta\rho_j d_j^2 / 18\mu$

where

$$\begin{aligned} \Delta\rho_i &= \rho_{si} - \rho_w; \\ \Delta\rho_j &= \rho_{sj} - \rho_w; \\ \rho_i, \rho_j &= \text{densities of } i \text{ and } j \text{ particles and} \\ \rho_w &= \text{water density.} \end{aligned}$$

Among others, Hunt (1982), Lick et al. (1992), and McAnally (1999) have described the manner in which the relative importance of the above three collision mechanisms changes as aggregation of particles proceeds. In Fig. 4-11 a comparison is made of these mechanisms based on Eq. (4-13) and typical water column conditions. Observe that as aggregation proceeds and the second particle size increases, fluid shear takes over as the dominant mechanism, while the influence of Brownian motion becomes negligible. Note also that when the two particles are of the same size, in this case 1  $\mu\text{m}$ , there is no contribution from differential settling because the two particles settle at the same rate, and therefore do not collide by that mechanism.

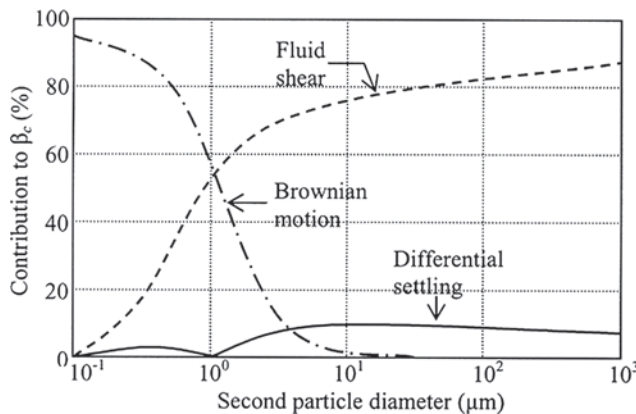


**Fig. 4-11.** Simulated relative contributions to the collision frequency for typical water column conditions in the estuary. First particle diameter is 1  $\mu\text{m}$  (after McAnally 1999).

In general, fluid shear is the most important of the three collision mechanisms, because it produces relatively tightly packed, durable flocs in comparison with the other two mechanisms (Krone 1963; 1986). Differential settling is important during and close to times of slack water. At very low flow shear Brownian motion becomes responsible for aggregation; however, the flocs thus produced tend to be weakly bonded.

#### 4.5.2 Settling Velocity and Concentration

Floc settling velocities typically range from  $1 \times 10^{-5}$  to  $1 \times 10^{-1}$  m/s for particles of size 10 to 1,000  $\mu\text{m}$  (Dyer 1989; van Leussen 1994; Moudgil and Vasudevan 1989). The settling velocity depends on the floc properties, especially size, density, and shape, which in turn are governed by the interparticle collision frequency and the outcome of collisions. Inasmuch as collisions depend on particle concentration in the suspension, suspended sediment concentration can be used as an approximate lumped parameter for estimating the settling velocity of flocs (Krone 1962). As a result, and given the convenience with which concentration can be measured, formulas relating the settling velocity to concentration have been proposed.

Following Wolanski et al. (1989), a general expression for the mean settling velocity divides the settling range into four zones—free settling, flocculation settling, hindered settling, and negligible settling. The settling velocity,  $w_s$ , in each zone can be expressed as (Hwang 1989)

$$w_s = \begin{cases} w_{sf} & C < C_1 \\ a_w \frac{C^{n_w}}{(C^2 + b_w^2)^{m_w}} & C_1 < C < C_3 \\ \sim \text{negligible} & C_3 < C \end{cases} \quad (4-14)$$

where

$w_{sf}$  = free settling velocity;  
 $C$  = suspension concentration;  
 $a_w$  = velocity scaling coefficient;  
 $n_w$  = flocculation settling exponent;  
 $b_w$  = hindered settling coefficient;  
 $m_w$  = hindered settling exponent and  
 $C_1, C_3$  = zone concentration limits defined in Fig. 4-12.

Free settling occurs at low suspension concentrations when  $w_s$  is independent of  $C$ , and can be calculated from Stokes' law, especially when settling occurs under quiescent conditions. Between  $C_1$  and  $C_2$ ,  $w_s$  increases with concentration due to the formation of stronger, denser and larger flocs. In the hindered settling zone between  $C_2$  and  $C_3$ , the occurrence of an aggregated particulate network inhibits, or hinders, the upward transport of interstitial water in the deposit. As a result,  $w_s$  decreases with increasing  $C$  in this zone. At concentrations above  $C_3$ , settling becomes comparatively small as consolidation takes over.

Values of coefficients  $a_w$ ,  $b_w$ ,  $m_w$ , and  $n_w$  along with  $C_1$  are given in Table 4-8 based on the application of Eq. (4-14) to measured variations of the settling velocity (m/s) with concentration ( $\text{kg/m}^3$ ). In general,  $C_1$  ranges between 0.1 and 0.3  $\text{kg/m}^3$ , in agreement with the original observations of Krone (1962). In reality, the transition between free and flocculation settling is gradual and may occur over a wider concentration range, e.g., on the order of 0.01 to 0.3  $\text{kg/m}^3$  (Krone 1962; Ozturk and Lavelle 1986). For computational purposes, it is convenient to select  $w_{sf}$  as the value of the settling velocity corresponding to the intersection of the curve for flocculation settling obtained from (4-14) with the vertical line corresponding to  $C_1 = 0.1 \text{ kg/m}^3$ .

The concentration  $C_2$ , corresponding to the peak settling velocity  $w_{sm}$ , can vary between 1 and 15  $\text{kg/m}^3$ . Odd and Cooper (1989) reported  $C_3$  to be on the order of 75  $\text{kg/m}^3$  in their measurements of settling rates of mud from the Severn

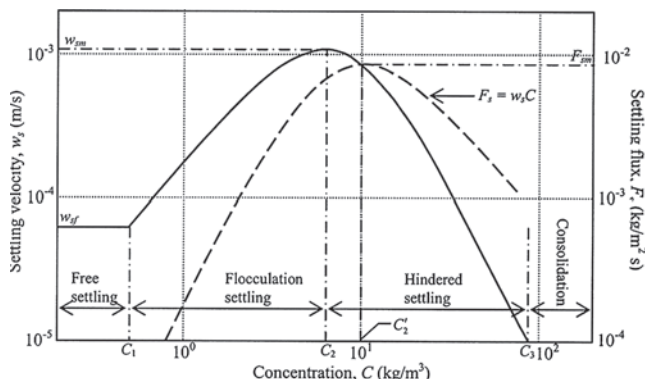


**Fig. 4-12.** A representative plot of settling velocity and associated settling flux variation with suspension concentration.

**Table 4-8 Values of Coefficients in (4-14) Derived from Several Studies**

Investigator(s)	Sediment source	$a_w$	$b_w$	$m_w$	$n_w$	$C_1$ (kg/m <sup>3</sup> )
Krone (1962)	San Francisco Bay, California	0.048	25.0	1.00	0.40	0.30
Owen (1970)	Severn River, U.K., salinity 2 g/L	0.140	17.0	1.40	1.10	0.20
Owen (1970)	Severn River, U.K., 8 g/L	0.110	11.0	1.53	1.50	0.20
Owen (1970)	Severn River, U.K., 17 g/L	0.160	15.0	1.15	0.50	0.20
Owen (1970)	Severn River, U.K., 32 g/L	0.100	10.0	1.30	1.00	0.20
Owen (1970)	Severn River, U.K., 48 g/L	0.080	9.50	1.34	1.00	0.20
Huang et al. (1980)	Yangtze River, China	0.012	1.70	2.80	2.20	0.20
Thorn (1981)	Severn River, U.K.	0.010	2.00	1.46	2.10	0.20
Burt and Stevenson (1983)	Thames River, U.K., 1981 sample	0.170	3.00	1.90	1.65	0.15
Burt and Stevenson (1983)	Thames River, U.K., 1982 sample	0.060	2.00	1.90	1.50	0.20
Nichols (1984/85)	James River, Va.	0.039	3.80	1.32	1.52	0.20
Odd and Rodger (1986)	Severn River, U.K.	0.080	6.50	1.35	1.42	0.10
Lott (1986)	Commercial kaolinite	0.010	3.00	1.60	1.30	0.20
Ross (1988)	Tampa Bay, Fla.	0.001	1.80	1.40	2.10	0.30
Hwang (1989)	Lake Okeechobee, Fla., 40% organic, particle size 10 µm	0.080	3.50	1.88	1.65	0.15
Hwang (1989)	Lake Okeechobee, Fla., 40% organic, particle size 15 µm	0.027	5.50	1.60	1.00	0.20
Hwang (1989)	Lake Okeechobee, Fla., 40% organic, particle size 7 µm	0.090	4.50	1.85	1.80	0.30
Costa (1989)	Hangzhou Bay, China	0.100	6.20	1.60	1.20	0.20
Wolanski et al. (1991)	Cleveland Bay, Australia, field test	0.200	1.40	2.25	2.45	0.10
Wolanski et al. (1991)	Cleveland Bay, Australia, laboratory tests	0.07	1.30	2.5	2.80	0.20
Jiang (1999)	Jiaojiang, China, neap tide	0.045	6.00	1.51	1.50	0.20
Jiang (1999)	Jiaojiang, China, spring tide	0.230	10.00	1.80	1.50	0.20
Marván (2001)	Ortega River, Fla.	0.160	4.50	1.95	1.70	0.20
Ganju (2001)	Loxahatchee River, Fla.	0.190	5.80	1.80	1.80	0.20

River estuary in United Kingdom. This value is in approximate agreement with the concentration at which a suspension changes to a bed due to the development of effective normal stress (Sills and Elder 1986).

From Eq. (4-14) we find that when  $C \ll b_w$ , i.e., the “low” concentration condition,

$$w_s = a_w b_w^{-2m_w} C^{n_w} \quad (4-15)$$

Equation (4-15), which describes flocculation settling, was derived by Krone (1962), who also provided a phenomenological explanation for the form of the equation. Using the data of Overbeek (1952) on the aggregation of initially dispersed particles, Krone determined the value  $n_w = 4/3$  and showed that it agreed with his data on settling of San Francisco Bay sediment in a flume as well as in a settling column.

When  $C \gg b_w$ , i.e., the “high” concentration condition, Eq.(4-14) reduces to

$$w_s = a_w C^{n_w - 2m_w} \quad (4-16)$$

where  $n_w - 2m_w$  must be less than zero, because hindered settling causes the settling velocity to decrease with increasing concentration. The form of Eq. (4-16) agrees with the experimental data of Richardson and Zaki (1954), who also derived it theoretically based on idealized geometric arrays of particles falling in the hindered settling mode.

From Eq. (4-14) the following useful quantities related to settling velocity and associated settling flux  $F_s = w_s C$  (Fig. 4-12) are obtained:

*Peak velocity,  $w_{sm}$ :*

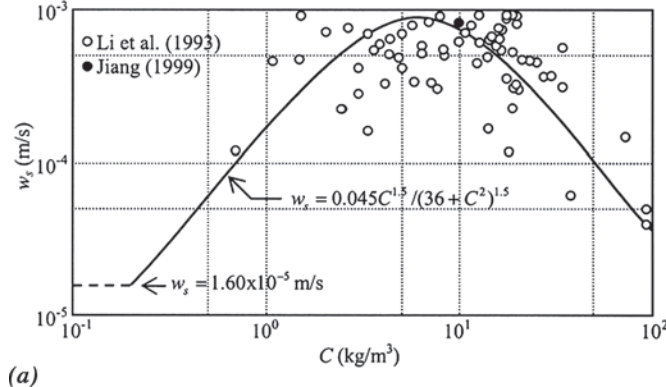
$$w_{sm} = a_w b_w^{n_w - 2m_w} \frac{\left(\frac{2m_w}{n_w} - 1\right)^{m_w - n_w/2}}{\left(\frac{2m_w}{n_w}\right)^{m_w}} \quad (4-17)$$

*Concentration,  $C_2$ :*

$$C_2 = \frac{b_w}{\left(\frac{2m_w}{n_w} - 1\right)^{1/2}} \quad (4-18)$$

*Settling flux,  $F_s (= w_s C)$ :*

$$F_s = a_w \frac{C^{n_w + 1}}{(C^2 + b_w^2)^{m_w}} \quad (4-19)$$



*Maximum settling flux,  $F_{sm}$ :*

$$F_{sm} = a_w b_w^{n_w - 2m_w + 1} \frac{\left(\frac{2m_w}{n_w} - 1\right)^{m_w - \frac{n_w + 1}{2}}}{\left(\frac{2m_w}{n_w} + 1\right)^{m_w}} \quad (4-20)$$

*Concentration at maximum flux,  $C'_2$ :*

$$C'_2 = \frac{b_w}{\left(\frac{2m_w}{n_w} - 1\right)^{1/2}} \quad (4-21)$$

Inasmuch as  $C'_2$  is obtained from Eq. (4-18) by replacing  $n_w$  by  $n_w + 1$ , it is characteristically greater than  $C_2$ . Physically this is so because of the dependence of settling velocity on concentration, which means that the settling flux is a nonlinear function of concentration. Thus, for example, from the data of Nichols (1984/1985) in Table 4-8 we find that  $C_2 = 4.4$  kg/m<sup>3</sup> and  $C'_2 = 17.4$  kg/m<sup>3</sup>. In a depositional environment, i.e., in the absence of significant reentrainment of sediment,  $C'_2$  marks the level of the lutocline. Consequently, in Fig. 4-4 this concentration corresponds to the upper level of the fluid mud layer. Likewise,  $C_3$  very approximately marks the transition between the fluid mud layer and the bed. The concentration  $C_1$  defines the transition between the mixed suspension layer and the stratified suspension layer. When entrainment is significant these concentration limits and the elevations at which they occur in the concentration profile tend to change, depending on the importance of entrainment in relation to settling.

An example of settling velocity data from the Jiaojiang estuary in China and data fit using Eq. (4-14) is shown in Fig. 4-13a. An illustration of settling flux variation with

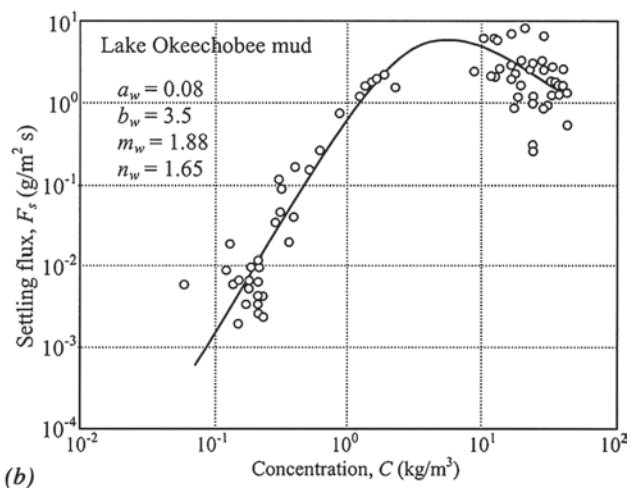


**Fig. 4-13.** Settling velocity as a function of (a) suspension concentration during a neap tide in the Jiaojiang estuary, China (after Jiang 1999) and (b) suspended sediment concentration for Lake Okeechobee, Fla. mud (data from Hwang 1989; the curve is based on Eq. (4-19)).

concentration is shown in Fig. 4-13b, based on the data of Hwang (1989) from Lake Okeechobee in Florida. The curve is obtained from Eq. (4-19).

#### 4.5.3 Other Effects on Settling

Jiang (1999) found that deposition data from the flume experiments of Lau (1994) using a kaolinite under controlled conditions of fluid temperature showed a well-defined temperature dependence of the form

$$w_{s50}(C, T_c) = \Phi w_{s50}(C, 15) \quad (4-22a)$$

where

$w_{s50}(C, 15)$  = concentration-dependent median settling velocity as defined by Eq. (4-14) at temperature  $T_c = 15^\circ\text{C}$ , and

$$\Phi = 1.776(1 - 0.875T') \quad (4-22b)$$

where

$$T' = T_c / 15.$$

This finding suggests that the mean floc size decreases with increasing temperature, which is a reasonable conclusion because thermal activity of the clay micelle ions tend to increase the repulsive effect between grains, reducing the number of collisions available to pump sediment mass up the size distribution in an environment in which continued aggregation occurs.

In order to account for the effect of flow shear on the settling velocity, van Leussen (1994) and Teeter (2001a) proposed equations relating  $w_s$  to the flow shear rate, whereas Burban et al. (1990) relate  $w_s$  to shear stress. Winterwerp (1998) used Kranenburg's (1994) fractal model as a framework to formulate settling velocity relationships based directly on grain and floc sizes. Following van Leussen (1994), Malcherek and Zielke (1996) and Teisson (1997), Teeter (2001a), used the expression:

$$\frac{w_s}{w_{s|\dot{\gamma}=0}} = \frac{(1 + \lambda_1 \dot{\gamma})}{1 + \lambda_2 \dot{\gamma}^2} \quad (4-23)$$

in which  $w_{s|\dot{\gamma}=0}$  is obtained from a concentration dependent settling velocity function such as (4-14),  $G$  is the shear rate (Hz or  $\text{s}^{-1}$ ), and  $\lambda_1$  and  $\lambda_2$  are sediment-specific coefficients. From laboratory work on mud from San Francisco Bay, the values of these two coefficients are found to be 266 and 9, respectively.

Sheng (1986) showed that submerged vegetative canopies offer considerable resistance to settling and deposition. Ganju (2001) found that for Florida sediments the coefficient  $a_w$  in (4-14) depends on the organic content  $OC(\%/100)$  according to  $a_w = a_{w0} + a_1 OC + a_2 OC^2 + a_3 OC^3 + a_4 OC^4$ , with  $a_{w0} = 0.2$ ,  $a_1 = 6.67 \times 10^{-4}$ ,  $a_2 = -1.7 \times 10^{-4}$ ,  $a_3 = 7.1 \times 10^{-6}$ , and  $a_4 = -1.3 \times 10^{-7}$ . Note that  $a_{w0}$  is the value of  $a_w$  when  $OC = 0$ . This relationship amounts to the trend of decreasing aggregate diameter and settling velocity with increasing organic content, because the aggregates become both smaller and lighter as the density and cohesion of the composite material decrease with increasing organic fraction.

## 4.6 DEPOSITION UNDER FLOW

### 4.6.1 Rate of Deposition

Referring to Fig. 4-6, if a settling floc approaches a bed where concentration, collision frequency, and shearing rate are high, it will either break apart and be reentrained or bond with particles at the bed surface and be deposited. Deposition can be characterized as the outcome of interaction between two stochastic processes occurring just above the bed—interfloc collisions causing both floc breakup and growth that creates a distribution of floc sizes and strengths, and the probability that a floc of a given strength and size will be deposited (Stolzenbach et al. 1992). Thus, the deposition rate is a function of floc settling velocity, concentration, and the near-bed shearing rate. The shearing rate is conveniently characterized by the bed shear stress.

A widely used expression for the sediment mass deposition rate  $\Psi$ , when only one size class is considered, is

$$\Psi = \frac{d\bar{C}}{dt} = -\frac{w_s \bar{C}}{h} \left( 1 - \frac{\tau_b}{\tau_d} \right); \quad \tau_b < \tau_d \quad (4-24)$$

where

$\bar{C}$  = depth-averaged suspended sediment concentration;  
 $h$  = water depth;  
 $\tau_b$  = bed shear stress; and  
 $\tau_d$  = critical stress for deposition.

When  $\tau_b \leq \tau_d$  all initially suspended sediment deposits and, conversely, no sediment deposits when  $\tau_b > \tau_d$ . Thus, in the free settling range ( $w_s = \text{constant}$ ), an exponential law of concentration decay is obtained from (4-24) by integration;

$$\frac{C}{C_0} = \exp \left[ - \left( 1 - \frac{\tau_b}{\tau_d} \right) \frac{w_s}{h} t \right]; \quad \tau_b < \tau_d \quad (4-25)$$

where

$C_0$  = initial suspension concentration;  
 $t$  = time;

and the bar over  $C$  is omitted for convenience of further treatment.

In the flocculation settling range, in which the settling velocity increases with increasing concentration, e.g., according to Eq. (4-15), the concentration-time relationship becomes logarithmic; i.e.,  $\log C$  decreases linearly with  $\log t$  (Krone 1993; Shrestha and Orlob 1996). However, Eq. (4-25) has been found to hold reasonably well up to concentrations on the order of  $1 \text{ kg/m}^3$  (Mehta and Lott 1987).

#### 4.6.2 Multiclass Deposition

Among others, Ockenden (1993) and Teeter (2001a; 200b) extended Eq. (4-24) to multiple grain sizes using

$$\Psi_i = \frac{dC_i}{dt} = -\frac{w_{si}}{h} C_i \left( 1 - \frac{\tau_b}{\tau_{di}} \right); \tau_b < \tau_{di} \quad (4-26)$$

where for each size class  $i$ ,

$\Psi_i$  = mass deposition rate;  
 $C_i$  = depth-mean concentration;  
 $w_{si}$  = settling velocity; and  
 $\tau_{di}$  = critical shear stress for deposition.

Assumed  $\tau_d$  to vary between a minimum value  $\tau_{d1}$  for the finest sediment size class and a maximum  $\tau_{dm}$  for the coarsest class  $M$ , the concentration-time variation during deposition can be shown to depend on the magnitude of  $\tau_b$  in relation to  $\tau_{d1}$  and  $\tau_{dm}$ . The three types of curves that can result are shown schematically in Fig. 4-14. In this plot,  $C_f$  is the final, steady-state suspension concentration attained at the end of the transient period, during which the concentration decreases from its initial value. For further illustration, flume data on the deposition of a kaolinite and curves based on the multiclass relation of Mehta and Lott (1987) are shown in Fig. 4-15. The simulations are based on the equation

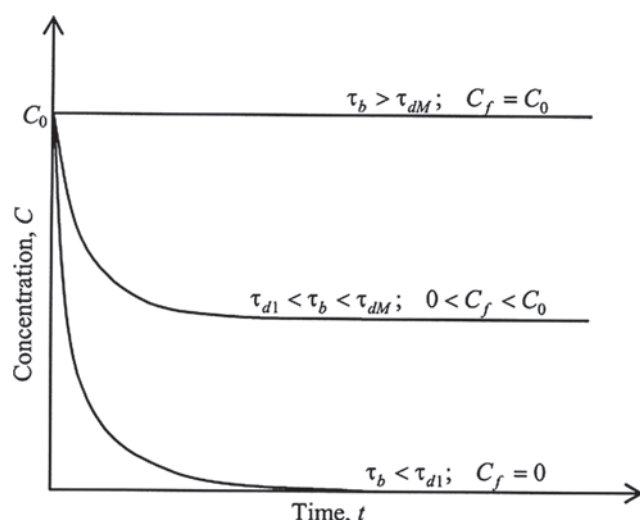


Fig. 4-14. Schematic drawing of concentration-time relationships during multiclass sediment deposition.

$$\frac{C}{C_0} = \frac{1}{C_0} \sum_{i=1}^M C_i = \sum_{i=1}^M \phi(w_{si}) \times \exp \left\{ - \left[ 1 - \frac{\tau_b}{\tau_{dl}} \left( \frac{w_{sl}}{w_{si}} \right)^{\frac{\ln(\tau_{dm}/\tau_{d1})}{\ln(w_{sm}/w_{s1})}} \right] \frac{w_{sl}}{h} t \right\} \quad (4-27)$$

which is subject to the condition  $C_i = C_{0i}$ , the initial concentration for each class  $i$ , for all  $\tau_b \geq \tau_{di}$ , also for each class  $i$ . For a single-size sediment  $M=1$ , and Eq. (4-27) reduces to Eq. (4-25). It must be pointed out that Eq. (4-27) is based on multiclass distribution of floc settling velocity, rather than size. Given the histogram of  $w_{si}$  values obtained from settling velocity tests,  $\phi(w_{si})$  is the frequency of the  $i$ th class and  $w_{s1}$  is the smallest value of the settling velocity in the histogram. For simulation of the curves in Fig. 4-15, the range  $\tau_{d1}$  to  $\tau_{dm}$  was 0.04 to 1 Pa, which is typical in laboratory flumes. The histogram of settling velocity was derived from settling tests conducted with flocculated kaolinite in a settling column (Yeh 1979) and assumed to be applicable to flume conditions. A limitation of this approach is that the settling velocity is assumed to be unaffected by ongoing aggregation. Therefore, in those water bodies in which the flocs are composed of highly cohesive sediment and floc

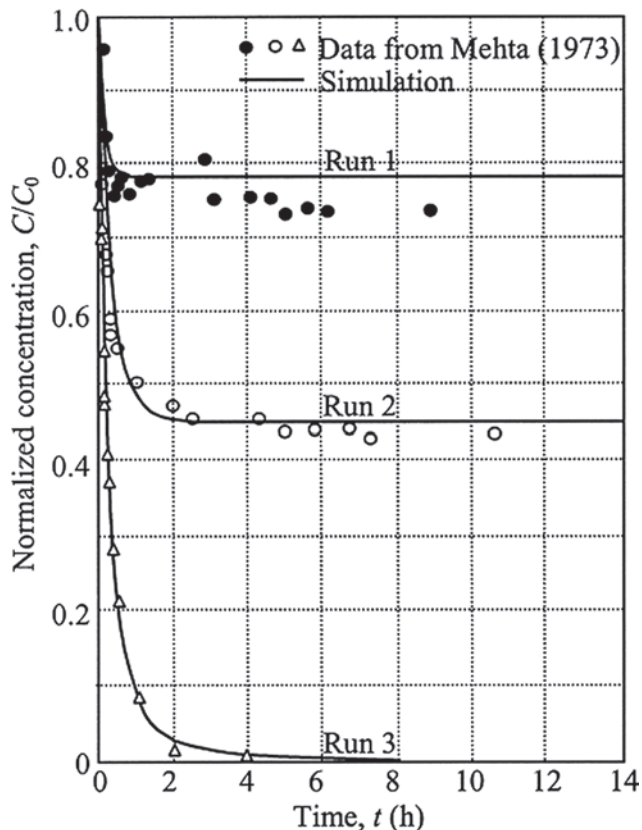


Fig. 4-15. Concentration-time relationships for kaolinite deposition in a flume (after Mehta and Lott 1987).

growth/breakup is strongly influenced by flow shear, Eq. (4-27) as used may lead to errors in the prediction of the time-concentration history. Thus for example, whereas kaolinite, which is weakly cohesive, may be appropriate for (4-27), answers obtained using cohesive mud from the San Francisco Bay must be interpreted carefully (McAnally and Mehta 2000; 2002).

In a depositional environment such as a dead-end or finger canal, or wherever deposition is the dominant process, multiclass simulation enables the prediction of sorting by size (Lau and Krishnappan 1992), which typically manifests as a decrease in grain size with distance from the initial point of deposition (Lin 1986; Lin and Mehta 1997; McAnally 1999). However, in cases where resuspension cannot be ignored, the use of either Eq. (4-24) or (4-26) effectively amounts to a simulation of nonsimultaneous bed sediment exchange when the bed shear stress exceeds the critical stress for deposition. Size sorting also occurs during resuspension, particularly when the sediment is only weakly cohesive, such as a kaolinite, and this leads to a bed armoring effect because larger, especially unaggregated, grains erode less easily than the finer fractions (Teeter et al. 1997). However, since this selective resuspension process is less well understood than multiclass deposition, tracking particles, especially in the presence of ongoing aggregation of suspended matter, becomes cumbersome. To obviate this complexity in process modeling, it is convenient to assume a single size class only and to further consider  $\tau_d$  to be equal to the maximum value of  $\tau_b$  expected to be encountered in the simulation process (Jiang 1999). Then Eq. (4-24) reduces to  $\Psi = -w_s \bar{C}/h$ , which allows deposition to occur at all prevailing shear stresses.

It should be emphasized that (4-24) and (4-26) are based on laboratory data. Their applicability to the field requires a careful interpretation of the relationship between vertical gradients of concentration and their role in influencing the deposition rate. Also, when the total water depth is large, deposition is found to correlate with sediment concentration in the near-bed suspension layer, in contrast to depth-mean concentration, used in Eq. (4-24) and (4-26). Scale effects associated with the structure of turbulence also play a role (Sanford and Chang 1997).

## 4.7 CONSOLIDATION AND GELLING

### 4.7.1 Settling and Consolidation

If a clay mixture in water is allowed to settle, three stages of the settlement process can be identified, as shown schematically in Fig. 4-16 (Schiffman et al. 1985). In the first, flocculation stage, aggregation is important but no significant settling occurs. For some slurries, e.g., those of kaolinite, this stage may be only tens of seconds long, but for a bentonite slurry it may last effectively up to tens of minutes. In the second stage, flocs gradually settle and form a bed

layer, which undergoes what is called primary consolidation and associated dewatering. The initial settling process is complicated by a significant change in the structure of the newly deposited flocs. Krone (1963) conceptualized this change in terms of the aggregate order—when aggregates of order  $n$  deposit they form an initial “fluffier” and weaker layer of aggregates of order  $n + 1$ . When this layer exceeds a thickness on the order of 2.5 cm, overburden crushes the  $n + 1$  order aggregates to  $n$  order aggregates, which are then crushed further by overburden to result in aggregates of order  $n - 1$ ,  $n - 2$ , and so on.

The upper boundary of the settling zone in the second stage, which can generally be defined as a lutocline, drops with time until it meets the rising bed boundary at the onset of the third stage. In this stage, settling is terminated and bed consolidation continues. Accordingly, the bed surface gradually drops until no further consolidation takes place. Whereas the second stage may last from minutes to hours, the third stage can range between hours to days or months. In some case it may take years for full consolidation. During this stage, even after dewatering ends, internal rearrangements of particles may occur under secondary consolidation. It should be noted however, that in a large number of cases involving fresh estuarine deposits, consolidation is practically over in one to two weeks. Because this time scale coincides with the synodic spring-neap tidal cycle, consolidation plays an important role in governing estuarine sediment transport and budget.

The rate of settling, which is typically in the hindered mode, and consolidation are both governed by the rate at which interstitial or pore water escapes the particle matrix. Within the settling zone there is no significant effective normal stress; i.e., the pore water pressure is practically equal to the total hydrostatic pressure. Within the consolidation zone, because a part of the total weight

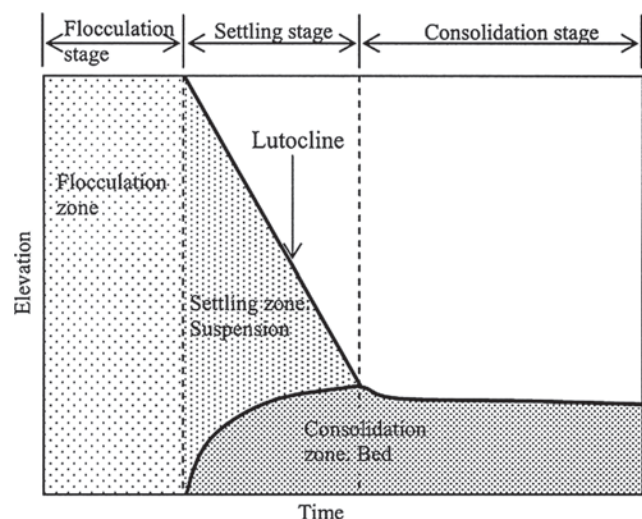


**Fig. 4-16.** Flocculation, settling, and consolidation zones (adapted from Schiffman et al. 1985).

of the slurry is supported by the particle matrix, the pore pressure is less than the total pressure, with the difference, equal to the effective stress, representing the particle-supported load. Figure 4-17a shows an instantaneous density profile within a settling silty clay in an experimental column, 4.75 h after test initiation starting with a uniformly mixed suspension having a density of  $1,090 \text{ kg/m}^3$  (Sills and Elder 1986). The corresponding measured profiles of total pressure (i.e., normal stress) and pore pressure are shown in Fig. 4-17b. The elevation separating the settling suspension (without effective stress) from the consolidating bed (with effective stress) is practically at 60 cm, close to the level of the lutocline at that point in time.

The settling behavior can be analyzed through the sediment continuity equation in the vertical direction, which yields the time-variation of the lutocline as it settles, and also the associated density profile within the suspension. Consolidation of soils in general has been simulated with non-linear, finite strain models (Gibson et al. 1967; 1981). For the estuarine environment, models for self-weight consolidation, i.e., settling due to the weight of the deposit itself, have been developed through linearized analytic solutions (e.g., Been and Sills 1981; Govindaraju et al. 1999) and nonlinear numerical solutions (e.g., Papanicolaou and Diplas 1999). Interest with respect to fine sediment transport is in tracking the change in the density of deposit, because both the bed shear strength and the mass of material eroded per unit time depend on density. Change in bottom elevation due to consolidation is usually of lesser interest, inasmuch as generally it is only a small fraction of the total water depth.

With regard to density determination during consolidation, the commonly used correlations between density and bed shear strength are empirical and inherently approximate. As a result the calculation of rate of erosion, which depends on the shear strength, is also approximate. Thus it often suffices to calculate the density to first-order accuracy. For this requirement, it is useful to consider simple approaches to track density though (hindered) settling and consolidation combined. Such approaches rely on the physical similarities between these two processes (e.g., Schiffman et al. 1985).

Following the continuity approach of Kynch (1952), and accounting for the accumulation or depletion of bed deposit by deposition or erosion, respectively, the sediment continuity equation can be written as

$$\frac{\partial h' C}{\partial t} = \frac{\partial w_{sc} C}{\partial z'} + q \quad (4-28)$$

where

$h'$  = thickness of the consolidating layer;

$w_{sc}$  = velocity or rate of consolidation;

$z' = z / h'$ ;

$z$  = vertical coordinate originating at the bottom and positive upward; and

$q$  = net settling flux (i.e., deposition less erosion) of sediment mass at the top of the consolidating layer (Jiang 1999).

In general, two modes of consolidation can be recognized from the plot of consolidation rate against concentration,

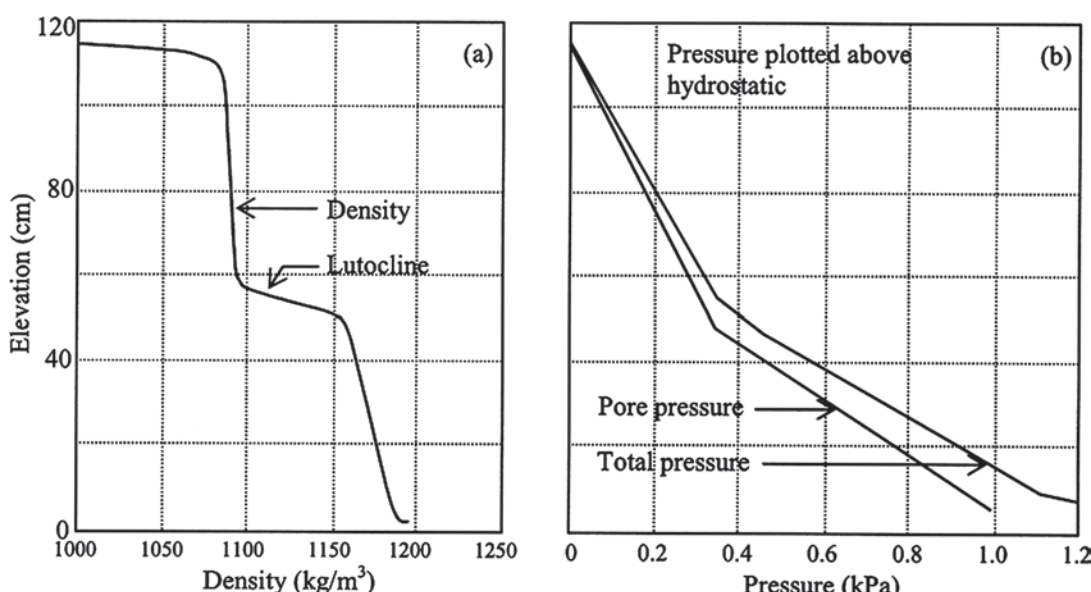


Fig. 4-17. (a) Instantaneous density profile during settling of a silty clay in tap water; (b) corresponding total and pore pressure profiles (adapted from Sills and Elder 1986).

**Table 4-9 Compilation of Parameters for (4-29)**

Reference(s)	Sediment source	$w_{sc1}$ (m/s)	$C_{s1}$ (kg/m <sup>3</sup> )	$w_{sc2}$ (m/s)	$C_{s2}$ (kg/m <sup>3</sup> )	$C_t$ (kg/m <sup>3</sup> )	$m_t$	$n_t$
Burt and Parker (1984); Jiang (1999)	Estuarine mud, UK	— <sup>a</sup>	— <sup>a</sup>	$4.2 \times 10^{-6}$	680	15	6.0	15
Toorman and Berlamont (1993)	Doel Dock, Belgium	$5.0 \times 10^{-4}$	20	$7.0 \times 10^{-6}$	205	160	3.0	13
Jiang (1999)	Jiaojiang estuary, China	$1.0 \times 10^{-4}$	31	$6.0 \times 10^{-6}$	350	210	4.5	15
Marván (2001)	Ortega River, Florida	$6.0 \times 10^{-5}$	15	$3.0 \times 10^{-6}$	1000	83	5.5	18

<sup>a</sup>First mode absent.

namely loose soil consolidation and compact soil consolidation. For these two modes, Toorman and Berlamont (1993) developed a combined relationship of the form

$$w_{sc} = w_{sc1} \exp\left(-\frac{C}{C_{s1}}\right) F_t + w_{sc2} \left(1 - \frac{C}{C_{s2}}\right)^{m_t} (1 - F_t); \quad (4-29)$$

$$F_t = \exp\left[-\left(\frac{C}{C_t}\right)^{n_t}\right]$$

where

$F_t$  = characteristic mode transition (from loose soil to compact soil) function with  $n_t > 10$ ;  
 $m_t$  = sediment-dependent constant;  
 $C_t$  = mode transition concentration;

$w_{sc1}, w_{sc2}$  = rates of consolidation for the first and the second modes, respectively;

$C_{s1}$  = concentration corresponding to the maximum settling flux; and

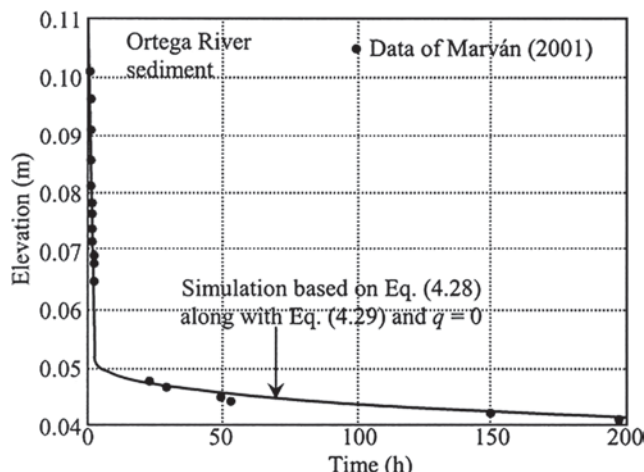
$C_{s2}$  = saturation concentration, i.e., maximum attainable compaction concentration.

Table 4-9 gives representative values of these coefficients. Data points for sediment from the Ortega River in Florida (Marván 2001) are shown in Fig. 4-18 along with a comparison with Eq. (4-28) assuming  $q=0$ , Eq. (4-29), and the corresponding coefficients from Table 4-9. Note that in addition to Eq. (4-28) the equation of conservation of total mass is needed to solve for  $h'$  and  $C$  (Jiang 1999). In Fig. 4-18 both the data and computations start with a uniformly mixed suspension of constant concentration (38.7 kg/m<sup>3</sup>). Observe the two identifiable (initially rapid, then slow) trends in the rate of fall of the bed deposit elevation. It can be shown that whereas the initial consolidation time is inversely proportional to the thickness of the deposit, subsequently this time becomes inversely proportional to the square of the bed thickness (Toorman 1996; Winterwerp 1999).

#### 4.7.2 Gelling

Clayey muds exhibit various degrees of thixotropy depending on composition. Thixotropy is an isothermal, reversible, time-dependent process occurring under conditions of constant composition and volume, whereby a material stiffens, or gels, while at rest and softens or liquefies upon remolding (Mitchell 1993). Once mud gels it is harder to erode than when it is remolded.

Day and Ripple (1966) showed that a bed of kaolinite in water practically lost its strength upon shearing, but the strength was recovered in about a day. This process is schematized in Fig. 4-19, in which  $S_p$  is the peak undisturbed strength and  $S_R$  is the remolded strength. These values can be determined from the unconfined compression test, or



**Fig. 4-18.** Settling consolidation of sediment from the Ortega River, Florida.

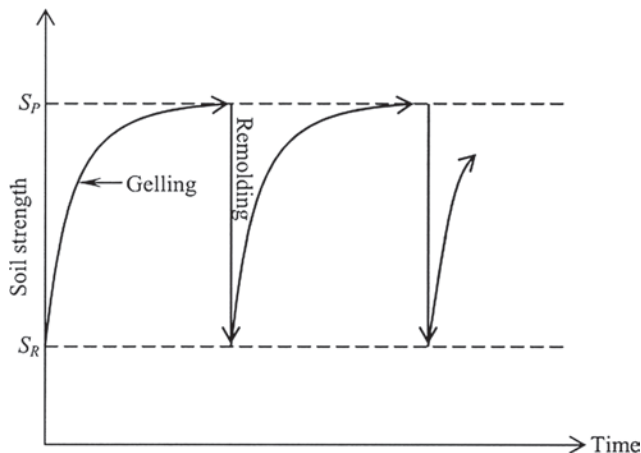


**Fig. 4-19.** Schematic drawing of changes in soil strength due to repeated cycles of gelling and remolding (based on Mitchell, 1976).

vane shear test, for low strength soils (Lambe and Whitman 1969). A measure of the gelling effect is the sensitivity,  $S_t = S_p/S_R$ . Accordingly,  $S_t = 1$  implies no sensitivity, and 4 to 5 is considered very sensitive (Mitchell 1976). Gelling occurs because water molecules within the pore fluid and close to the clay surface form a “solid” layered structure through hydrogen bonding. When the sample is disturbed this structure collapses and water molecules are randomized. Gelling therefore can be detected through changes in the pore water pressure. Starting with a disturbed sample, as the material gels the pore water pressure drops with increasing ordering of water molecules. A tensiometer is commonly employed to record these changes (Kirkham and Powers 1972).

## 4.8 EROSION

### 4.8.1 Modes of Erosion

The four modes of erosion mentioned in Section 4.3.2 are surface erosion, mass erosion, fluid mud generation, and fluid mud entrainment. Note that generation of fluid mud is considered to be erosion because in this process there is a phase change from a bed to a suspension. This fourfold classification of erosion is meant mainly to understand and treat a very complex set of mechanisms through simplified analytic and empirical treatments. These treatments are considered in what follows.

### 4.8.2 Surface Erosion

Modeling surface erosion continues to pose problems, largely due to a lack of basic understanding of the way in which

the bed-water interface responds to flow-induced stress. For steady or quasi-steady (e.g., tidal) flows, numerous formulas relating the rate of bed surface erosion to the bed shear stress have been proposed. In this mode of erosion, particles or flocs at the bed surface are detached and entrained, thus causing bed scour. Some of the early formulas have been summarized by Mehta et al. (1982). Subsequent developments may be found in, among others, Jepsen et al. (1997); Piedra-Cueva and Mory (2001); and Taki (2001). These formulas are generally applicable to cases of low to moderate suspended sediment concentrations, up to about  $C_2$  in Fig. 4-12. At high concentrations settling of eroded sediment is hindered, and a layer of fluid mud is formed over the bed. The mechanism by which this layer erodes is not modeled well by simple, stress-based formulations used for surface erosion. Furthermore, damping of turbulence within fluid mud alters the bed shear stress from its value under clear or nearly clear water conditions. In that regard, Bedford et al. (1987) showed that, at least in the context of their experiments in Long Island Sound, the turbulent kinetic energy proved to be better correlated with resuspension than the Reynolds stress.

Following the stochastic theory of Einstein (1950) for coarse grain transport, and considering erosion to occur in the absence of deposition, Partheniades (1962; 1965) developed a phenomenological formula relating the rate of erosion to the bed shear stress. This formula and the flume data on mud erosion with which the formula was compared showed a nonlinear relationship between erosion rate and bed shear stress. Subsequently, Ariathurai (1974) assumed a straight line approximating the nonlinear relation, and attributed the resulting linearized formula to Partheniades (1962). This linear “Ariathurai-Partheniades” formula, which was essentially empirical, led to the expression, investigated extensively by Kandiah (1974),

$$\epsilon = \epsilon_M \left( \frac{\tau_b - \tau_s}{\tau_s} \right) \quad (4-30)$$

in which

$\epsilon$  = erosion rate or mass flux (mass eroded per unit bed area per unit time);

$\tau_b$  = bed shear stress;

$\tau_s$  = bed shear strength with respect to erosion; and

$\epsilon_M$  = the erosion rate constant, the value of  $\epsilon$  when

$$\tau_b = 2\tau_s$$

Equation (4-30) is characteristically applicable to homogeneous beds of uniform (i.e., nonstratified) density and indicates that  $\epsilon$  varies with the excess shear stress  $\tau_b - \tau_s$ . Thus, a plot of  $\epsilon$  versus  $\tau_b - \tau_s$  ideally appears as a straight line as illustrated in Fig. 4-20, in which the erosion rate and the shear strength (determined by the intercept of a given line with the horizontal axis) are seen to depend on the percentage (by weight) of montmorillonite in a mixture of this clay with Yolo loam from California. Also observe that the effect of the highly cohesive montmorillonite was to decrease the

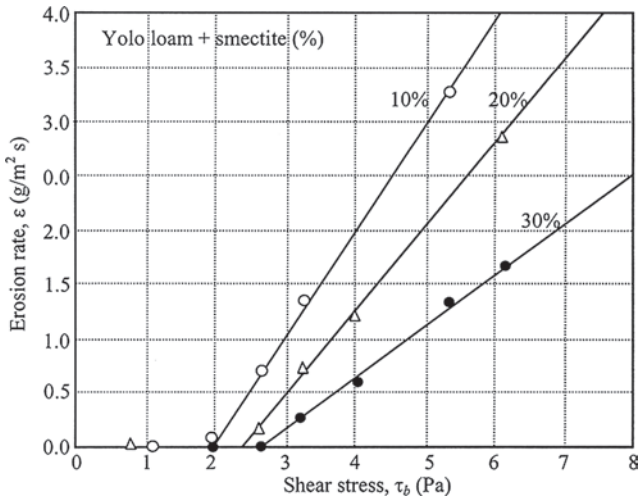


Fig. 4-20. Erosion rate versus bed shear stress for mixtures of Yolo loam and montmorillonite. Percent indicates montmorillonite by weight (adapted from Kandiah 1974).

line slope due to an increase in the shear strength of the mixture.

For beds that are stratified with respect to density and shear strength, formulas that account for the variation in  $\tau_s$  with depth have been developed, e.g., by Parchure (1984) and Piedra-Cueva and Mory (2001). Although such formulas differ from (4-30), in most of them the erosion rate varies with the excess shear stress. This similarity, as well as experience from modeling applications, suggests that (4-30) can also be used for stratified beds with a reasonable degree of accuracy by allowing  $\tau_s$  to vary with depth, i.e., by replacing  $\tau_s$  by  $\tau_s(z)$ , where  $z$  denotes the vertical coordinate (Ariathurai et al. 1977; Hayter 1983).

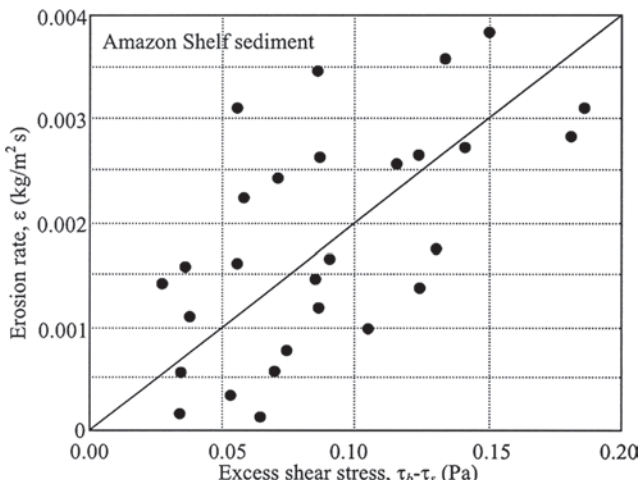


Fig. 4-21. Erosion rate versus excess shear stress based on the analysis of Vinzon (1998) using data from Kineke (1993).

Vinzon (1998) used measured time series of near-bed velocities and suspended sediment concentrations at sites on the Amazon shelf off Brazil reported by Kineke (1993) to develop the linear plot shown in Fig. 4-21. The observed relationship is akin to the lines in Fig. 4-20 and therefore conforms to Eq. (4-30), but with a considerably greater degree of data scatter. Similar plots have been developed by, among others, Sanford et al. (1991) and Sanford and Halka (1993) using data from the Chesapeake Bay.

#### 4.8.3 Shear Strength

Although bed shear strength and bed density are neither uniquely interrelated nor are dimensionally homogeneous, efforts have been made to correlate these two parameters empirically, recognizing that, in general, the denser the soil the harder it is to erode. Thus, given  $\tau_{sh}$  as a measure of soil shear strength, relationships have been developed of the general form (Table 4-10)

$$\tau_{sh} = \zeta_s (\phi - \phi_e)^{\xi_s} \quad (4-31)$$

where

$\phi$  = solids volume fraction;

$\phi_e$  = limiting or minimum value of  $\phi$  below which

$\tau_{sh}=0$ ; and

$\zeta_s, \xi_s$  = sediment-specific coefficients.

Thus, according to Eq. (4-31),  $\tau_{sh}$  depends on the excess solids volume fraction,  $\phi - \phi_e$ . Measures of shear strength in general include the apparent Bingham yield strength ( $\tau_y$ ), the vane shear strength ( $\tau_v$ ) and the surface erosion shear strength ( $\tau_s$ ). Among these,  $\tau_y$  and  $\tau_v$  are representative of the bulk physical properties of the soil. As noted in Section 4.2.2,  $\tau_y$  is associated with soil rheology, and has been used, for example, to determine the bottom slope required to generate mud underflows (Mei and Liu 1987). Wotherspoon and Ashley (1992) correlated  $\tau_y$  to the liquid content of sewer sediment deposit. The quantity  $\tau_y$  is a measure of the bulk strength of the soil and has been used in geotechnical evaluations of cohesive soil consistency. Thus, for example, Annandale (1995) has suggested the classification given in Table 4-11.

Most studies on the erosion of submerged soils in the estuarine and marine environments are limited to "very soft" to "soft" cohesive materials identified in Table 4-11. This is because wave- and current-induced bed shear stresses in these environments are usually not large enough to erode stiffer soils. On the other hand, in rivers with high flow velocities, even firm soils can erode significantly over months and years (Jiang 1999). Thus, the vane shear strength is a convenient parameter commonly used to assess the erosion potential of cohesive soils in a given flow environment, even though it is not a highly accurate measure (Lee 1985).

**Table 4-10 Expressions Relating Shear Strength to Solid Volume Fraction**

Investigator(s)	Sediment	Shear strength, $\tau_{sh}$ (Pa)	$\phi_\ell^a$	$\zeta_s$	$\xi_s$	$\phi$ range <sup>a</sup>
Krone (1963)	Estuary muds	Apparent Bingham yield ( $\tau_y$ )	— <sup>b</sup>	466	2.55	0.008–0.57
Migniot (1968)	Marine muds	Apparent Bingham yield ( $\tau_y$ )	—	Variable	4.00	0.094–0.19
Owen (1970)	Estuary mud	Apparent Bingham yield ( $\tau_y$ )	—	1110	2.33	0.042–0.11
Vinzon (1998)	Shelf mud	Apparent Bingham yield ( $\tau_y$ )	—	2024	2.62	0.021–0.19
Hwang (1989)	Lake mud	Vane ( $\tau_v$ )	0.06	22.6	1.00	0.060–0.26
Thorn and Parsons (1980)	Estuary muds	Surface erosion ( $\tau_s$ )	—	37.5	2.28	0.014–0.12
Kusuda et al. (1984)	Estuary mud	Surface erosion ( $\tau_s$ )	—	6.50	1.60	0.032–0.11
Villaret and Paulic (1986)	Bay mud	Surface erosion ( $\tau_s$ )	—	1.65	1.00	0.10–0.38
Black (1991)	Estuary mud	Surface erosion ( $\tau_s$ )	—	1.88	2.30	0.13–0.25
Berlamont et al. (1993)	Marine muds	Surface erosion ( $\tau_s$ )	—	5.41	0.90	0.02–0.07

<sup>a</sup>Use  $\rho_s = 2,650 \text{ kg/m}^3$  to convert  $\phi (=C/\rho_s)$  to dry density or concentration  $C$ , except for the relationship of Hwang (1989) for which  $\rho_s = 2,140 \text{ kg/m}^3$ .

<sup>b</sup>Not determined.

Source: Mehta and Parchure (2000).

**Table 4-11 Soil Consistency Classification Based on Vane Shear Strength**

Soil consistency	Identification	Vane shear strength (kPa)
Very soft	Easily molded by fingers	0–80
Soft	Molded by fingers with some pressure	80–140
Firm	Very difficult to mold; can be penetrated by a hand-spade	140–210
Stiff	Requires a hand pick for excavation	210–350
Very stiff	Requires a power tool for excavation	350–750

Source: Annandale (1995).

In contrast to  $\tau_y$  and  $\tau_v$ , the parameter  $\tau_s$ , which occurs in Eq. (4-30), is related to the strength of surface flocs. Referring to the results in Table 4-10, the characteristic difference between  $\tau_y$  and  $\tau_s$  is reflected in the value of the proportionality coefficient  $\zeta_s$ , which is considerably higher for  $\tau_y$  (mean  $\zeta_s = 1,200$ , excluding the data of Migniot 1968) than for  $\tau_s$  (mean  $\zeta_s = 10.6$ ). Likewise, the exponent  $\xi_s$  is higher for  $\tau_y$  (mean value 2.88) than for  $\tau_s$  (mean value 1.62). With respect to the sole correlation for  $\tau_v$ , observe that  $\xi_s = 1$ . It should be noted that this relationship of Hwang (1989) was developed for a lacustrine mud that contained a high amount (40% by weight) of organic material.

Conceptually the minimum value of  $\phi$ , namely  $\phi_p$ , is analogous to the space-filling volume fraction at which the particle matrix begins to exhibit a measurable shear modulus of elasticity, which increases with increasing  $\phi (> \phi_p)$  (James et al. 1988). The same threshold condition, sometimes referred to as the “gelling point,” may apply to the development of

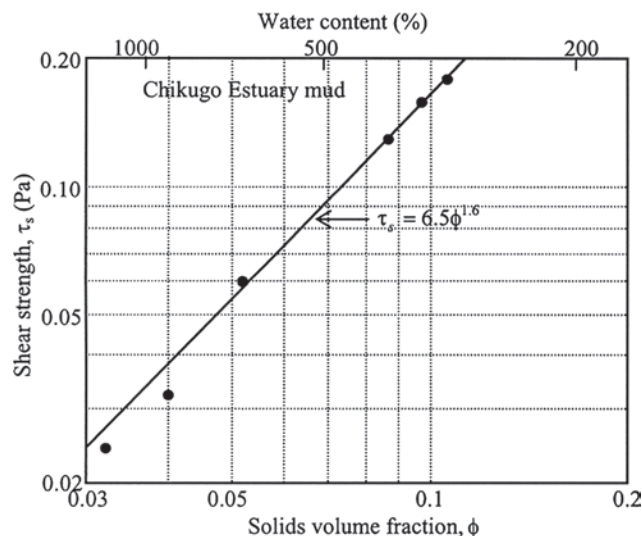


**Fig. 4-22.** Bed shear stress versus solids volume fraction and water content for Chikugo estuary (Japan) mud (after Kusuda et al. 1985).

normal effective stress in the soil (Ross 1988). Hwang (1989) determined that  $\phi_e = 0.06$  from a plot of measured  $\tau_v$  versus  $\phi$  by extrapolating the linear relationship ( $\xi_s = 1$ ) to  $\tau_v = 0$  when  $\phi = \phi_e$ . He further showed that this value of  $\phi_e$  ( $= 0.06$ ) was commensurate with the density below which the mud was in a fluid-like state, and was therefore devoid of measurable strength. As seen from Table 4-10, other investigators did not report  $\phi_e$ , and therefore only limited use can be made of this parameter at present. An example of data conforming to (4-31) but without a knowledge of  $\phi_e$  is shown in Fig. 4-22, based on the work of Kusuda et al. (1985) on mud from the Chikugo River estuary in Japan.

Two factors on which  $\zeta_s$ ,  $\xi_s$ , and  $\phi_e$  can be expected to depend are bed sediment composition and fluid chemistry. This dependence is reflected in the variability in the values of  $\zeta_s$  and  $\xi_s$  associated with  $\tau_s$  in Table 4-10. The relative importance of composition and chemistry cannot be separated easily in these cases, because the shear strength of a given soil can be significantly influenced by even minor changes in the chemical composition of pore water (Ravisangar et al. 2001). Furthermore, even though salinity is reported in many investigations on estuarine and marine muds, other chemical factors can also affect the soil fabric, thereby influencing soil erodibility. For example, Fig. 4-23 shows the results of Kandiah (1974) for a montmorillonite based on measurements of the sodium adsorption ratio (SAR). This ratio of sodium ions ( $\text{Na}^+$ ) to the sum of calcium ( $\text{Ca}^{++}$ ) and magnesium ions ( $\text{Mg}^{++}$ ) in the bed pore fluid is defined as

$$\text{SAR} = \frac{\text{Na}^+}{[0.5(\text{Ca}^{++} + \text{Mg}^{++})]^{1/2}} \quad (4-32)$$

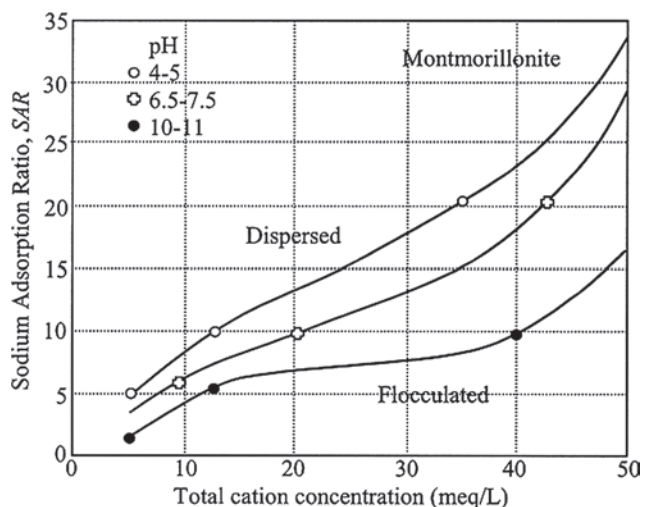


**Fig. 4-23.** Flocculation-dispersion boundary curves for a montmorillonite at three pH ranges (adapted from Kandiah 1974).

where the ionic concentrations are measured in milliequivalents per liter. Figure 4-23 shows that this montmorillonite could be altered between dispersed (i.e., nonflocculated) and flocculated states merely by changing the pH of the pore fluid, either holding SAR constant or holding constant the total cation concentration in the pore fluid. Since a dispersed clay bed can erode with considerably greater ease than a flocculated bed of the same clay, Fig. 4-23 demonstrates that sediment composition alone cannot be a unique, or even dominant, determinant of bed erosion potential. This consideration underscores the need to use native water in laboratory erosion tests, or to reconstitute the eroding fluid based on an analysis of the native water with regard to its ionic composition. It is also a reason for in situ testing of bed erodibility in the prototype environment (Maa et al. 1993).

Inasmuch as  $\tau_s$  is a measure of the strength of flocs at the bed surface, it reflects the order of aggregation of these surface flocs. In a bed prepared by allowing suspended sediment to deposit, the bed density characteristically increases with depth due to sorting and consolidation. The rate of increase is usually the highest just below the surface and gradually decreases with depth until the overburden is no longer sufficient to cause further consolidation. In the estuarine environment, beds formed by deposition in this way tend to increase in density until they reach ~1,300 to ~1,400 kg/m<sup>3</sup> at depths on the order of 20–60 cm. Increasing density with depth decreases the order of aggregation and increases the shear strength.

The trend of increasing shear strength with depth is seen in Fig. 4-24, in which shear strength profiles are given for the same bed of flocculated kaolinite in salt water, but after different periods of consolidation (Parchure 1984). The shear strength at a given consolidation period  $T_{dc}$  was determined by eroding the bed layer by layer. This procedure,

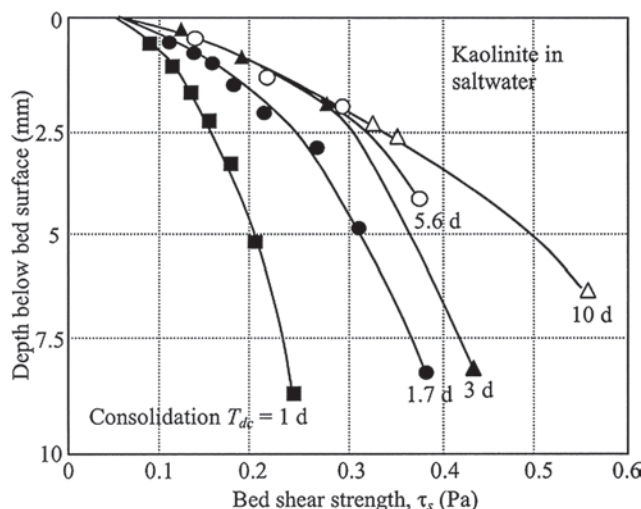


**Fig. 4-24.** Bed shear strength profiles for a bed of kaolinite in salt water (adapted from Parchure 1984).

credited to Thorn and Parsons (1980), was accomplished by increasing the flow-induced bed shear stress in steps, allowing the test to run at each step for a sufficiently long duration to cause bed scour to proceed to a depth at which no further erosion took place, because the shear stress at that depth was equal to the shear strength. In this way, the profile of strength variation with depth was constructed by knowing the applied stress at each depth. In Fig. 4-24 observe that because the aggregate order did not change at the surface due to the absence of overburden, the shear strength remained independent of the period of consolidation. Such a finding was also reported previously by Partheniades (1965), who correctly pointed out that this independence means that erosion occurs by breakup of inter particle bonds, and hence that this breakup process cannot be parameterized by such bulk soil indices as the

Atterberg indices. Beneath the surface however, increasing shear strength reflects increasing floc strength with decreasing aggregate order. Recognizing that the time-variation of erosion rate depends on the shear strength profile, which in turn depends on the density profile, Jepsen et al. (1997) correlated the erosion rate directly with bed density.

When inorganic fine sediment is mixed with other materials, the effect on shear strength can be significant (Ashley and Verbanck 1996). Two common cases of interest are mixtures of mineral particles with organic material and with sand. In Table 4-12, shear strength parameters of Eq. (4-31) from three studies are summarized (Mehta and Parchure 2000; Marván et al. 2002). In all cases the experiments were conducted in the laboratory using muds from water bodies in Florida. These bodies receive organic sediments from a variety of terrigenous and aqueous sources. Observe that the exponent  $\xi_s$  is 0.83 for sediment from the Ortega River with 28% (by weight) organic matter. This value may be compared with the mean value of 1.62 from Table 4-10 for largely inorganic sediment beds. The organic-rich samples from the Rodman Reservoir (45% organic content) and the Lower Kissimmee River basin (50% organic content) showed practically no dependence ( $\xi_s=0$ ) of shear strength on density. Furthermore, these samples had very low shear strengths, on the order of 0.1 Pa.

The usually (but not always; see, e.g., Dennett et al. 1998) high erosion potential of organic-rich sediments is due to the comparatively light and weakly bound nature of the flocs or floccules. The lack of significant dependence of erosion on bed density may be explained as follows. Unlike clayey beds whose interface with water can be reasonably well defined, especially for dense beds, the organic-rich bed-water interface tends to develop a layer of “fluff” consisting of flocs released by way of elastic rebound from the bed with a thickness of a few floc diameters. Due to its low excess density, this fluff layer does not consolidate easily. Thus when fluid stress is applied, it is this layer of weakly interconnected particles,

**Table 4-12 Shear Strength Parameters for Organic-Rich Sediments**

Location	Organic fraction by weight (%)	Mixture granular density, $\rho_s$ (kg/m <sup>3</sup> )	$\phi_e$	$\zeta_s$	$\xi_s$	$\phi$ range
Ortega River, Florida	28	2,032	NN. D. <sup>a</sup>	1.1	0.83	0.06 – 0.07
Lake Okeechobee, Florida	40	2,140	00.06	1.0	0.2	0.06 – 0.17
Rodman Reservoir, Florida	45	1,914	NN. D.	0.105	0	0.02 – 0.28
Lower Kissimmee River basin, Florida	50	1,586	NN. D.	0.099	0	0.08 – 0.38

<sup>a</sup>Not determined.

Sources: Mehta and Parchure (2000); Marván et al. (2002).

with a low negative buoyancy, that is entrained. Further, as the layer erodes it is replenished by continual “release” of flocs from within the bed that is disturbed by flow-induced deformations. As a result, since the density of the fluff layer is determined by the released flocs rather than the bed, the shear strength is largely unaffected by bed density.

#### 4.8.4 Shear Strength of Fine/Coarse Sediment Mixtures

Fine sediment and sand can occur as interbedded layers alternating between fine- and coarse-grain layers (Jaeger and Nittrouer 1995), or as more homogenous mixtures. In general, bed stratigraphy reflects the depositional history of the accumulated sediment, and any subsequent changes brought about by physicochemical transformations and biogenic effects. Among the latter, bioturbation usually enhances homogeneity and causes the bed to become less resistant to erosion (Jaeger and Nittrouer 1999). In turn, coring data that show intact laminated structures may imply the absence of bioturbation (Kirby et al. 1994).

In a nonstratified bed composed of a mixture of sand and fine sediment, the shear strength may vary in a nonlinear way with the proportion of fine fraction. In order to demonstrate this effect, Torfs et al. (2001) derived the following expression for the critical shear stress of the homogeneous mixture:

$$\tau_{cm} = \left[ \frac{\alpha_{1cg} \tan \Phi_{cg}}{(\alpha_{1cg} + \alpha_{2cg} \tan \Phi_{cg})} + \frac{K' \zeta_s (\Phi_v - \Phi_{vc})}{g (\rho_{sm} - \rho) d_m} \right] \times g (\rho_{sm} - \rho) d_m \quad (4-33)$$

where  $\alpha_{1cg}$ ,  $\alpha_{2cg}$ ,  $\alpha_{3cg}$ ,  $\phi_{cg}$ , and  $K'$  are sediment-specific constants,  $\zeta_s$  and  $\xi_s$  are defined per (4-31), and

$\rho_{sm}$  = representative granular density of the mixture;

$\rho$  = fluid density;

$\phi_v$  = solids volume fraction of the fine sediment-water mixture before it is mixed with sand;

$\phi_{vc}$  = value of  $\phi$  below which the bed has practically no shear strength;

$g$  = acceleration due to gravity; and

$d_m$  = representative mixture diameter.

Torfs et al. have provided the necessary equations for the selection and calculation of these parameters.

In Fig. 4-25,  $\tau_{cm}$  is plotted against the fine sediment weight fraction of the mixture,  $\psi$ . The dependence of  $\tau_{cm}$  on  $\psi$  is embodied in the empirical relations  $K' = 60|\psi - 0.018|^{1.9} - 0.029$  for  $\psi \leq 0.018$  and  $K' = 0.88 - (1 - \psi)^{3.5}$  for  $\psi > 0.018$ . The comparison between (4-33) and the data of Torfs (1995) is wholly diagnostic, because these relations, as well as parameters in (4-33), were derived from the experimental data included in the figure. These data, obtained in a laboratory flume, were on the erodibility of mixtures of a

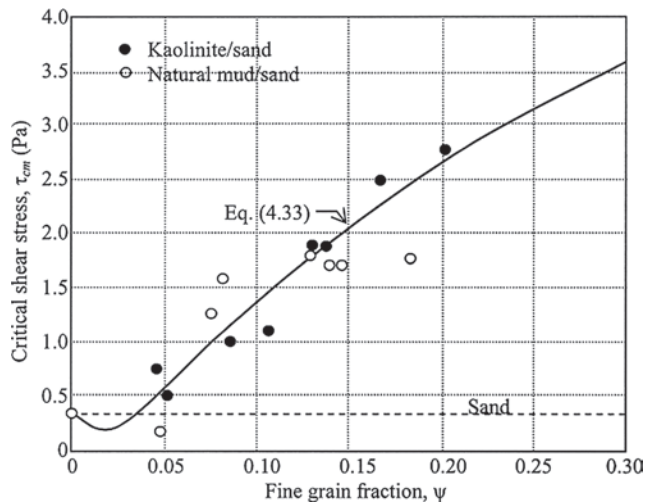
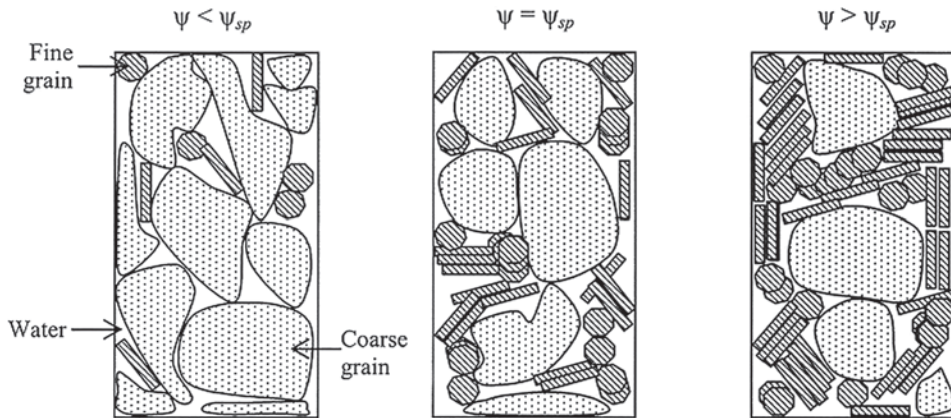


Fig. 4-25. Critical shear stress for erosion of kaolinite/sand and natural mud/sand mixtures versus fine-grain weight fraction: data points of Torfs (1995) and curve based on (4-33) (after Torfs et al. 2001).

kaolinite with 0.23 mm diameter sand and, also, mixtures of a natural mud with the same sand. Starting with  $\psi=0$  corresponding to pure sand (at a nominal bulk density of 1,850 kg/m<sup>3</sup>), the fine fraction was increased without changing the mixture bulk density, up to a maximum value of  $\psi=0.38$ . The variation of  $\tau_{cm}$  with  $\psi$  is observed to be nonmonotonic and seemingly passes through a minimum, yielding values of  $\tau_{cm}$  that may at first be lower than those for sand (0.35 Pa), then increase to values larger than for sand, and increase further with increasing  $\psi$ . Notwithstanding the fact that this description is constrained by the paucity of data, and by possible albeit unquantified uncertainties in the estimates of the bed shear stress (Torfs 1995), it can be elaborated upon as follows.

Referring to Fig. 4-26, when a small quantity of fines is added to sand, a reduction in the intergranular friction between sand particles due to partial filling of pore spaces by the fines causes sand grains to erode with greater ease than in the absence of fines, thus lowering the critical stress for erosion below that for pure sand. This effect increases with increasing fine fraction until an interconnected, “space-filling” network of fines is established, when the threshold of motion becomes minimum. Given this condition, any further increase in the fine fraction causes the bed surface to be increasingly influenced by the fines. This is so because as clayey particles increasingly surround sand grains, sand-sand contacts decrease and also, the number of sand grains per unit surface area of bed decreases. Finally, as the fine fraction approaches unity, one can expect  $\tau_{cm}$  to approach  $\tau_s$ , the bed shear strength of the fine sediment (Panagiotopoulos et al. 1997).



**Fig. 4-26.** Schematic drawings of a saturated bed composed of large and small grain populations. Left: small grain fraction is less than space-filling; center: small grain fraction is space-filling; right: small grain fraction exceeds space-filling value (after Torfs et al. 2001).

#### 4.8.5 Erosion Rate Constant

The erosion rate constant  $\epsilon_M$  in (4-30) generally depends on the same factors that influence  $\tau_s$ . A noteworthy effect studied in the laboratory is the variation of  $\epsilon_M$  with fluid temperature. In that regard, surface erosion of cohesive beds has been treated as a mechanism that is phenomenologically akin to the rate process theory for chemical reactions (Paaswell 1973). Conceptually, erosion occurs when a threshold “energy of activation” is exceeded, and interparticle electrochemical bonds are broken. Following this concept it can be shown that  $\epsilon_M$ , and hence the rate of erosion  $\epsilon$ , increases with increasing temperature in such a way that  $\log(\epsilon/T)$  varies linearly with  $1/T$ , where  $T$  is the absolute temperature. This behavior can be represented by

$$\frac{\epsilon}{T} = \exp\left(\Delta - \frac{\Lambda}{T}\right) \quad (4-34)$$

Equation (4-34) was shown by Kelly and Gularce (1981) to hold for the erosion of a bed of grondite, with  $\Delta = 34.7$  and  $\Lambda = 10,145$ . These coefficients are specific to the sediment-fluid mixture used and were obtained at a constant eroding flow velocity of 0.18 m/s. Their magnitudes conform to the units of  $\epsilon$  in  $\text{g/m}^2 \text{s}$  and  $T$  in K. In general, these coefficients can be expected to depend on the physicochemical properties of the sediment and fluid, on the solids weight fraction  $\phi$  and, especially with respect to  $\Delta$ , on the applied bed shear stress. As Lau (1994) indicated, an increase in temperature only marginally affects the van der Waals attractive force at the particle surface, but the interparticle repulsive force increases significantly. As a result, particle-particle bonds rupture more easily at higher temperatures, thereby leading to enhanced erosion.

Based on the observation that the rate of erosion decreases as the shear strength increases, Arulanandan et al. (1980) defined another erosion rate constant  $\epsilon_N = \epsilon_M/\tau_s$ , and plotted it against  $\tau_s$  derived from erosion tests on a large number of

soil samples. Introducing this modified rate constant conveniently redefines (4-30) in terms of  $\epsilon_N$  and  $\tau_s$  as

$$\epsilon = \epsilon_N (\tau_b - \tau_s) \quad (4-35)$$

It was found that, notwithstanding data scatter, in the mean  $\epsilon_N$  decreased monotonically and exponentially with increasing  $\tau_s$ . Compilation of laboratory data from numerous studies in addition to those of Arulanandan et al. (1980), when examined collectively, suggests that the empirical relationship between  $\epsilon_N$  and  $\tau_s$  may be extended to include data grouped by sediment and fluid composition. Despite the evidently approximate nature of the resulting curves relating  $\epsilon_N$  to  $\tau_s$ , this approach affords a crude means to calculate the erosion rate from (4-30) knowing the bed density, inasmuch as the shear strength is related to density via (4-31). Accordingly, the plot shown in Fig. 4-27 was prepared based on the relationship

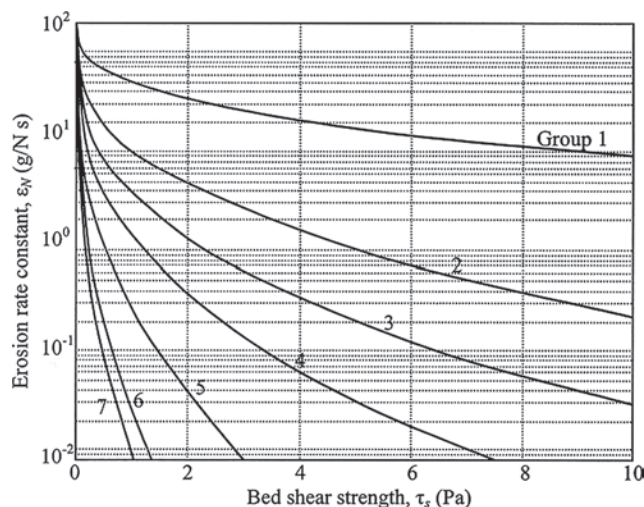


**Fig. 4-27.** Erosion rate constant  $\epsilon_N$  versus bed shear strength  $\tau_s$  for different bed groups identified in Table 4-13. (after Mehta and Parchure 2000).

**Table 4-13 Coefficients for (4-36) and Properties of Groups 1–7**

Group no.	Coefficients in (4-36) <sup>a</sup>		Clay content (%)	Cation exchange capacity (meq/100 g)
	$\chi_s$	$\lambda_s$		
1	1.345	0.368	24	13
2	2.892	0.372	27	18
3	3.905	0.356	28	15
4	4.938	0.355	23	15
5	6.594	0.382	27	15
6	9.011	0.386	33	16
7	10.582	0.252	19	23

<sup>a</sup>These values of  $\chi_s$  and  $\lambda_s$  apply when  $\tau_s$  is in Pa and  $\epsilon_N$  is in g/N s.

Source: Mehta and Parchure (2000).

$$\epsilon_N = \epsilon_{N0} \exp(-\chi_s \tau_s^{\lambda_s}) \quad (4-36)$$

for which the value of  $\epsilon_{N0}$  was conveniently chosen as 200 g/N s. Mehta and Parchure (2000) provide actual fits of (4-36) with data within each of seven groups. These groups and the coefficients  $\chi_s$  and  $\lambda_s$  for each group are given in Table 4-13. As observed therein,  $\chi_s$  and  $\lambda_s$  show a weak correlation with the cation exchange capacity of the sediment, although evidently the exchange capacity is by no means the sole determinant of soil erodibility. Observe also that while  $\lambda_s$  varies within a narrow range (0.252 to 0.386),  $\chi_s$  varies over an order of magnitude (1.345 to 10.582), which implies that this parameter is sensitive to soil composition. The curves in Fig. 4-27 highlight the wide range of  $\epsilon_N$  values that can occur for a given  $\tau_s$ . The form of (4-36) is consistent with the observation of, among others, Galami et al. (1991), who showed that  $\epsilon_N$  decreases with increasing duration of consolidation of the bed, which essentially increases the bed shear strength.

Using Eq. (4-35) along with (4-31), (4-34), and (4-36), the following erosion rate expression is obtained:

$$\epsilon = \epsilon_{N0} T \exp\left(\Delta - \frac{\Lambda}{T}\right) \exp\left(-\chi_s \left[ \zeta_s (\phi - \phi_l)^{\xi_s} \right]^{\lambda_s} \right) \quad (4-37)$$

$$\times \left[ \tau_b - \zeta_s (\phi - \phi_l)^{\xi_s} \right]$$

The application of (4-37) can be illustrated by the following example of erosion in a channel. Consider values of the coefficients  $\epsilon_{N0}=200$  g/N s,  $\chi_s=2.892$ ;  $\lambda_s=0.372$ ,  $\zeta_s=1.65$ ,  $\xi_s=1.00$ ,  $\phi_l=0$ ,  $\Delta=27.0$ , and  $\Lambda=10,145$ . Now consider a bed of density  $\rho=1,545$  kg/m<sup>3</sup> subject to a flow-induced bed shear stress  $\tau_b=1$  Pa at a water temperature  $T=27^\circ\text{C}$  ( $300^\circ\text{K}$ ). With  $\rho_w=1,000$  kg/m<sup>3</sup> and  $\rho_s=2,650$  kg/m<sup>3</sup>, we

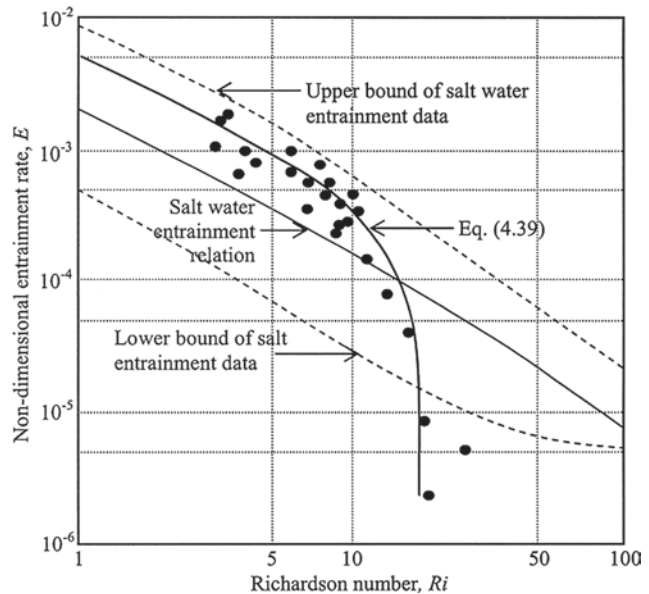


**Fig. 4-28.** Nondimensional entrainment rate against Richardson number. Comparison between data on fluid mud entrainment (dark circles), corresponding curve based on (4-39), salt entrainment data (upper and lower bounds) reported by Christodoulou (1986) and salt entrainment relation obtained from (4-39) (after Mehta and Srinivas, 1993).

obtain  $\phi=0.33$  from Eq. (4-5). Equation (4-37) then yields  $\epsilon=2.98$  g/m<sup>2</sup> s.

#### 4.8.6 Mass Erosion

Mass erosion, in which the bed fails and releases chunks or clasts of material, has been modeled on Eq. (4-30), even though this relation was derived for surface erosion (Mehta and Lee 1994). This approach, although very approximate, is convenient because one merely has to calibrate for  $\epsilon_M$  and  $\tau_s$ . Mass erosion is often considered to occur when stiff beds are subjected to high stresses (Ariathurai et al. 1977). However, even weak beds can mass erode at comparatively low stresses. In flume tests, Hwang (1989) reported mass erosion of beds of organic-rich sediment from Lake Okeechobee in Florida (Table 4-4). Starting with no flow and increasing the bed shear stress in steps, resuspension initially occurred by surface erosion, and at high stresses (but low compared to those for stiff clays, for example) the 3- to 4-cm-thick bed failed almost entirely. A feature of the erosion process was that in some cases  $\epsilon_M$  and  $\tau_s$  were considerably higher for mass erosion than for surface erosion of the same bed. Thus, for example, for a bed of density 1,200 kg/m<sup>3</sup>,  $\epsilon_M$  and  $\tau_s$  for surface erosion were  $5.6 \times 10^{-6}$  kg/m<sup>2</sup> s and 0.65 Pa, respectively, whereas the corresponding values for mass erosion were  $5.6 \times 10^{-4}$  kg/m<sup>2</sup> s and 1.8 Pa.

Recognizing the rapidity with which mass erosion occurs, Ariathurai et al. (1977) introduced a simple model, which

essentially amounts to instantaneous erosion of a bed layer of thickness  $\Delta z_b$  in time  $\Delta t$ ,

$$\epsilon = \rho_b \frac{\Delta z_b}{\Delta t} \quad (4-38)$$

where  $\epsilon$  is the mass rate of erosion (or erosion flux) and  $\rho_b$  is the bed density. Equation (4-38) applies when the bed shear stress exceeds the shear strength for mass erosion. The thickness  $\Delta z_b$  was determined by calibration against data on the time-variation of the suspended sediment concentration in the Savannah River estuary, Georgia.

When a water jet impinges on a fine-grained soil a hole develops when the jet momentum exceeds the requisite critical value. In this mass erosion process, the rate of erosion is usually measured as the time-rate of change of the cube-root of the hole volume. Traditionally, this rate is expressed as a function of the erosion-governing parameters through dimensional analysis (Hanson 1990; Hollick 1976; Moore and Masch 1962).

#### 4.8.7 Fluid Mud Entrainment

Sediment entrainment can occur due to hydrodynamic instabilities at the interface between very soft mud and water, resulting in the generation and breakup of the interfacial bilows by shear flow. This process has been described in terms of a balance between production of turbulent kinetic energy, buoyancy work in entraining the sediment, and viscous energy dissipation (Uittenbogaard 1995; Kranenburg 1994b; Scarlatos and Mehta 1993; Winterwerp et al. 1993; Winterwerp and Kranenburg 1997a). Bottom response in this case is distinct from surface erosion of sediment flocs, which occurs over typically harder cohesive beds (Taki 1990). In the prototype environment, interfacial undulations can occur at the frequency of surface wave forcing, i.e., in the forced mode, and also in the free mode. In the forced mode, additional, low-frequency oscillations can occur as a result of interactions among the forcing wave frequencies (Jiang 1993). In the free mode the interface tends to oscillate at the buoyancy (Brunt-Väisälä) frequency (Jiang 1999; Wright et al. 1988).

Based on laboratory tests in a flume, Mehta and Srinivas (1993) proposed the relation for the rate of sediment entrainment

$$E = \frac{dz_b/dt}{U} = A \cdot Ri^{-1} - D \cdot Ri \quad (4-39)$$

where

$E$  = dimensionless entrainment rate, i.e., the rate of change of bottom height,  $dz_b/dt$ , divided by  $U$ , the characteristic flow velocity above the water-mud interface;

$A$  and  $D$  = sediment dependent coefficients; and

$Ri$  = the global Richardson number, defined as

$$Ri = \frac{hg(\rho - \rho_w)/\rho_w}{U^2} \quad (4-40)$$

In Eq. (4-40),  $h$  is a characteristic water depth above the interface,  $\rho$  is the suspension density, and  $\rho_w$  is water density. In Fig. 4-28,  $E$  is plotted against  $Ri$  and compared with data on the entrainment of a clayey fluid mud in a laboratory flume. Values of the coefficients are  $A = 5.2 \times 10^{-3}$  and  $D = 1.6 \times 10^{-5}$ . Since the second term on the right hand side of (4-39) arises from the effect of settling,  $D$  depends on the settling velocity. Setting  $D=0$  leads to the inverse dependence of  $E$  on  $Ri$ , as in salt entrainment. In Fig. 4-28, the resulting expression is compared with data on the entrainment of salt water into fresh water compiled by Christodoulou (1986). Observe that due to the settling effect, at relatively high values of  $Ri$  sediment entrains much less efficiently than salt. Several factors are responsible for the drop in the entrainment rate at high  $Ri$ , including the viscous effect and wall friction. In addition, increased resistance to entrainment due to density stratification plays a role. When these and related effects can be explicitly included in the entrainment rate formulation, the final equation is found to be similar in form to Eq. (4-30) (Kranenburg and Winterwerp 1997; Winterwerp and Kranenburg 1997b). Referring to Eq. (4-40), one may define a critical value  $Ri_c$  of the Richardson number above which sediment entrainment can be assumed to be zero, as suggested by Odd and Cooper (1989). In Fig. 4-28  $Ri_c$  is seen to be close to 20.

When fluid mud is mobile, i.e., has been set in motion by flow above the interface,  $U$  must be replaced by  $\Delta U$ , the characteristic difference between the velocity above and below the interface. It is common to find layers of fluid mud set in motion by tidal flows, as shown in Fig. 4-29 from measurements in the Avon River, U.K. (Kendrick and Derbyshire 1985). Ross (1988) examined fluid mud layer motion as a simple Rayleigh flow problem (Phan-Thien 1983) in which the layer is set in motion by the downward diffusion of momentum. Trowbridge and Kineke (1994) provided a fuller treatment, both datawise and from the perspective of non-Newtonian flow modeling of fluid mud driven by flow over the Amazon Shelf.

## 4.9 WAVE-INDUCED EROSION

### 4.9.1 Nearshore Zone

In shallow nearshore waters the mode of erosion of bottom mud depends on waves and on the bottom condition. As schematized in Fig. 4-30, the sediment-active zone is bounded by the shoreline and the terminal depth, defined as that depth seaward of which wave action is unable to reach the bottom to cause significant changes in the bed profile. The nearshore profile is subdivided by the wave breakerline

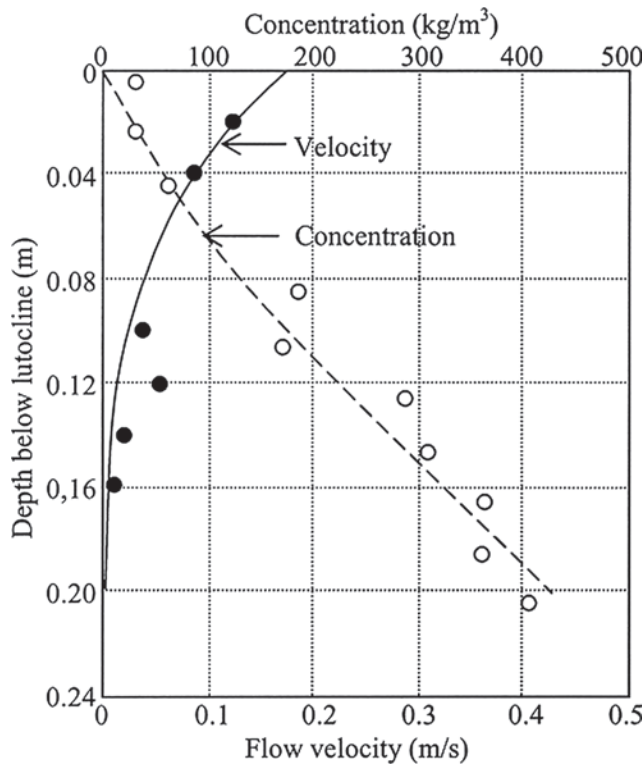


Fig. 4-29. Flow velocity and concentration profiles below lutocline in the Avon River, UK (adapted from Kendrick and Derbyshire, 1985).

into the surf zone and the offshore zone between this line and the terminal depth.

Although the terminal depth has been shown to be a reasonably well-defined parameter (depth of closure) characterizing the active sand profile, for fine sediment profiles laden with fluid mud it is a notional depth that requires quantitative assessment. Fluid mud generation has been examined in laboratory flumes and in the lacustrine environment where wave forcing dominates (e.g., Lindenbergh et al. 1989; Li 1996), and it appears that rough estimates of the thickness of the fluid mud layer formed under sustained wave action can be obtained by calculating the depth, i.e., the lower level of the fluid mud layer, at which the wave-induced (maximum) lift on a unit sediment mass balances

the resistance to liquefaction due to gravity and cohesion (Li and Mehta 2001). Hence the terminal depth,  $h_c$ , corresponds to the critical condition when the layer thickness reduces to nil. Accordingly, it can be shown that this depth can be estimated from  $h_s = \alpha_d \log(\beta_d H_s)$ , where  $H_s$  is a characteristic maximum wave height, and  $\alpha_d$ ,  $\beta_d$  are coefficients that depend on the bed properties and also on the wave period (Rodriguez 2000). This equation is applicable to areas where the terminal depth is on the order of 1 m or higher. Very little prototype information on  $\alpha_d$ ,  $\beta_d$  is available, inasmuch as the distance from the shoreline up to which the muddy bottom is regularly or episodically turned over by waves has not been explored in any systematic way. From data on waves, water depths, and fluid mud thickness in Lake Okeechobee in Florida,  $\alpha_d = 20.4$  and  $\beta_d = 0.73$  have been obtained, with the wave height and water depth measured in meters (Rodriguez 2000; Li 1996).

The position of the breakerline, and hence the breaker (water) depth below mean water level, depends on the shape of the profile and the degree of wave damping. Profile shape, in turn, depends on the composition of bottom material and also on whether it is molded by waves or tide (Friedrichs 1993; Roberts et al. 2000). Wave breaking in the surf zone tends to erode and rapidly disperse the eroded material over the water column. In the comparatively less energetic zone seaward of the breakerline mud liquefaction by waves can occur, and transport of the resulting soft mud is often the main reason for profile changes. It appears that apart from gravity slide, which is typically seaward, fluid mud transport can occur landward due to streaming, a second-order hydrodynamic effect associated with wave propagation at the water surface and at the interface between water and fluid mud, and the associated fluid velocities. Depending on the direction of wave incidence, streaming can be in the cross-shore direction or both cross-shore and alongshore directions (Shibayama et al. 1986; Sakakiyama and Bijker 1989; Jiang and Mehta 1996; Rodriguez and Mehta 1998).

Depending on tide and wave conditions, bottom sediment properties and sediment sources and sinks, muddy coast profile shapes can be "convex-upward" or "concave-upward," the latter being qualitatively akin to sandy beach profiles (Kirby 1992; Friedrichs 1993; Lee 1995). By assuming wave height to decrease with distance by damping due to viscous dissipation within bottom mud, and wave breaking in the surf zone, Lee (1995) obtained the following expression for the profile depth,  $h(y)$ , below mean water level

$$h = h_0 e^{4k_i(y_0 - y)} \left( \frac{y}{y_0} \right)^2 + F_0 y e^{-\beta_0 y} \quad (4-41)$$

where

$y$  = distance from shoreline;

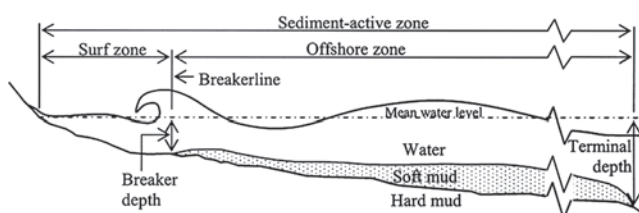


Fig. 4-30. Definitions related to the sediment-active nearshore zone (after Rodriguez 2000).

$h_0, y_0$  = coordinates of the offshore end of the profile;  
 $k_i$  = wave damping coefficient;  
 $F_0$  = bottom slope at  $y = 0$ ;

and the coefficient  $\beta_0$  accounts for the offshore extent of the combined influence of bottom slope at the shoreline and scour due to wave breaking at the shoreline.

Relatively few measurements of the wave-damping coefficient applicable to muddy coast profile dynamics seem to have been made. From two nearshore wave gages that were 3.4 km apart in the Gulf of Mexico off Louisiana, Tubman and Suhayda (1976) recorded a 48% reduction in wave energy corresponding to  $k_i = 0.00020 \text{ l/m}$ . Near Triangular

Marsh in Corte Madera Bay, California, Liang and Williams (1993) also reported  $k_i = 0.00020 \text{ l/m}$  based on wave data. An example of fitting Eq. (4-41) to a convex-upward profile measured along the coast of Louisiana (Kemp 1986) is shown in Fig. 4-31 (Lee 1995). A similar comparison for a concave-upward profile is shown in Fig. 4-32. When the profile is molded by tide, the shape is different from (4-41) and is strongly influenced by the tidal range (Kirby 1992; Friedrichs 1993; Roberts and Whitehouse 2001).

The coefficient  $k_i$  is particularly sensitive to mud density. Lee and Mehta (1997) for instance showed that in the muddy bottom environment of the Gulf of Mexico off Mobile Bay in Alabama,  $k_i$  increased from 0.0005 l/m to 0.023 l/m as the

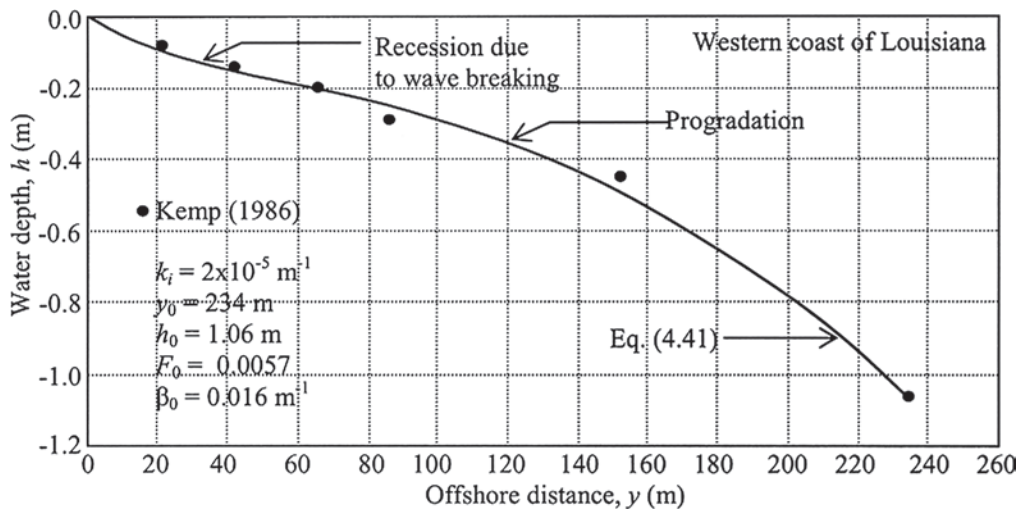


Fig. 4-31. Comparison of (4-41) with profile data from Louisiana coast obtained by Kemp (1986).

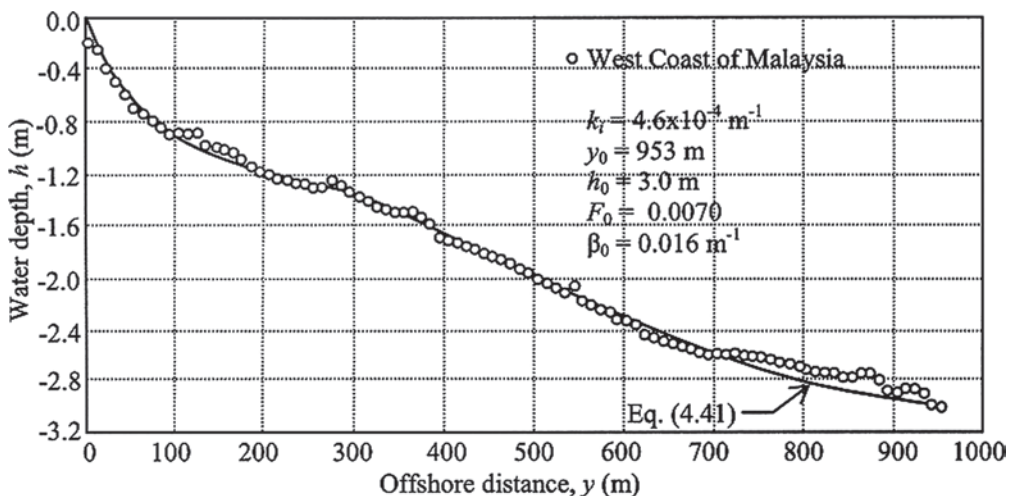


Fig. 4-32. Comparison of Eq. (4-41) with profile from the west coast of Malaysia (after Lee and Mehta, 1997).

**Table 4-14 Coefficients in (4-41) for Concave and Convex Profile Configurations**

Location (source)	Profile state	$F_0$		$\beta_0$ (1/m)		$k_i$ (1/m)	
		Mean	Std. dev.	Mean	Std. dev.	Mean	Std. dev.
Malaysia, China, U.S. (Lee and Mehta 1997)	Concave (81 profiles)	0.059	0.083	0.046	0.054	0.42	0.13
	Convex (15 profiles)	0.026	0.019	0.015	0.0084	0.016	0.027

mud density decreased from 1,302 to 1,139 kg/m<sup>3</sup>. In general, the wave attenuation coefficient,  $k_i$ , is related to wave amplitude according to  $k_i = -(1/\ell)\ln(a_i/a_0)$ , where  $a_0$  is the wave amplitude at  $y=y_0$  and  $a_i$  is the amplitude at a shoreward distance  $\ell$ . Based on 96 profiles,  $F_0$ ,  $\beta_0$ , and  $k_i$  were correlated with the state of the profile (Lee 1995), considering concave-upward profiles to be “erosional” and convex-upward profiles to be “accretionary.” The resulting values (means and standard deviations) of these three parameters are given in Table 4-14.

#### 4.9.2 Profile Stability Factor

Profile stability, i.e., whether a given profile will accrete, will remain as it is, or will erode, can be characterized by the ratio of an overall shore stabilizing factor,  $F_s$ , to an overall shore destabilizing factor,  $F_d$ . A profile stability number,  $S$ , can then be defined (Mehta and Kirby 1996) as

$$S = 1 - \frac{F_s}{F_d} \quad (4-42)$$

With respect to Eq. (4-42) the three cases that can arise are (1)  $F_d = F_s$  or  $S = 0$ , signifying marginal stability; (2)  $F_d > F_s$  or  $S > 0$ , for destabilizing or eroding conditions; and (3)  $F_d < F_s$  or  $S < 0$ , for stable or accretionary conditions. Summing the corresponding individual stabilizing and destabilizing factors,  $f_{di}$  and  $f_{si}$ , respectively,  $F_d$  and  $F_s$  are obtained from  $F_d = \sum \alpha_{di} f_{di}$  and  $F_s = \sum \alpha_{si} f_{si}$ , where  $\alpha_{di}$  and  $\alpha_{si}$  are weighting coefficients, subscript  $i$  represents a particular factor, and  $\Sigma$  denotes summation. By definition, the weighting coefficients must satisfy the conditions:  $\sum \alpha_{di} = 1$ ;  $\sum \alpha_{si} = 1$ . Equation (4-42) can now be stated as

$$S = 1 - \frac{\sum \alpha_{si} f_{si}}{\sum \alpha_{di} f_{di}} \quad (4-43)$$

To calculate  $S$  from Eq. (4-43) for a given shoreline, all relevant factors and the corresponding weighting coefficients must be evaluated. For a broad categorization stability, the effectiveness of individual factors contributing to  $S$  can be considered to assume the following values and associated effects on stability: 0 = no or low effect,

±1 = moderate effect, ±2 = significant effect, and ±3 = very significant effect. Further, one may conveniently consider that “moderate” effect for any particular factor corresponds to marginal stability ( $S = 0$ ), i.e., a noneroding, nonaccreting profile. Thus, in Eq. (4-43), setting  $S=0$  and each  $f_{di}$  and  $f_{si}$  to unity yields  $0 = 1 - (\sum \alpha_{si}/\sum \alpha_{di})$ , which is consistent with the definition of the weighting coefficients. It follows from this qualitative assignment of parametric values that the weighting coefficients represent the relative magnitudes of the various factors when they individually have moderate effects.

Although numerous shore destabilizing factors actually contribute to profile stability, noteworthy factors include waves and storm surge, structures, tides, and biophysicochemical processes. The corresponding stabilizing factors are sediment supply, bottom hardness, structures, morphologic control, sediment composition, vegetative cover, and biophysicochemical processes.

Waves, storm surge, and intrusive structures often contribute significantly to erosion, as do tides (and associated currents) when they are strong. Because storm surge data are not commonly available, one may consider waves as surrogates for the storm surge effect, even though wave and storm surge statistics are often not entirely interdependent. Also, an influence not easily quantified is the sediment transporting role of a storm surge and the ensuing change in the profile.

Among biological processes, bioturbation is probably the most important destabilizing factor, although biochemical production of gas, e.g., methane, can also destabilize the bottom. Such factors as air and water temperature, salinity and water quality parameters, and the various positive and negative feedbacks linking physical and biophysicochemical processes further complicate biologically driven systems, which tend to play an important role, at times even a dominant one, in areas where waves and tides are comparatively weak.

Sediment supply is a characteristically significant factor governing shore stability because, irrespective of the magnitude of the erosive forces, a profile can hold fast or accrete as long as the rate of sediment supply equals or exceeds the rate of depletion. Conversely, if sediment supply becomes

insufficient, the likelihood of a shoreline remaining static is low, especially in the long run, except perhaps through hardening by structural means. Bottom hardness, as defined by standard measures of soil strength, can be quite important in distinguishing between overconsolidated and weakly consolidated beds.

Some structures can promote stability by sheltering a coast from erosive forces, and their role can be as noteworthy as that of bottom hardness. Other structures can have the opposite effect, namely, one of shoreline destabilization by reduction or elimination of sediment supply. In a similar vein, morphologic control can be exerted by offshore bathymetry on wave action and associated alongshore water and sediment transport. Shoreline configuration can be equally significant, for instance by promontories in sequestering sediment and thereby enhancing stability. Sediment composition partly determines hardness, although hardness also depends on consolidation and gelling. On the other hand, given two sediment beds of the same density, the less cohesive material is likely to erode more easily than the other.

Vegetative canopies tend to impart stability, as do certain benthic biological processes, e.g., surficial mats produced by secretions including mucopolysaccharides. Finally, tide and tidal currents can also influence stability through intertidal wetting and drying, because desiccation can measurably enhance profile hardness by soil encrustation.

From an inspection of the effects of the various factors at several muddy coasts, the following expression for  $S$  can be defined:

$$S = 1 - \frac{0.25f_{S\text{sed}} + 0.20f_{S\text{bh}} + 0.15f_{S\text{st}} + 0.15f_{S\text{mor}} + 0.10f_{S\text{com}} + 0.10f_{S\text{veg}} + 0.05f_{S\text{bio}}}{0.40f_{D\text{wv}} + 0.30f_{D\text{st}} + 0.25f_{D\text{tc}} + 0.05f_{D\text{bio}}} \quad (4-44)$$

where subscripts are wv for waves, st for structures, tc for tide and tidal currents, sed for sediment supply, bh for bottom hardness, mor for morphology, com for sediment composition, veg for vegetation, and bio for biophysicochemical effects.

To fully assess the applicability of Eq. (4-44) in predicting shore stability, extensive data sets for evaluating the coefficients and factors are required. Here we will illustrate how this might be accomplished by considering some diagnostic examples, giving consideration only to the most important factors contributing to stability.

The Gulf of Mexico shoreline of Louisiana near Cheniere au Tigre undergoes seasonal fluctuations due to a variable wave climate, and its mean position is stabilized by mud supply derived ultimately from the Mississippi River (Kemp 1986). In this moderate coastal environment, the mean astronomical tidal range is on the order of 0.5 m, which is modulated by frequency contributions from frontal-wind-induced oscillations, especially in winter. The shore, backed by marsh

vegetation, has a biogenically active mud flat morphology with sediment diameter in the range 1 to 5  $\mu\text{m}$  and is dominated by fluid mud. On the basis of a scale for effects ranging from 0 to  $\pm 3$  the following values will be assigned:  $f_{D\text{wv}}$ ,  $f_{S\text{sed}}$ ,  $f_{S\text{bh}}$ ,  $f_{S\text{veg}}$ , and  $f_{S\text{bio}}$  all equal to unity, and the remainder equal to zero. Equation (4-44) then yields  $S = -0.50$ , which is less than zero, and correlates with the observed seasonal mean stability of the shoreline, notwithstanding longer term changes due to the relative rise in sea level experienced in this region.

The value of  $S$  for Louisiana and other sites including India (Mathew and Baba 1995), Indonesia (Tarigan et al. 1996), and Suriname (Eisma et al. 1991; Wells 1983), are given in Table 4-15. Along the coast of Kerala in India, mudbanks are believed to be enhanced in part by the inclement monsoonal waves but are less active in fair weather, because the high monsoonal waves are able to transport quantities of mud from an offshore pool to the shore by streaming. At the end of the monsoon, in the absence of significant streaming, the nearshore-transported mud is thought to slide offshore and to not return until the onset of the following monsoon (Mathew and Baba 1995).

The shorelines of Indonesia at Teluk Waru, Madura, and Surabaya are partly sheltered against waves by neighboring islands, and in conjunction with the absence of significant sediment supply they exhibit marginal stability. In general, notwithstanding the example from India, which is unique in

**Table 4-15 Calculated Stability Numbers versus Observed Shore Stability**

Location	Stability number, $S$	Observed profile stability
Louisiana	-0.50	Generally stable, with seasonal variability
Kerala (monsoon), India	~0	Shore-attached mudbanks occur at specific locations
Kerala (fair weather), India	0.75	Mudbanks are absent
Teluk Waru, Indonesia	~0	Marginally stable environment
Surinam	~0	Mudbanks are stable over short term; translate alongshore over a decadal time scale
Selangor, Malaysia	0.67	Eroding coast
Madura, Indonesia	~0	Marginally stable environment
Surabaya, Indonesia	~0	Marginally stable environment

terms of the historically transient nature of the mudbanks, if a long-established muddy coast is currently eroding, it is natural to look for possible anthropogenic causes of the altered state of the shoreline. Thus, for example, at the Selangor coast of Malaysia where  $S = 0.67$ , this once-stable mangrove-fringed coast has been eroding in recent decades due to reduced detrital supply from rivers as a result of diversion of river waters for agricultural usage (Midun and Lee 1989).

#### 4.9.3 Erosion by Breaking Waves

Referring to the surf zone in Fig. 4-30, among others, Azam (1998) and Yamanishi et al. (1998) have shown that the erosion of mud bed is caused by the impact force as the wave breaks. An expression for the mass flux or the rate of bed erosion,  $\epsilon_b$ , can be introduced as (Rodriguez 2000)

$$\epsilon_b = \epsilon_{bw} \left( \frac{H_b - H_{bc}}{H_{bc}} \right)^{\delta_b} \quad (4-45)$$

where  $H_b$  is the breaker height,  $H_{bc}$  is the critical value of  $H_b$  below which there is no measurable erosion,  $\epsilon_{bw}$  is the value of  $\epsilon_b$  when  $H_b = 2H_{bc}$  and  $\delta_b = 1$ , and  $\delta_b$  is a sediment-specific coefficient. In (4-45)  $\epsilon_b$  is conveniently considered to depend on the breaker height, i.e., the wave height at the seaward end of the surf zone, rather than the local wave height within the surf zone, and thus represents a mean value applicable over the entire surf zone. This is often a reasonable approximation because, as a result of wave damping by bottom mud, the surf zone over a muddy bottom tends to be considerably narrower than that over a rigid or sandy bottom. However, in general, with increasing surf zone width the applicability of Eq. (4-45) becomes increasingly qualitative, unless  $H_b$  is replaced by the corresponding local wave height and the equation is locally calibrated for  $\epsilon_{bw}$ ,  $H_{bc}$ , and  $\delta_b$ .

Coefficients in Eq. (4-45) from some studies are given in Table 4-16. In each case the rate of erosion was determined by comparing nearshore bottom profiles at different

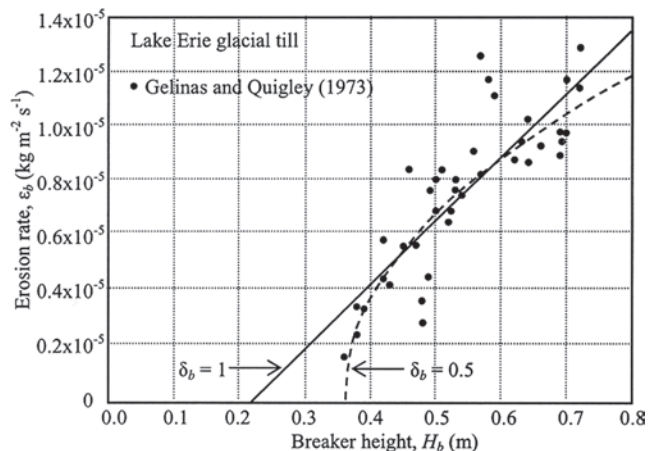


**Fig. 4-33.** Erosion rate within the surf zone as a function of breaking wave height for the northern shore of Lake Erie using data of Gelinis and Quigley (1973). Curves are based on Eq. (4-45) (after Rodriguez 2000).

times, calculating the associated volumetric changes, and from these the corresponding mass changes, given the bottom density. Illustrative plots of Eq. (4-45) are shown in Fig. 4-33. The data are for a consolidated glacial till from the northern shore of Lake Ontario in Canada (Gelinis and Quigley 1973). With regard to Eq. (4-45) it is observed that, although both a linear regression fit ( $\delta_b = 1$ ) and a power-law fit ( $\delta_b = 0.5$ ) appear to be reasonable, the power-law fit is better (regression coefficient  $r^2 = 0.80$ ) than the linear fit ( $r^2 = 0.71$ ). In all other cases given in Table 4-16,  $\delta_b = 1$  was found to be reasonable, contingent upon the typically sparse data sets used to fit Eq. (4-45) (Rodriguez 2000).

#### 4.9.4 Erosion by Nonbreaking Waves

Here we will consider the offshore zone (Fig. 4-30), i.e., the zone seaward of the surf zone up to the depth of closure, under nonbreaking waves and when the bed is not liquefied, i.e., no significant layer of fluid mud is present. In this case,

**Table 4-16 Coefficient Values for Eq. (4-45) for Breaking Wave-Induced Erosion**

Sediment source and investigator(s)	$\epsilon_{bw}$ (kg/m <sup>2</sup> s)	$H_{bc}$ (m)	$\delta_b$
50/50 (by weight) mixture of a kaolinite and an attapulgite: laboratory tests (Lee 1995; Tarigan 1996)	$7.56 \times 10^{-6}$	0.027	1
Louisiana coast mud (Kemp 1986)	$2.37 \times 10^{-6}$	0.087	1
Lake Erie glacial till: laboratory tests (Bishop and Skafel 1992; Bishop et al. 1992; Skafel and Bishop 1994)	$1.39 \times 10^{-3}$	0.083	1
Lake Ontario glacial till (Nairn 1992)	$4.18 \times 10^{-5}$	0.57	1
Lake Erie glacial till (Kamphuis 1986)	$7.34 \times 10^{-6}$	0.29	1
Lake Erie glacial till (Gelinis and Quigley 1973)	$5.48 \times 10^{-6}$	0.23	1
Lake Erie glacial till (Gelinis and Quigley 1973)	$1.07 \times 10^{-5}$	0.36	0.5

Source: Rodriguez (2000).

erosion rate formulas determined for wind-generated as well as mechanically produced waves in flumes tend to support the validity of the functional form of Eq. (4-30), i.e., the erosion rate expression developed for steady flows. Relevant information is summarized in Table 4-17, in which characteristic parameters are given for the expression

$$\epsilon = \epsilon_w \left( \frac{\tau_b - \tau_s}{\tau_s} \right)^{\delta_w} \quad (4-46)$$

For  $\delta_w = 1$ , Eq. (4-46) reduces to Eq. (4-30). In fact, as seen from Table 4-17, experimental data at times have yielded values of  $\delta_w$  close to unity. In Eq. (4-46),  $\tau_b$  is the peak value of the bed shear stress during the wave cycle, and the shear strength  $\tau_s$  can differ from that associated with current-induced erosion due to the effect of cyclic loading on the soil matrix (Maa 1986; Mimura 1993). An example of (4-46) is shown in Fig. 4-34 based on the work of Maa (1986) in a flume in which a kaolinite, as well as mud from Cedar Key in Florida, was eroded by waves. The associated wave characteristics are given in Table 4-17.

#### 4.9.5 Fluid Mud Entrainment by Waves

Laboratory flume tests show that when wave action above a threshold value necessary for bed liquefaction continues for a sufficient length of time, an equilibrium thickness of the fluid mud layer occurs. This threshold depends on bottom mud density and rheology, and fluid layer thickness increases with increasing wave height (Li 1996). Results from some laboratory tests are given in Table 4-18. On the prototype scale, in Lake Okeechobee, Florida, fluid mud thickness ranges between 0.05 and 0.20 m, depending on the water depth (Li and Mehta 2001). Thicker layers of fluid mud are found off the coast of Louisiana (Kemp 1986); the coast of Suriname/Guayana (Augustinus 1987; Eisma et al.

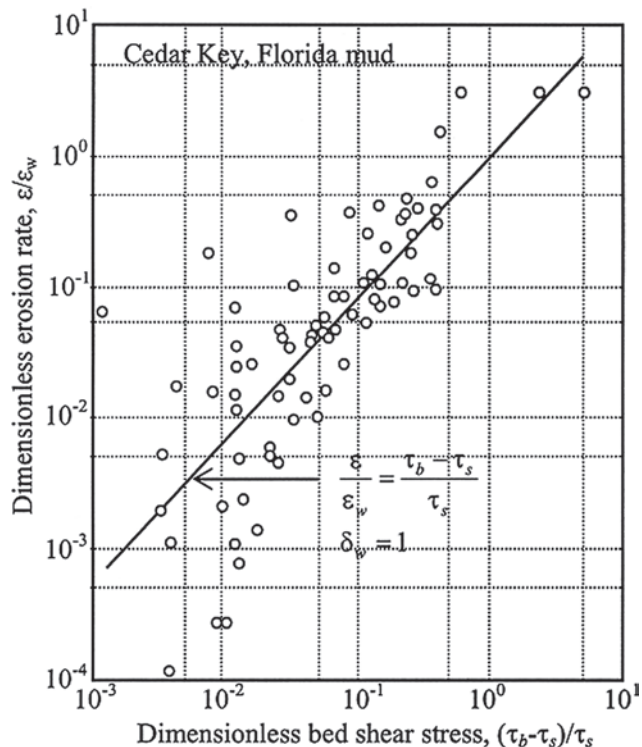


**Fig. 4-34.** Erosion rate relationship for nonbreaking waves obtained by Maa (1986).

1991); the Amazon shelf (Kineke and Sternberg 1995); and the southwestern coast of India (Mathew and Baba 1995).

In the offshore zone (Fig. 4-30), when the surficial layer at the bottom occurs as very soft or fluid mud, its entrainment can be described by an expression paralleling that used to quantify fluid entrainment from a stratified flow interface, e.g., Eq. (4-39). Li (1996) developed the following relation for the net rate entrainment by waves over fluid mud,  $\epsilon_f$  (mass per unit bottom area per unit time), in which the first

**Table 4-17 Parameters for Eq. (4-46) for NonBreaking Wave-Induced Erosion**

Investigator(s)	Mode of wave generation	Sediment	Parameter ranges <sup>a</sup> a (cm); ω (rad/s); k (1/cm)	Parameter values in Eq. (4-46)		
				$\epsilon_w$ (g/m <sup>2</sup> s)	$\tau_s$ (Pa)	$\delta_w$
Alishahi and Krone (1964)	Wind	Bay mud	0.9 ≤ a ≤ 3.4	Test 1: 0.48 Test 2: 11.2	0.29 0.39	1.72 1.15
Thimakorn (1984)	Mechanical	River mud	3.1 ≤ ω ≤ 12.6 0.16 ≤ ak ≤ 1.60	= $\mu_b \delta_{bl} / 2\tau_s^b$	Variable	1.00
Maa (1986)	Mechanical	Kaolinite; bay mud	1.4 ≤ a ≤ 3.7 3.3 ≤ ω ≤ 6.3	Kaolinite: 131 Mud: 30	Depth-varying Depth-varying	1.15 0.95
Mimura (1993)	Mechanical	Clays; bay mud	0.6 ≤ a ≤ 6.9 4.8 ≤ ω ≤ 8.2	0.27	0.15	1.82

<sup>a</sup>a = wave amplitude =  $H/2$ , H = wave height, ω = wave angular frequency ( $=2\pi f$ ); k = wave number.

<sup>b</sup> $u_b$  = amplitude of bottom (or near-bottom) orbital velocity;  $\delta_{bl}$  = wave boundary layer thickness =  $(v/f)^{1/2}$  and v = kinematic viscosity of water.

Source: Mehta (1996).

**Table 4.18 Summary of Selected Fluid Mud Generation Experiments in Flumes**

Source	Mud	Water depth (cm)	Bed thickness (cm)	Mud density (kg/m <sup>3</sup> )	Wave amplitude (cm)	Wave frequency (Hz)	Mud viscosity (Pa.s)	Mud rigidity (Pa)	Fluid mud thickness (cm)
Ross (1988)	Tampa Bay, Florida	31.4–31.7	11.8–13.0	1,080	3.1–3.6	1.0–1.1	25.0	100	5.0–6.3
Lindenberg et al. (1989)	Kaolin	25	4.8–4.9	1,300	2.4–3.6	0.4–0.7	3.0	5	1.0–2.5
Feng (1992)	AK <sup>a</sup>	18.4–20.2	14.7–16.6	1,170	1.9–4.0	1.0	6.1	295	2.0–3.5

<sup>a</sup>A 50/50 (by weight) clayey mixture of an attapulgite and a kaolinite; see Table 4-4.

Source: Li (1996).

term represents upward entrainment and the second embodies entrained sediment settling onto the fluid mud:

$$\epsilon_f = \begin{cases} \alpha_w \rho u_b \left( \frac{R_c^2}{R_g} - R_g \right) - w_s C_a & R_g < R_c \\ 0 & R_g \geq R_c \end{cases} \quad (4-47)$$

In Eq. (4-47),

$\rho$  = density of the fluid mud;

$u_b$  = near-bottom velocity amplitude;

$\alpha_w$  = sediment-dependent coefficient;

$C_a$  = near-bottom sediment concentration; and

$R_g$  = Richardson number, given by:

$$R_g = \frac{(\rho_m - \rho_w)g\delta_{bl}^2}{\rho_w \Delta u_i^2} \quad (4-48)$$

In Eq. (4-48),  $\delta_{bl}$  = wave boundary layer thickness (see footnote of Table 4-17) and  $\Delta u_i$  = absolute value of the maximum (horizontal) wave velocity difference across the interface. In Eq. (4-47)  $R_c$  is the critical value of  $R_g$  below which no entrainment is assumed to occur. This equation is plotted in Fig. 4-35 using the laboratory data of Maa (1986) and Li (1996) on the entrainment of natural and clayey sediments by waves in a flume. The coefficients  $\alpha_w = 2 \times 10^{-6}$  and  $R_c = 0.043$  were selected for both sets of data. In general, when direct measurements are not available, the calculation of the velocities  $u_b$  and  $\Delta u_i$  can be carried out as follows.

When bottom mud is soft, wave-induced orbital motion tends to penetrate the water-mud interface and, in turn, due to the high viscosity of mud (Table 4-6), wave damping often becomes significant. Several models have been used to determine the velocity field in two-layered (water and mud) flows in which energy dissipation is significant in the lower (mud) layer. An early model is due to Gade (1958), who assumed the lower layer to be a viscous fluid and the water layer above to be inviscid. He further limited his solution

for the velocity field to waves in shallow water. Dalrymple and Liu (1978) considered both layers to be viscous and did not restrict the water depth. MacPherson (1980) assumed the lower layer to be viscoelastic and water to be inviscid. Piedra-Cueva (1993) extended the work of MacPherson by introducing a boundary layer at the water-mud interface. Jiang (1993) expanded on the solution of Dalrymple and Liu by including second order effects. The velocities  $u_b$  and  $\Delta u_i$  for the plot of Eq. (4-44) in Fig. 4-34 were derived by Li (1996) using the solutions of Jiang. A brief review of these and other models is provided in Rodriguez (2000).

A case of a simple flow field is one in which damped oscillation of the fluid mud layer is ignored in comparison with the orbital velocity above the interface. Then one has  $\Delta u_i \approx u_b$ , which can be easily calculated assuming the applicability of, for instance, the Airy wave theory (e.g., Dean and Dalrymple 1991) by ignoring the boundary layer effect in the water layer. In the simplest case of a shallow water wave the bottom velocity can be obtained from

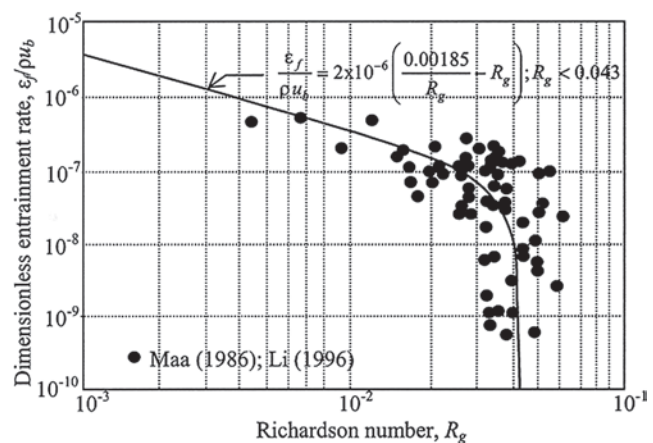


**Fig. 4-35.** Dimensionless wave-induced entrainment flux as a function of Richardson number (after Li and Parchure 1998).

$$u_b = \frac{H}{2} \left( \frac{g}{h} \right)^{1/2} \quad (4-49)$$

where  $H$  is the local wave height and  $h$  is the water depth.

## 4.10 DIFFUSION

### 4.10.1 Diffusion and Stratification

The (negative) buoyancy effect due to sediment-induced stratification tends to restore fluid lumps moved upward by turbulent diffusion back to their original positions, and thereby restricts the vertical transfer of momentum and sediment mass. This effect can be simply characterized by the way in which the momentum and mass mixing lengths vary with sediment concentration. In general, as the concentration increases the mixing length decreases, and below the lutocline almost complete turbulent collapse may occur, essentially leading to viscous flow (Jiang 1999; Winterwerp 1999; Jiang and Mehta 2000).

The Fickian flux due to vertical diffusion is

$$F_d = K_v \frac{\partial C}{\partial z} \quad (4-50)$$

where

$K_v$  = diffusion coefficient.

From the analogy between sediment-induced density stratification and that induced by salinity and thermal gradients, along with the so-called Reynolds analogy between momentum and mass transport (Bird et al. 1960), expressions relating  $K_v$  to turbulence-mean flow and sedimentary parameters have been derived. Thus, for example, based on the phenomenological development of Rossby and Montgomery (1935), Munk and Anderson (1948) proposed the semiempirical formula

$$K_v = K_{v0} \left( 1 + \beta_v R_i g \right)^{\gamma_v} \quad (4-51)$$

where

$K_{v0}$  = “neutral” diffusivity in homogenous flow and  $\beta_v$  and  $\gamma_v$  are sediment-dependent coefficients.

In Eq. (4-51), in which the second term within parentheses represents buoyancy correction to neutral diffusion, the gradient Richardson number  $R_i g$  is defined as

$$R_i g = \frac{g}{-\rho} \frac{\partial \rho / \partial z}{(\partial u / \partial z)^2} \quad (4-52)$$

where

$u$  = local horizontal velocity.

With reference to the well-known mixing length concept of Prandtl and von Karman,  $K_{v0}$  can be stated as

$$K_{v0} = \kappa u_* z \left( \frac{(h-z)}{h} \right) \quad (4-53)$$

where

$$\begin{aligned} \kappa &= \text{Karman constant and} \\ u_* &[=(\tau_b/\rho_w)^{1/2}] = \text{friction velocity (Guo and Wood, 1995).} \end{aligned}$$

The use of (4-53) (with a nominal value of  $\kappa=0.4$ ) is contingent on the assumption of a logarithmic boundary layer velocity profile in the nonstratified water column. In reality, a Monin-Obukhov correction to the boundary layer velocity profile must be applied when stratification is significant (Friedrichs et al. 2000).

Jobson and Sayre (1970) noted that vertical mixing of suspended sediment in open-channel flow occurs as a result of two diffusion processes that can be shown to be additive. These processes include diffusion due to tangential components of turbulent velocity fluctuations and the centrifugal force arising from the curvature of fluid particle path lines. Based on these observations, they derived the following expressions for  $K_{v0}$ :

$$K_{v0} = \alpha_j \kappa u_* z \left( 1 - \frac{z}{h} \right) + \beta_j u_* h \left( \frac{1-z/h}{0.9} \right)^3 \quad \text{for } \frac{z}{h} \geq 0.1 \quad (4-54)$$

$$K_{v0} = \alpha_j \kappa u_* z \left( 1 - \frac{z}{h} \right) + \beta_j u_* h \left( \frac{z/h}{0.1} \right)^3 \quad \text{for } \frac{z}{h} \leq 0.1$$

Coefficients values from flume tests were reported to be  $\alpha_j = 0.038$  and  $\beta_j = 0.98$ .

Values of the coefficients in Eq. (4-51) for forcing by current and applicable to fine sediment transport are given from some sources in Table 4-19. In general, fewer sets of values of these coefficients are available than for momentum transfer (Ross 1988; Jiang 1999). Momentum diffusivity can be converted to mass diffusivity if the turbulent Schmidt number  $S_c$ , i.e., the ratio of momentum to mass diffusivity, is known from measurement. From estuarine measurements, Oduyemi

**Table 4-19 Parameters for (4-48) for Stratification Correction**

Source/forcing	$\beta_v$	$\gamma_v$
Ross (1988)/current	4.2	-2.0
Ross (1988)/waves	2.0	-0.5
Costa (1989)/current	1.0–8.0	-2.0
Hwang (1989)/waves	0.5	-0.5
Jiang (1999)/current	10	-0.5

(1986) found that the behavior of these two diffusivities over a tidal cycle was not self-similar, meaning that the  $S_c$  varied over the tide. Costa (1989) also reported that  $S_c$  varied with tide in Hangzhou Bay in China, in the range of 0.94 to 2.45.

Starting with a homogeneous suspension, the behavior of the diffusive flux  $F_d$  according to Eq. (4-50) along with Eq. (4-51) and (4-52) can be examined as a function of the concentration gradient,  $\partial C/\partial z$ . The resulting trend is illustrated in Fig. 4-36. It is assumed that  $\rho$  in the denominator of Eq. (4-51) is equal to water density  $\rho_w$ . Furthermore, the velocity gradient  $\partial U/\partial z = u_*/\kappa z$  is based on the logarithmic velocity profile, and  $\partial \rho/\partial z = [1 - (\rho_w/\rho_s)] \partial C/\partial z$ . Relevant values are  $h = 3$  m,  $u_* = 0.1$  m/s,  $z = 0.1$  m,  $\kappa = 0.4$ ,  $\rho_w = 1,000$  kg/m<sup>3</sup>,  $\rho_s = 2,650$  kg/m<sup>3</sup>,  $\beta_v = 4$ , and  $\gamma_v = -2$ . Observe the effect of increasing negative buoyancy in limiting upward diffusion.

Glenn and Grant (1987) developed a correction factor for sediment-induced stratification due to the effects of waves superimposed on current. In general, the use of higher order turbulence closure schemes for modeling diffusion partially obviates the empirical limitations of Fickian closure described here (Nunes Vaz and Simpson 1994). Among others, Sheng and Villaret (1989) modeled resuspension using a second-order closure model for turbulence, which also yielded a better measure of the bottom stress than from the usual assumption of a constant bottom drag coefficient and wave-induced velocity unaffected by suspended sediment. In fact, turbulence damping due to suspended sediment was shown to measurably reduce bottom drag, hence resuspension. The same trend was found by Adams and Weatherly (1981) using a similar modeling approach.

#### 4.10.2 Wave Effect

To model diffusion according to Eq. (4-50) for wave-induced processes, appropriate formulations for  $K_{v0}$  must be used.

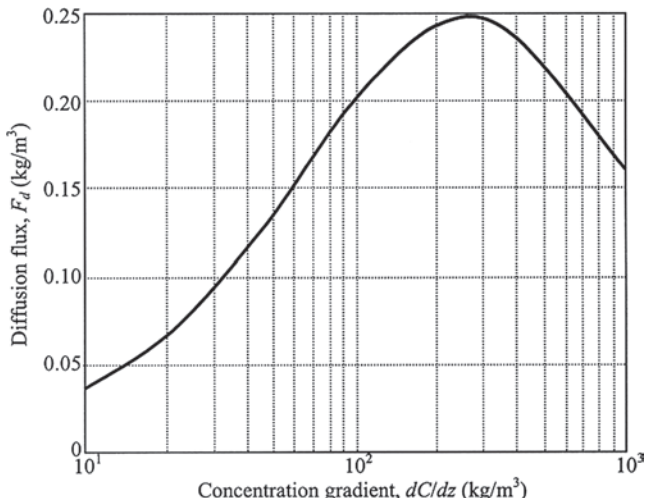


Fig. 4-36. Dependence of vertical mass diffusive flux on suspended sediment concentration gradient.

Several formulas have been proposed (e.g., Homma et al. 1965; Bhattacharya 1971; Kennedy and Locher 1972). A brief review of the subject is found in Dyer (1986). Focusing on the ambient water column rather than the near-bottom wave boundary layer, Hwang and Wang (1982) proposed the expression

$$K_{v0} = \alpha_{wd} \frac{H^2}{2} \frac{\sinh^2 k(h+z)}{\sinh^2 kh} \quad (4-55)$$

in which

$H$  = wave height,

$h$  = water depth,

$k$  = wave number,

and the diffusion scaling coefficient  $\alpha_{wd}$  for a given sediment depends on the flow field.

In Eq. (4-55), the vertical coordinate  $z$  is measured positive upward from the mean water level, so at the bottom  $z = -h$ . Based on wave energy dissipation in the water column and experimental data, Thimakorn (1984) arrived at an expression for  $K_{v0}$  that is akin to Eq. (4-55), with  $\alpha_{wd} = 1.77/\sinh kh$ . In Lake Erie, Lick (1982) reported a mass diffusivity, value  $K_{v0}$ , of 25 cm<sup>2</sup>/s. For calculation of  $K_v$  from  $K_{v0}$  using Eq. (4-51), Table 4-19 provides values of the coefficients  $\beta_v$  and  $\gamma_v$  from wave-induced resuspension studies by Ross (1988) and Hwang (1989).

Under wave action, vertical diffusion of sediment tends to be considerably less efficient than in a current in the sense that whereas, under waves, the sediment tends to remain sequestered within a comparatively thin bottom boundary layer, under a current-induced thicker boundary layer the material is swept upward much more easily, thus resulting in a greater suspension height (Li and Parchure 1998). Furthermore, release of bed pore water and associated chemical constituents appears to be influenced by a diffusive sublayer close to the bed, which seemingly restricts upward entrainment. On the other hand, heaving motion of mud, especially when it is soft, enhances upward transport (Li et al. 1997). When heaving and relative motion between water and mud at the interface become significant, the calculation of bed shear stress must also account for the “slippage” between the two layers (Maa 1986). In addition, there seems to be an effect on bottom drag associated with the flocs at the bed. Typically, the drag coefficient for a cohesive bed, especially one composed of soft mud, tends to be low. For example, from flume experiments Dixit (1982) reported values of the Manning’s bed resistance coefficient,  $n$ , to be on the order of 0.011. As postulated by Gust (1976), such a low value may in part be due to an elastic deformation of flocs induced by flow at the bed surface. Bed resistance is also mitigated by the effect of sediment-induced buoyancy. Li and Gust (2000) further ascribe the reduction effect to severe damping of turbulence in the wall boundary layer.

## 4.11 APPLICATIONS

The description of fine sediment behavior given in the preceding sections is used in engineering studies to predict sediment movement and deposition and to design sediment management measures (Zeigler and Nisbet 1994; 1995). A few examples will illustrate how they are used.

### 4.11.1 Measurement

Measurement of fine sediment transport rate and bed changes is accomplished by several methods, none of which provides a complete picture of the important processes. The greatest difficulty lies in measuring near the active bed-water interface and at lutoclines, where intrusive instruments may disrupt the processes to be measured.

The depth-mean suspended sediment mass transport rate is obtained from

$$\mathbf{q}(x, y, t) = \int_0^{h(x, y, t)} C(x, y, z, t) \mathbf{u}_s(x, y, z, t) dz \quad (4-56)$$

in which

$x$  and  $y$  = the longitudinal and transverse coordinates, respectively;

$z$  = the vertical coordinate;

$h(x, y, t)$  = the instantaneous water depth; and

$\mathbf{u}_s$  = the sediment velocity vector.

Because it is currently unrealistic to deal with the sediment velocity, which is difficult to quantify, especially for flocculated sediments,  $\mathbf{u}_s$  is characteristically replaced by the corresponding fluid velocity,  $\mathbf{u}$ . Thus, assuming isokinetic motion of water and sediment, we restate Eq. (4-56) as

$$\mathbf{q}(x, y, t) = \int_0^{h(x, y, t)} C(x, y, z, t) \mathbf{u}(x, y, z, t) dz \quad (4-57)$$

Suspended sediment load in the water column away from the bed is obtained by direct or indirect methods. Direct sampling involves collecting water samples at several depths while simultaneously measuring the flow velocity profile, and repeating these measurements at several locations along a cross section. The water samples may be taken by submerged bottle-type samplers or by pumping to a bottle on a vessel or platform. Samples are then analyzed for sediment concentration, usually by filtration and drying. Integration of the product of sediment concentration, flow velocity, and cross-sectional area over the profile yields an estimate of sediment discharge. Flow velocities can be measured by devices using vanes or propellers held at the sampling point, but the preferred method is now an acoustic Doppler current profiler (ADCP), either sitting on the bed or held just below the water surface, which emits multiple sound pulses and measures the time and frequency of reflected sound waves to compute three-dimensional velocities. Analysis of the

reflected wave intensity can also be used to estimate suspended sediment concentration, but requires careful, site-specific calibration of the signal against standard methods (Teeter et al. 1996; Land et al. 1997).

Other methods of measuring the sediment load include optical backscatter sensors (OBS), which emit a beam of light, measure the intensity of reflected light, and convert that reading to a sediment concentration. Such devices must be calibrated to the sediment in transport at each site, because the particle's reflectance is a function of shape, color, size, and surface coating (Downing and Beach 1989). Optical transmissometers are used in both low-concentration (Bocuniewicz et al. 1991) and high-concentration (Costa 1989) environments.

Measuring the location of the bed is commercially important for navigable waterways because it defines the depth available for navigation (Parker 1994), and scientifically important for defining rates of erosion and deposition. Despite its importance, the process is fraught with uncertainty in definition of what the bed surface is and where it is. Acoustic depth-sounding equipment is standard in most waterways and works well when the bed is composed of sand-size or larger sediment. For muddy beds the technique may or may not yield accurate results, because the acoustic signal is reflected by sharp density gradients, not by specific densities; thus the acoustic record may suggest that the bed occurs at the first fluid density inflection, such as is shown in Fig. 4-4, producing a bed elevation estimate that is one to several meters above the actual firm bed. In the presence of fluid mud, multiple density inflection points may produce multiple false bed locations (Parker and Kirby 1982). More accurate and reliable methods for locating the bed include nuclear density meters (Parker and Kirby 1982) and towed devices that respond to both suspension density and viscosity (Alexander et al. 1997).

### 4.11.2 Modeling

For many years physical models based on scaling principles were the primary engineering tool of choice for fine sediment studies (Herrmann and Letter 1990; Letter and McAnally 1977), but have now been largely replaced by numerical models which solve the equations of transport and bed change using computational methods.

In some situations involving steady or periodic flows, Eq. (4-57) can be solved through simple modeling techniques (e.g., McAnally 1999; Krone 1985). In steady and also quasi-steady flows such as those due to tides, and when the suspended concentration does not exceed a few tens of milligrams per liter, the classical Rouse (1937) profile of suspended sediment (Dyer 1986; Hill et al. 1988) is often found to be adequate to describe the variation of concentration  $C$  with depth. In this development the settling velocity is assumed to be independent of  $C$  and vertical diffusion is assumed to be neutral. Depth variation of  $C$  is obtained under the assumption of the equality of upward

diffusion and settling fluxes. The resulting profile of  $C$  along with the well-known logarithmic variation of flow velocity  $\bar{u}$  with depth (Dyer 1986) can be used to calculate the sediment load via (4-57).

Introduction of time-dependence of  $C$  in the Rouse formulation leads to a one-dimensional (vertical) model that has been used extensively in modeling the time-variation of the vertical profile of  $C$  due to tide as well as waves (e.g., Adams and Weatherly 1981; Maa and Mehta 1988; Sheng and Villaret 1989; Le Hir et al. 2001; Teeter 2001a, 2001b).

In most cases, it becomes essential to use complex two- or three-dimensional time-dependent numerical models to calculate  $\bar{u}$  and  $C$ , incorporating the described unit transport processes, i.e., settling and deposition of suspended material, consolidation of the fresh deposit, and erosion and entrainment of the fresh as well as of the consolidated deposit (Zeigler and Nisbet 1994; Cardenas et al. 1995; Costa 1995; Zeigler and Nisbet 1995; Jiang 1999).

The solved governing equations for transport of suspended sediment load, either cohesive or noncohesive, are usually the general advection-diffusion equations,

$$\frac{D}{Dt} = \frac{\partial}{\partial x} \left( K_x \frac{\partial C}{\partial y} \right) + \frac{\partial}{\partial y} \left( K_y \frac{\partial C}{\partial y} \right) + \frac{\partial}{\partial z} \left( K_z \frac{\partial C}{\partial z} \right) + \sum_{\text{sources}} - \sum_{\text{sink}} \quad (4-58)$$

where the left hand side is the total derivative and

$C$  = suspended sediment concentration;  
 $t$  = time,

$x$ ,  $y$ , and  $z$  = spatial coordinates, and

$K_x$ ,  $K_y$ , and  $K_z$  = directional diffusion coefficients.

The source term as represented in (4-58) denotes external sediment that enters the system being modeled, such as that due to shoreline or bluff erosion and river or slough runoff. Organic sediments can both be internally produced, e.g., by photosynthesis, and arrive from external sources. Sediments that leave the system are represented in the sink term. Erosion and deposition of sediment within the system is handled through the bottom boundary condition when the model includes the variation of flow and sediment properties in the vertical ( $z$ ) direction. In depth-averaged models, erosion and deposition become (external) source and sink, respectively.

A bed model, which describes the density, resistance to erosion, and other characteristics of the sediment bed, keeps track of the net deposition/erosion and thus the elevation of the bed and the variation of properties with depth into the bed (see, for example, McAnally and Thomas 1989). One of the first models in which the bed was discretized into horizontal layers, with density and erodibility indices changing from layer to layer, is due to Ariathurai et al. (1977), who applied the model to simulate tidally driven fine sediment

deposition in the dredged channel leading to the port of Savannah, Georgia. Maa (1986) extended this concept to wave modeling, in which the bottom density, erodibility, and rheological parameters were varied with depth. It is now recognized that an eventual goal of modeling should be to simulate the solid and fluid phases on a continuous rather than discretized basis (Teisson 1997; Toorman, 2001). Simulation of phase changes between the bed and suspension due to erosion/deposition must be integral to such a development, as opposed to the present piecemeal approach based on unit transport processes. It is certain that considerable additional experimental work will be required to fully evolve such a modeling approach.

Two aspects of modeling that are essential for simulating cohesive bottom related processes include fluid mud transport and bed stratification. In estuaries with large tidal ranges such as the Severn in the UK (Kirby 1986; Smith and Kirby 1989), the Loire in France (Le Hir et al. 2001), and the Amazon in Brazil (Kineke 1993; Geyer 1995; Vinzon and Mehta 2001), fluid mud tends to persist through the entire tidal cycle and plays a major role in determining the sediment budget. In the microtidal to mesotidal environment, such as along much of the U.S. coastal zone, thick layers of fluid mud are less common in fair weather, but can become significant in terms of their contribution to the total sediment load when, for example, storm waves occur (Kemp and Wells 1987).

The technology of sediment modeling has evolved rapidly in recent decades, and any description of the state of the art will quickly become obsolete. The one-dimensional numerical model HEC-6 and its variations are widely used for rivers and occasionally estuaries (e.g., Thomas et al. 1988). The TABS-MD and other systems of models have been extensively used for estuarine sediment transport (Donnell et al. 1991; McAnally 1989; Willis and Crookshank 1997), and the 2DV model LAEM-SED has been used in a few estuaries (Smith et al. 1987; Johnson et al. 1989). Three-dimensional models constitute the state of the art in fine sediment modeling, and are exemplified by applications reported by, among others, Teeter and Callegan (2000).

#### 4.11.3 Case Studies

Indian River Inlet, Delaware, connects Indian River Bay and Rehoboth Bay to the Atlantic Ocean on the U.S. East Coast. In 1938–1940 the previously ephemeral inlet was stabilized by parallel jetties 150 m apart with a maximum inlet depth of about 6 m below mean low water. Almost immediately the sandy inlet bed began to scour, and by 1991 nearly all of the inlet was deeper than 12 m and some holes exceeded 30 m in depth. Scour had uncovered lagoonal cohesive clay deposits at depths of about 11 m and the deepest holes had eroded through the clay layer, exposing consolidated Pleistocene sand and gravel (CTH 1994). Concern over the

possibility of further erosion undermining the jetties and a state highway bridge over the inlet prompted an analysis of the inlet's stability, a question usually associated with cohesionless sediments, but in this case one in which the erodibility of cohesive sediments was a controlling factor. The Corps of Engineers CTH (1994) analyzed the inlet's stability, employing a mix of field, laboratory, and desktop calculations as summarized below.

The average depth of the bays is 1.5 m below mean low water. Mean tide range is approximately 1 m in the offshore area, 0.6 m in Indian River Bay and 0.3 m in Rehoboth Bay. Small freshwater inflows (usually less than 100 m<sup>3</sup>/s) create a longitudinal salinity gradient in the bays, with minor to no vertical stratification occurring under normal conditions. In 1992 the inlet had an average cross-sectional area of about 2,100 m<sup>2</sup>. Tidal flow speeds through the inlet exceeded 2 m/s under spring tides.

A vessel-mounted 1,200-KHz ADCP was used to measure current speed and direction profiles along 12 ranges. Each range was profiled during peak ebb and peak flood flows for two tidal cycles. The ADCP measured three-dimensional velocity vectors, averaging within zones, or bins, approximately 50 cm deep. Sediment samples were taken to characterize the erodibility of the cohesive sediments and to obtain grain size distributions of the exposed bed sands. Clam-shell samples, drag bucket samples, and cores were taken at 10 locations throughout the inlet. Laboratory erosion tests were conducted to define the two characteristic parameters of Eq. (4-30) for the cohesive sediment samples. Tests were conducted in a particle entrainment simulator (PES) (Tsai and Lick 1986), a vertical loop sediment tunnel (VOST) (Teeter and Pankow 1989), and a rotating cylinder erosion device (see, e.g., Chapuis and Gatien 1986). Lee and Mehta (1994) have reviewed these and several other types of erosion-measuring devices reported in the literature. The PES induced bed stresses up to 0.7 Pa by means of a vertically oscillating grid, whereas the VOST generated horizontal flow stresses up to 3 Pa and the rotating cylinder generated stresses up to 16 Pa. The value of the erosion shear strength  $\tau_s$  developed from those experiments was 4 Pa for an intact sample and 5.8 Pa for a remolded sample. The erosion rate constant for the tested sediments ranged from  $5.8 \times 10^{-4}$  to  $1 \times 10^{-3}$  kg/m<sup>2</sup> s.

Typical mean flow velocities for the inlet were obtained by smoothing measured values and then adjusting them to an appropriate tide range and inlet cross-sectional area by means of the Keulegan (1967) tidal inlet method. Half-hourly shear stresses on the bed were estimated via Manning's flow velocity equation. These stresses were used to compute erosion rates for neap, mean, and spring tides using Eq. (4-30) and then composited to create annual erosion rates. Comparison with observed historical rates led to adjustment of the laboratory-derived erosion rate coefficients to make the bed somewhat more erodible, which was probably caused by

sand abrasion of the clay bed leading to more rapid erosion than by water flow alone.

The calculations showed that the clay bed would stop eroding at an inlet size of about 2,800 m<sup>2</sup>, or about 30% larger than the then existing inlet size. Based on these and other, sand-based calculations, it was decided to do nothing other than continue monitoring the inlet to ensure that the predicted size stability would occur.

Hayter and Gu (2001) applied a two-dimensional numerical model (HSCTM-2D) to the problem of contaminated sediment transport in the Maurice River-Union Lake, New Jersey, system in order to predict the effects of dredging on sediment and arsenic distribution in the system. Union Lake is a 4-km-long impoundment on the Maurice River about 40 km upstream of Delaware Bay. Its average width is 1.6 km. Bed sediments were contaminated with arsenic concentrations above 0.05 mg/l, and the model was used to compare natural flushing of arsenic from the system to a proposed remedial plan that would remove some contaminated sediments by dredging. Data collected for the modeling effort included daily stages and discharges; suspended sediment concentrations and arsenic concentrations in the river, tributaries, and lake during storms and normal conditions; cross-sectional hydrographic surveys; sediment cores that were analyzed for grain size distribution, mineral composition, density, organic content, and arsenic concentration; and bed pore water samples that were analyzed for arsenic, pH, and conductivity. Sedimentation traps were deployed in the system to accurately measure deposition rates; however, the traps were lost during high flow events and provided no data.

The model solved the depth-averaged form of Eq. (4-58) for three sediment size classes, plus selected dissolved and suspended contaminants, using the finite element method. Depth-averaged water velocities and water surface elevations were computed by a companion module that solved the Reynolds form of the Navier-Stokes equations. The cohesive sediment source-sink terms in Eq. (4-58) employed Eq. (4-26) for deposition rate to the bed and a form of Eq. (4-37) for bed erosion rate. The bed sediment density structure and thickness were computed by a one-dimensional finite strain model developed by Cargill (1982).

The model was validated by adjustment to, and comparison with, 3-year-long data as described above. As is the case in most engineering studies, the data were less complete and comprehensive than in the ideal case, and the results were interpreted in light of those limitations. Numerical experiments were then performed, using a synthetic typical year's flows that included four storm events. Model results showed that arsenic flushing times (time required for arsenic concentrations to decline to less than 120 mg/kg throughout the system) ranged from 15 years for the no-action alternative to 4 years for dredging contaminated sediments out of the river and lake. The estimated error in flushing times was  $\pm 1.2$  years, based on the model validation and a sensitivity analysis of arsenic desorption rates.

Rodriguez (2000) examined the problem of assessing the fate of mud placed off the beach, from where it may be carried away mainly by wave-induced currents. Referring to the elemental control volume in Fig. 4-37, and considering the cross-shore distance coordinate  $y$  to be the dependent variable and water depth  $h$  to be the independent one, the sediment continuity equation can be conveniently stated as

$$\frac{\partial y}{\partial t} = -\frac{1}{m\rho_D} \frac{\partial q_x}{\partial x} - \frac{1}{\rho_D} \frac{\partial q_y}{\partial h} \quad (4-59)$$

where

$q_x$  and  $q_y$  = the components of mass sediment fluxes per unit length in the  $x$  and  $y$  directions, respectively;

$\rho_D$  = the dry density of the deposit; and

$m = \partial h/\partial y$  = the local bottom slope.

Equation (4-59) makes possible tracking changes in the bottom contour position with time, as opposed to tracking water depth. The output at every time step is therefore a bottom contour "map" dependent on the fluxes  $q_x$  and  $q_y$  (Perlin and Dean 1983).

In Eq. (4-59),  $q_x$  must be determined in accordance with Eq. (4-57) from the product of the cross-shore distributions of suspension concentration and water velocity (Rodriguez and Mehta 2000). The corresponding cross-shore flux  $q_y$  can be related to the difference in the instantaneous rate of wave energy dissipation and the corresponding dissipation rate over an "equilibrium" or "target" profile (Lee and Mehta 1997).

The simplest application of Eq. (4-59) is to waves normally incident on a coast with shore-parallel contours (Coakley et al. 1988). In this case the alongshore transport mode is switched off in the model, so that profile change, either accretion or erosion, is due to sediment moving landward or seaward. The erosion of a beach consisting of over-consolidated till along Lake Ontario in Canada was reported by Davidson-Arnott (1986), who also noted that as the

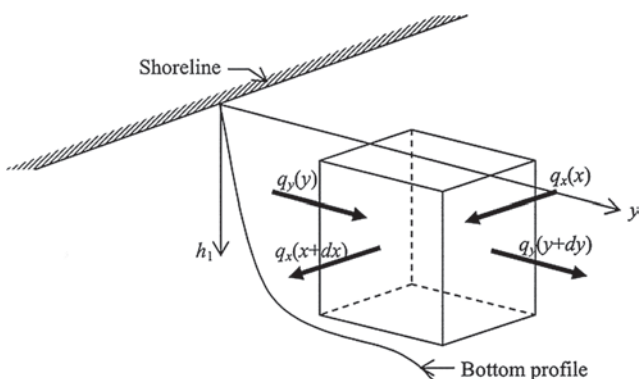


Fig. 4-37. Elemental control volume and suspended sediment fluxes in open coast waters.

profile translated landward the eroded material was carried away beyond the sediment-active profile, leaving practically no sediment deposit within this zone. Profile evolution over the period 1980–1984 is simulated in Fig. 4-38 (Rodriguez 2000).

When obliquely incident waves and alongshore current occur, simulation of profile evolution becomes considerably more complicated, due to the effects of alongshore as well as cross-shore forcing on shore processes. At the Mahin coast in Nigeria, waves are dominated by swell originating at storm centers in the southern Atlantic region. The tide is semidiurnal with a mean range of 1.5 m, and the beach and nearshore material consist mainly of poorly sorted silt with mean size ranging from 20 to 50  $\mu\text{m}$ . Due to submarine canyons that act as sinks of littoral drift, this region is starved of sediment supply. In the 1970s a navigation cut was dredged perpendicular to the coast near the village of Awoye about 20 km west of the Benin River (Fig. 4-39) to connect inland creeks and canals with the ocean. This cut apparently enabled larger waves to penetrate inland, exacerbating the erosion of the shoreline in the vicinity. In addition, salt water intrusion occurred, which in turn affected vegetation sensitive to brackish water. The ensuing die-back exposed bottom sediment otherwise protected by rooting and considerably increased land loss (Eedy et al. 1994).

Shoreline erosion adjacent to the cut was in response to a combination of wave-induced and tidal forcing, consistent with sediment transport associated with the typical flood and ebb flow distributions that develop near a tidal inlet or cut. Accordingly, sediment eroded by wave action along the shoreline was drawn toward the cut by flood flow. During ebb flow, the material that had accumulated near the entrance was jetted offshore. Since the lost nearshore sediment was not replenished by alongshore drift, shoreline recession occurred. As observed from Fig. 4-39,

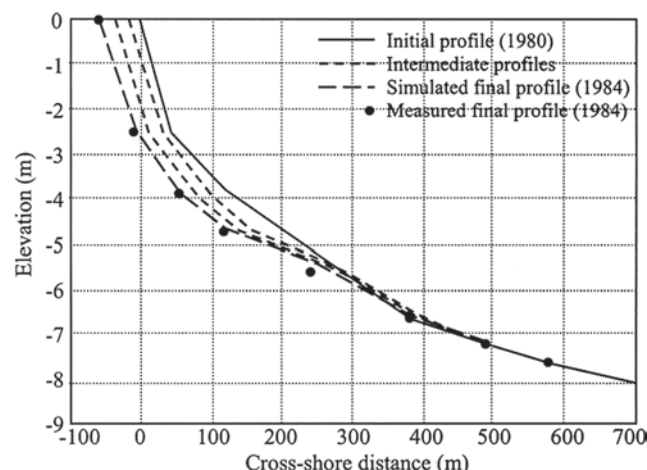
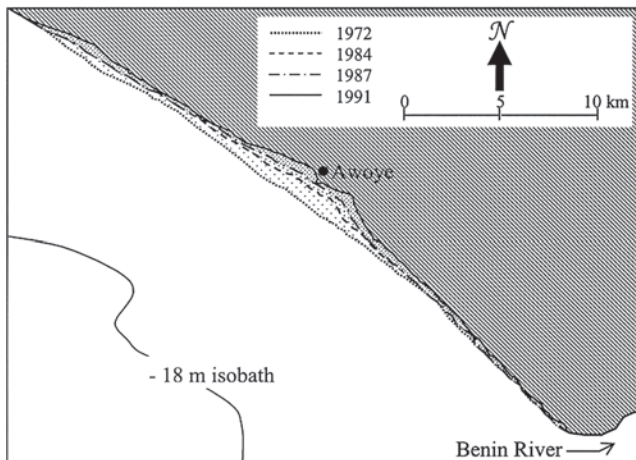


Fig. 4-38. Glacial till profiles at Grimsby, Lake Ontario, Canada measured by Davidson-Arnott (1986) and comparison with simulated profiles (after Rodriguez 2000).



**Fig. 4-39.** Shoreline recession in the vicinity of Awoye (after Rodriguez 2000).

erosion was rapid in the first few years, and a recession on the order of 1.5 to 2.0 km occurred near Awoye between 1972 and 1991.

It is instructive to examine the bathymetric change near Awoye by considering it to be due to an equivalent effect of shore-normal waves over a bottom with shore-parallel contours disturbed by a cut acting as a sediment sink. The resulting change in the bottom, in this case due to increasing deviation from the initial “target” profile, is shown in Fig. 4-40 (Rodriguez and Mehta 2001). In order to mimic the observed (Fig. 4-39) pattern of bottom change, sediment was withdrawn through the cut at a rate of 800 kg/s. This exceptionally high rate merely reflects the rapid rate of erosion that actually occurred. At the end of the initial period of 7 years covered in the simulation the shoreline was recessed by about 1 km.

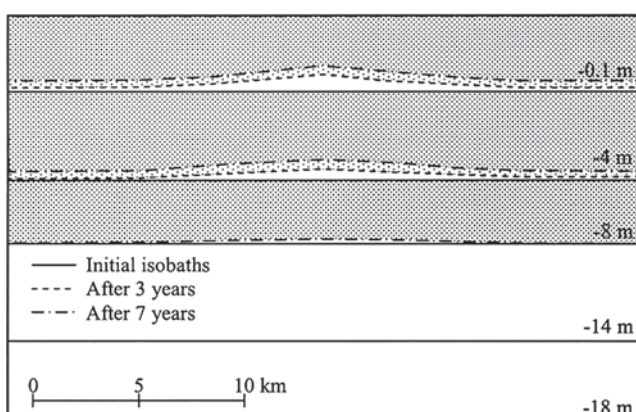


**Fig. 4-40.** Simulated contour recession due to the effect of a dredged channel (after Rodriguez and Mehta 2001).

## REFERENCES

- Adams, C. E., Jr., and Weatherly, G. L. (1981). “Some effects of suspended sediment stratification on an oceanic boundary layer.” *Journal of Geophysical Research*, 86(C5), 4,161–4,172.
- Alexander, M. P., Teeter, A. M., and Banks, G. E. (1997). “Development and verification of an intrusive hydrographic survey system for fluid mud in channels.” *Technical Rep. DRP-97-1*, U. S. Army Engineer Waterways Experiment Station, Vicksburg, Miss.
- Ali, K. H. M., and Georgiadis, K. (1991). “Laminar motion of fluid mud.” *Proceedings of the Institution of Civil Engineers, Part 2, Research and Theory*, 91, 795–821.
- Alishahi, M. R., and Krone, R. B. (1964). “Suspension of cohesive sediments by wind-generated waves.” *Technical Rep. HEL-2-9*, Hydraulic Engineering Laboratory, University of California, Berkeley, Calif.
- Amos, C. L., Brylinsky, M., Sutherland, T. F., O’Brien, D., Lee, S., and Cramp, A. (1998). “The stability of a mudflat in the Humber estuary, South Yorkshire, UK.” *Sedimentary processes in the intertidal zone*, K. S. Black, D. M. Paterson, and A. Camp, eds., The Geological Society, London, 25–44.
- Annandale, G. W. (1995). “Erodibility.” *Journal of Hydraulic Research*, 33(4), 471–493.
- Ariathurai, R. (1974). “A finite element model for sediment transport in estuaries.” PhD thesis, University of California, Davis, Calif.
- Ariathurai, R., MacArthur, R. C., and Krone, R. B. (1977). “Mathematical model of estuarial sediment transport.” *Technical Rep. D-77-12*, U. S. Army Engineer Waterways Experiment Station, Vicksburg, Miss.
- Arulanandan, K., Gillogly, E., and Tully, R. (1980). “Development of a quantitative method to predict critical shear stress and rate of erosion of natural undisturbed cohesive soils.” *Technical Rep. GL-805*, U. S. Army Waterways Experiment Station, Vicksburg, Miss.
- Ashley, R. M., and Verbanck, M. A. (1996). “Mechanics of sewer sediment erosion and transport.” *Journal of Hydraulic Engineering*, 34(6), 753–769.
- ASTM (1993a). “Standard test method for amount of material in soils finer than the no. 200 (75- $\mu$ m) sieve.” *Annual Book of ASTM Standards*, Section 4, Vol. 04.08, American Society for Testing and Materials, Philadelphia, 191–193.
- ASTM (1993b). “Standard test methods for moisture, ash, and organic matter of peat and other organic soils.” In: *Annual Book of ASTM Standards*, Section 4, Vol. 04.08, American Society for Testing and Materials, Philadelphia, 400–402.
- ASTM (1993c). “Standard test methods for operating performance of particulate cation-exchange materials.” *Annual Book of ASTM Standards*, Section 11, Vol. 11.02, American Society for Testing and Materials, Philadelphia, 772–776.
- ASTM (1993d). “Standard test for particle-size analysis of soils.” *Annual Book of ASTM Standards*, Section 4, Vol. 04.08, American Society for Testing and Materials, Philadelphia, 93–99.
- Augustinus, P. G. E. F. (1987). “The geomorphologic development of the coast of Guyana between the Corentyne River and the Essequibo River.” *International Geomorphology 1986 Part I*, V. Gardener, ed., Wiley, London, 1,281–1,292.

- Azam, M. H. (1998). "Breaking wave over mud flats." PhD thesis, Universiti Teknologi Malaysia, Kuala Lumpur, Malaysia.
- Barnes, H. A., Hutton, J. F., and Walters, K. (1989). *An introduction to rheology*. Elsevier, Amsterdam.
- Bedford, K. W., Onyx, W., Libicki, C. M., and Van Evra, R. (1987). "Sediment entrainment and deposition measurements in Long Island Sound." *Journal of Hydraulic Engineering*, 113(10), 1,325–1,342.
- Been, K., and Sills, G. C. (1981). "Self-weight consolidation of soft soils: An experimental and theoretical study." *Geotechnique*, 31(4), 519–535.
- Bentley, S. J., and Nittrouer, C. A. (1997). "Environmental influences on the formation of sedimentary fabric in the fine-grained carbonate-shelf environment: Dry Tortugas, Florida Keys." *Geo-Marine Letters*, 17, 268–275.
- Berlamont, J., Ockenden, M., Toorman, E., and Winterwerp, J. (1993). "The characterisation of cohesive sediment properties." *Coastal Engineering*, 21(1–3), 105–128.
- Bhattacharya, P. (1971). "Sediment suspension in shoaling waves." PhD thesis, University of Iowa, Iowa City, Iowa.
- Bird, R. B., Stewart, W. E., and Lightfoot, E. N. (1960). *Transport Phenomena*. Wiley, New York.
- Bishop, C. T., and Skafel, M. G. (1992). "Detailed description of laboratory tests on the erosion by waves of till profiles." *NWRI Contribution No. 92-26*, National Water Research Institute, Burlington, Ont., Canada.
- Bishop, C. T., Skafel, M. G., and Nairn, R. (1992). "Cohesive profile erosion by waves." *Proceedings of the 23rd Coastal Engineering Conference*, B. L. Edge, ed., ASCE, New York, 2,976–2,989.
- Black, K. S. (1991). "The erosion characteristics of cohesive estuarine sediments: Some in situ experiments and observations." PhD thesis, University of Wales, Menai Bridge, UK.
- Black, K. S., Paterson, D. M., and Cramp, A. (1998). Preface. In: *Sedimentary processes in the intertidal zone*, K. S. Black, D. M. Paterson, and A. Camp, eds., The Geological Society, London, vii–ix.
- Bocuniewicz, H., McTiernan, L., and Davis, W. (1991). "Measurement of sediment resuspension rates in Long Island Sound." *Geo-Marine Letters*, 11(3/4), 159–161.
- Burban, P. Y., Lick, W., and Lick, J. (1989). The flocculation of fine-grained sediments in estuarine waters. *Journal of Geophysical Research*, 94(C6), 8,323–8,330.
- Burban, P. Y., Xu, Y. J., McNeil, J., and Lick, W. (1990). Settling speeds of flocs in fresh water and seawater. *Journal of Geophysical Research*, 95(C10), 18,213–18,220.
- Burt, T. N., and Parker, W. R. (1984). "Settling and density in beds of natural mud during successive sedimentation." *Rep. No. IT 262*, HR Wallingford, Wallingford, UK.
- Burt, T. N., and Stevenson, J. R. (1983). "Field settling velocity of Thames mud." *Rep. No. IT 251*, HR Wallingford, Wallingford, UK.
- Cardenas, M., Galiani, J., Zeigler, C. K. and Lick, W. (1995). "Sediment transport in Lower Saginaw River." *Marine and Freshwater Research*, 46(1), 337–347.
- Cargill, K. W. (1982). "Consolidation of soft layers by finite strain analysis." *Miscellaneous Paper GL-82-3*, U.S. Army Engineer Waterways Experiment Station, Vicksburg, Miss.
- Cervantes, E., Mehta, A. J. and Li, Y. (1995). "A laboratory-based examination of 'episodic' resuspension of fine-grained sediments by waves and current." *Proceedings of the International Conference on Coastal and Port Engineering in Developing Countries*, Rio de Janeiro, Brazil, 1–13.
- Chapuis, R. P., and Gatien, T. (1986). "An improved rotating cylinder technique for quantitative measurement of the scour resistance of clays." *Canadian Geotechnical Journal*, 23(1), 83–87.
- Chou, H. T. (1989). "Rheological response of cohesive sediments to water waves." PhD thesis, University of California, Berkeley, Calif.
- Christodoulou, G. G. (1986). "Interfacial mixing in stratified flows." *Journal of Hydraulic Research*, 24(2), 77–92.
- Coakley, J. P., Skafel, M. G., Davidson-Arnott, R. G. D., Zeman, A. J., and Rukavina, N. A. (1988). "Computer simulation of nearshore profile evolution in cohesive material." *Proceedings of the IAHR Symposium on Mathematical Modeling of Sediment transport*, Copenhagen, Denmark, 290–299.
- Committee on Tidal Hydraulics (CTH). (1960). "Soil as a factor in shoaling processes: A literature review." *Technical Bulletin No. 4*, U.S. Army Engineer Waterways Experiment Station, Vicksburg, Miss.
- Committee on Tidal Hydraulics (CTH). (1994). "Indian River Inlet: An evaluation by the Committee on Tidal Hydraulics." *Unpublished Rep.*, U.S. Army Engineer Committee on Tidal Hydraulics, Vicksburg, Miss.
- Costa, R. C. F. G. (1989). "Flow-fine sediment hysteresis in sediment-stratified coastal waters." *MS thesis*, University of Florida, Gainesville, Fla.
- Costa, R. C. F. G. (1995). "Three-dimensional modeling of cohesive sediment transport in estuarine environments." PhD thesis, University of Liverpool, Liverpool, UK.
- Dade, W. B., and Nowell, A. R. M. (1991). Moving muds in the marine environment. *Proceedings of Coastal Sediments'91*, N. C. Kraus, K. J. Ginerich, and D. L. Kriebel, eds., ASCE, New York, 54–71.
- Dalrymple, R.A., and Liu, P. L.-F. (1978). "Waves over soft muds: A two-layer fluid model." *Journal of Physical Oceanography*, 8(6), 1,121–1,131.
- Davidson-Arnott, R. G. D. (1986). "Erosion of the nearshore profile in till: Rates, controls, and implications for shore protection." *Proceedings of the Symposium on Cohesive Shores*, Burlington, Ont., Canada, 137–149.
- Day, P. R., and Ripple, C. D. (1966). Effect of shear on suction in saturated clays. *Soil Science Society of America Proceedings*, 30, 675–690.
- Dean, R. G., and Dalrymple, R. A. (1991). *Water wave mechanics for engineers and scientists*. World Scientific, Singapore.
- Delichatsios, M. A., and Probstein, R. F. (1975). "Coagulation in turbulent flow: Theory and experiment." *Journal of Colloid and Interface Science*, 51(3), 394–405.
- Dennett, K. E., Sturm, T. W., Amritrajah, A., and Mahmood, T. (1998). "Effects of adsorbed organic matter on the erosion of kaolinite sediments." *Water Environment Research*, 70(3), 268–275.
- Dixit, J. G. (1982). "Resuspension potential of deposited kaolinite beds." M S thesis, University of Florida, Gainesville, Fla.
- Donnell, B. P., Letter, J. V., and Teeter, A. M. (1991). "The Atchafalaya River delta, report 11: Two-dimensional modeling." *Technical Rep. HL-82-15*, U. S. Army Engineer Waterways Experiment Station, Vicksburg, Miss.

- Downing, J. P., and Beach, R. A. (1989). "A laboratory apparatus for calibrating optical suspended solids sensors." *Marine Geology*, 86, 243–249.
- Drapeau, D. T., Dam, H. G. (1994). "An improved flocculator design for use in particle aggregation experiments." *Limnology and Oceanography*, 39(3), 723–729.
- Dyer, K. R. (1986). *Coastal and estuarine sediment dynamics*. Wiley, Chichester, UK.
- Dyer, K. R. (1989). "Sediment processes in estuaries: Future research requirements." *Journal of Geophysical Research*, 94(C10), 14,327–14,339.
- Eddy, W., Rodgers, B., Saunders, K. E., and Akindunni, F. (1994). "Application of satellite remote sensing to coastal recession in Nigeria." *Proceedings of Coast. Zone Management Conference*, Halifax, Nova Scotia, Canada, 1–4.
- Einstein, H. A. (1941). "The viscosity of highly concentrated underflows and its influence on mixing." *Transactions of the 22nd Annual Meeting of the American Geophysical Union*, Part I, Hydrology Papers, National Research Council, Washington, D.C., 597–603.
- Einstein, H. A. (1950). "The bed-load function for sediment transportation in open channel flows." *Technical Bulletin No. 1026*, U.S. Department of Agriculture, Washington, D.C.
- Eisma, D., Augustinus, P. G. E. F., and Alexander, C. (1991). "Recent and subrecent changes in the dispersal of Amazon mud." *Netherlands Journal of Sea Research*, 28, 181–192.
- Engelund, F., and Zhaohui, W. (1984). "Instability of hyperconcentrated flow." *Journal of Hydraulic Engineering*, 101(3), 219–233.
- Faas, R. W. (1995). "Mudbanks of the southwest coast of India. III: Role of non-Newtonian flow properties in the generation and maintenance of mudbanks." *Journal of Coastal Research*, 11(3), 911–917.
- Feng, J. (1992). "Laboratory experiments on cohesive soil bed fluidization by water waves." MS thesis, University of Florida, Gainesville, Fla.
- Foda, M. A. (1987). "Internal dissipative waves in poro-elastic media." *Proceedings of the Royal Society of London, Series A* 413, 383–405.
- Friedrichs, C. T. (1993). "Hydrodynamics and morphodynamics of shallow tidal channels and intertidal flats." PhD thesis, Woods Hole Oceanographic Institution, Woods Hole, Mass.
- Friedrichs, C. T., Wright, D., Hepworth, D. A., and Kim, S. C. (2000). "Bottom-boundary-layer processes associated with fine sediment accumulation in coastal seas and bays." *Continental Shelf Research*, 20, 807–841.
- Gade, H.G. (1958). "Effects of a non-rigid, impermeable bottom on plane surface waves in shallow water." *Journal of Marine Research*, 16(2), 61–82.
- Galani, J., Zeigler, C. K., and Lick, W. (1991). "Transport of suspended solids in the lower Fox River." *Journal of Great Lakes Research*, 17(4), 479–494.
- Ganju, N. K. (2001). "Trapping organic-rich fine sediment in an estuary." MS Thesis, University of Florida, Gainesville, Fla.
- Gelinas, P. J., and Quigley, R. M. (1973). "The influence of geology on erosion rates along the north shore of Lake Erie." *Proceedings of the 16th Conference on Great Lakes Research*, International Association for Great Lakes Research, Ann Arbor, Mich., 421–430.
- Geyer, W. (1995). "Tide-induced mixing in the Amazon frontal zone." *Journal of Geophysical Research*, 100(C10), 2,341–2,353.
- Gibbs, R. J. (1985). "Estuarine flocs: Their size, settling velocity and density." *Journal of Geophysical Research*, 90(C2), 3, 249–3,251.
- Gibson, R. E., England, G. L., and Hussey, M. J. L. (1967). "The theory of one-dimensional consolidation of saturated clays. I: Finite nonlinear consolidation of thin homogeneous layers." *Geotechnique*, 17, 261–273.
- Gibson, R. E., Schiffman, R. L., and Cargill, K. W. (1981). "The theory of one-dimensional consolidation of saturated clays. II: Finite nonlinear consolidation of thick homogeneous layers." *Canadian Geotechnical Journal*, 18(2), 280–293.
- Glenn, S. M., and Grant, W. D. (1987). "A suspended sediment stratification for combined wave and current flows." *Journal of Geophysical Research*, 84(C4), 1,797–1,808.
- Govindaraju, R. S., Ramireddygari, S. R., Shrestha, P. L., and Roig, L. C. (1999). "Continuum bed model for estuarine sediments based on nonlinear consolidation theory." *Journal of Hydraulic Engineering*, 125(3), 300–304.
- Grim, R. E. (1968). *Clay mineralogy*. McGraw-Hill, New York.
- Guo, J., and Wood, W. L. (1995). "Fine suspended sediment transport rates." *Journal of Hydraulic Engineering*, 121(12), 919–922.
- Gust, G. (1976). "Observations of turbulent drag reduction in a dilute suspension of clay in seawater." *Journal of Fluid Mechanics*, 75(May–June), 29–47.
- Hanson, G. J. (1990). "Surface erodibility of earthen channels at high stresses. Part I Developing an in situ testing device." *Transactions of the American Society of Agricultural Engineers*, 33(1), 132–137.
- Hayter, E. J. (1983). "Prediction of cohesive sediment transport in estuarial waters." PhD thesis, University of Florida, Gainesville, Fla.
- Hayter, E. J., and Gu, R. (2001). "Predictions of contaminated sediment transport in the Maurice River-Union Lake, New Jersey, USA." *Coastal and estuarine fine sediment transport: Processes and applications*, W. H. McAnally and A. J. Mehta, eds., Elsevier, Amsterdam, 439–458.
- Herrmann, F. A., and Letter, J. V. (1990). "Advancements in tidal hydraulics." *50th Anniversary of the Hydraulics Division, American Society of Civil Engineers*, A. M. Alsaffar, ed., ASCE, New York, 36–80.
- Hill, P. S. (1992). "Reconciling aggregation theory with observed vertical fluxes following phytoplankton blooms." *Journal of Geophysical Research*, 97(C2), 2295–2308.
- Hill, P. S., and Nowell, A. R. M. (1995). "Comparison of two models of aggregation in the continental-shelf boundary layers." *Journal of Geophysical Research*, 100(C11), 22,749–22,763.
- Hill, P. S., Nowell, A. R. M., and Jumars, P. A. (1988). "Flume evaluation of the relationship between suspended sediment concentration and excess boundary shear stress." *Journal of Geophysical Research*, 93(C10), 12,499–12,509.
- Hill, P. S., Nowell, A. R. M., and Jumars, P. A. (1992). "Encounter rate by turbulent shear of particles similar in diameter to the Kolmogorov scale." *Journal of Marine Research*, 50(4), 643–667.
- Hollick, M. (1976). "Towards a routine assessment of the critical tractive forces cohesive soils." *Transactions of the American Society of Agricultural Engineers*, 19(6), 1076–1081.

- Homma, M., Horikawa, K., and Kajima, R. (1965). "A study of suspended sediment due to wave action." *Coastal Engineering in Japan*, 8, 85–103.
- Huang, S., Han, N., and Zhong, X. (1980). "Analysis of siltation at mouth bar of the Yangtze River estuary." *Proceedings of the International Symposium on River Sedimentation*, Paper C6, Chinese Society of Hydraulic Engineering, Beijing, China (in Chinese).
- Huang, X., and Garcia, M. H. (1996). "A perturbation solution for Bingham-plastic mudflows." *Journal of Hydraulic Engineering*, 123(11), 986–994.
- Huang, X., and Garcia, M. H. (1998). "A Herschel-Bulkley model for mud flow down a slope." *Journal of Fluid Mechanics*, 374, 305–333.
- Huang, X., and Garcia, M. H. (1999). "Modeling of non-hydroplaning mudflows on continental slopes." *Marine Geology*, 154, 131–142.
- Hunt, J. R. (1982). "Self-similar particle-size distributions during coagulation: Theory and experimental verification." *Journal of Fluid Mechanics*, 122(Sep.), 169–185.
- Hunt, J. R. (1986). "Particle aggregate breakup by fluid shear." *Estuarine cohesive sediment dynamics*, A. J. Mehta, ed., Springer-Verlag, Berlin, 85–109.
- Hwang, K.-N. (1989). "Erodibility of fine sediment in wave dominated environments." MS thesis, University of Florida, Gainesville, Fla.
- Hwang, P. A., and Wang, H. (1982). "Wave kinematics and sediment suspension at wave breaking point." *Technical Rep. No. 13*, Department of Civil Engineering, University of Delaware, Newark, Del.
- Jacinto, R. S., and Le Hir, P. (2001). "Response of stratified muddy beds to water waves." *Coastal and estuarine fine sediment transport processes*, W. H. McAnally and A. J. Mehta, eds., Elsevier, Amsterdam, 95–108.
- Jaeger, J. M., and Nittrouer, C. A. (1995). "Tidal controls on the formation of fine-scale sedimentary strata near the Amazon mouth." *Marine Geology*, 125, 259–281.
- James, A. E., Williams, D. J. A., and Williams, P. R. (1987). "Direct measurement of static yield properties of cohesive suspensions." *Rheologica Acta*, 26, 437–446.
- James, A. E., Williams, D. J. A., and Williams, P. R. (1988). "Small strain, low shear rate rheometry of cohesive sediments." *Physical processes in estuaries*, J. Dronkers and W. van Leussen, eds., Springer-Verlag, Berlin, 488–500.
- Jepsen, R., Roberts, J., and Lick, W. (1997). "Effects of bulk density on sediment erosion rates." *Water, Air and Soil Pollution*, 99(1–4), 21–31.
- Jiang, F. (1993). "Bottom mud transport due to water waves." PhD thesis, University of Florida, Gainesville, Fla.
- Jiang, F., and Mehta, A. J. (1993). "Some observations on water wave attenuation over nearshore underwater mudbanks and mud berms." *Rep. No. UFL/COEL/MP-93/01*, Coastal and Oceanographic Engineering Department, University of Florida, Gainesville, Fla.
- Jiang, F., and Mehta, A. J. (1995). "Mudbanks of the southwest coast of India. IV: Mud viscoelastic properties." *Journal of Coastal Research*, 11(3), 918–926.
- Jiang, F., and Mehta, A. J. (1996). "Mudbanks of the southwest coast of India. V: Wave attenuation." *Journal of Coastal Research*, 12(4), 890–897.
- Jiang, J. (1999). "An examination of estuarine lutocline dynamics." PhD thesis, University of Florida, Gainesville, Fla.
- Jiang, J., and Mehta, A. J. (2000). "Lutocline behavior in a high-concentration estuary." *Journal of Waterway, Port, Coastal and Ocean Engineering*, 126(6), 324–328.
- Jobson, H. E., and Sayre, W. W. (1970). "Vertical transfer in open channel flow." *Journal of the Hydraulics Division of ASCE*, 96(3), 7,148–7,152.
- Johnson, B. H., Trawle, M. J., and Kee, P. G. (1989). "A numerical model study of the effect of channel deepening in shoaling and salinity intrusion in the Savannah estuary." *Technical Rep. HL-89-26*, U.S. Army Engineer Waterways Experiment Station, Vicksburg, Miss.
- Jones, T. E. R. (1997). "A review of rheometric methods for use with fine sediments." *Cohesive sediments*, N. Burt, R. Parker, and J. Watts, eds., Wiley, Chichester, UK., 317–329.
- Kamphuis, J. W. (1986). "Erosion of cohesive bluffs, a model and a formula." *Proceedings of the Symposium on Cohesive Shores*, M. G. Skafel, ed., National Research Council Canada, Ottawa, Canada, 226–245.
- Kandiah, A. (1974). "Fundamental aspects of surface erosion of cohesive soils." PhD thesis, University of California, Davis, Calif.
- Keedwell, M. J. (1984). *Rheology and soil mechanics*, Elsevier, London, 339p.
- Kelly, W. E., and Gularce, R. C. (1981). "Erosion resistance of cohesive soils." *Journal of the Hydraulics Division of ASCE*, 107(10), 1,211–1,224.
- Kemp, G.P. (1986). "Mud deposition at the shoreface: Wave and sediment dynamics on the chenier plain of Louisiana." PhD thesis, Louisiana State University, Baton Rouge, La.
- Kemp, G. P., and Wells, J. T. (1987). "Observations of shallow-water waves over a fluid mud bottom: Implications to sediment transport." *Proceedings of Coastal Sediments'87*, N. C. Kraus, ed., ASCE, New York, 363–378.
- Kendrick, M. P., and Derbyshire, B. V. (1985). "Monitoring of a near-bed turbid layer." *Rep. No. SR44*, HR Wallingford, Wallingford, UK.
- Kennedy, J. F., Locher, F. A. (1972). "Sediment suspension by waves." *Waves on beaches and resulting sediment transport*, R. E. Meyer, ed., Academic Press, New York, 249–296.
- Keulegan, G. H. (1967). "Tidal flow in entrances: Water level fluctuations of basins in communication with seas." *Technical Bulletin No. 14*, Committee on Tidal Hydraulics, U.S. Army Corps of Engineers, Vicksburg, Miss.
- Kineke, G. C. (1993). "Fluid muds on the Amazon continental shelf." PhD thesis, University of Washington, Seattle.
- Kineke, G. C., and Sternberg, R. W. (1995). "Distribution of fluid muds on the Amazon Continental Shelf." *Marine Geology*, 125, 193–223.
- Kirby, R. (1986). "Suspended fine cohesive sediment in the Severn estuary and Inner Bristol Channel." *Rep. No. ESTU-STP-4042*, Department of Atomic Energy, Harwell, UK.
- Kirby, R. (1992). "Effect of sea-level rise on muddy coastal margins." *Dynamics and exchanges in estuaries and the coastal zone*, D. Prandle, ed., American Geophysical Union, Washington, D.C., 313–334.
- Kirby, R., Hobbs, C. H., and Mehta, A. J. (1994). "Shallow stratigraphy of Lake Okeechobee, Florida: A preliminary reconnaissance." *Journal of Coastal Research*, 10(2), 339–350.

- Kirby, R., and Parker, W. R. (1977). "The physical characteristics and environmental significance fine sediment suspensions in estuaries." *Estuaries, geophysics and the environment*, National Research Council, National Academy Press, Washington, D.C., 110–120.
- Kirkham, D., and Powers, W. L. (1972). *Advanced soil physics*, Wiley, New York.
- Kranck, K. (1986). "Settling behavior of cohesive sediment." *Estuarine cohesive sediment dynamics*, A. J. Mehta, ed., Springer-Verlag, Berlin, 151–169.
- Kranck, K., and Milligan, T. G. (1980). "Macroflocs: Production of marine snow in the laboratory." *Marine Ecology Progress Series*, 3(July), 19–24.
- Kranck, K., and Milligan, T. G. (1992). "Characteristics of suspended particles at an 11-hour anchor station in San Francisco Bay, California." *Journal of Geophysical Research*, 97(C7), 11,373–11,382.
- Kranck, K., Petticrew, E., Milligan, T. G., and Droppo, I. G. (1993). "In situ particle size distributions resulting from flocculation of suspended sediment." *Nearshore and estuarine cohesive sediment transport*, A. J. Mehta, ed., American Geophysical Union, Washington, D.C., 60–74.
- Kranenburg, C. (1994a). "The fractal structure of cohesive sediment aggregates." *Estuarine, Coastal and Shelf Science*, 39(5), 451–460.
- Kranenburg C. (1994b). "An entrainment model for fluid mud." *Rep. No. 93-10*, Faculty of Civil Engineering, Delft University of Technology, Delft, The Netherlands.
- Kranenburg, C., and Winterwerp, J. C. (1997). "Erosion of fluid mud layers. I: Entrainment model." *Journal of Hydraulic Engineering*, 123(6), 504–511.
- Krishnappan, B. G. (1990). "Modeling settling and flocculation of fine sediments in still water." *Canadian Journal of Civil Engineering*, 17, 763–770.
- Krizek, R. J. (1971). Rheological behavior of clay soils subjected to dynamic loads. *Transactions of the Society of Rheology*, 15(3), 433–489.
- Krone, R. B. (1962). "Flume studies of the transport of sediment in estuarial shoaling processes." *Final Rep.*, Hydraulic Engineering Laboratory and Sanitary Engineering Research Laboratory, University of California, Berkeley, Calif.
- Krone, R. B. (1963). "A study of rheological properties of estuarial sediments." *Technical Bulletin No. 7*, Committee on Tidal Hydraulics, U.S. Army Engineer Waterways Experiment Station, Vicksburg, Miss.
- Krone, R. B. (1983). "A viscosity-temperature relation for Newtonian liquids." *Chemical Engineering Communications*, 22(3–4), 161–180.
- Krone, R. B. (1985). "Simulation of marsh growth under rising sea levels." *Proceedings of the Conference on Hydraulics and Hydrology in the Small Computer Age*, W. R. Waldrop, ed., ASCE, New York, 106–115.
- Krone, R. B. (1986). "The significance of aggregate properties to transport processes." *Estuarine cohesive sediment dynamics*, A. J. Mehta, ed., Springer-Verlag, Berlin, 66–84.
- Krone, R. B. (1993). "Sedimentation revisited." *Nearshore and estuarine cohesive sediment transport*, A. J. Mehta, ed., American Geophysical Union, Washington, D.C., 108–125.
- Kusuda, T., Umita, T., Koga, T., Futawatari, T. and Awaya, Y. (1985). "Erosional process of cohesive sediments." *Water Science and Technology*, 17(6–7), 891–901.
- Kynch, G. J. (1952). "A theory of sedimentation." *Transactions of Faraday Society*, 48, 166–176.
- Lambe, T. W., and Whitman, R. V. (1969). *Soil mechanics*. Wiley, New York.
- Land, J. M., Kirby, R., and Massey, J. B. (1997). "Developments in the combined use of acoustic doppler current profilers and profiling siltmeters for suspended solids monitoring." *Cohesive sediments*, N. Burt, R. Parker, and J. Watts, eds., Wiley, Chichester, UK., 187–196.
- Lau, Y. L. (1994). "Temperature effect on settling velocity and deposition of cohesive sediments." *Journal of Hydraulic Research*, 32(1), 41–51.
- Lau, Y. L., and Krishnappan, B. G. (1992). "Size distribution and settling velocity of cohesive sediments during settling." *Journal of Hydraulic Research*, 30(5), 673–683.
- Law, D. J., and Bale, A. J. (1998). "In situ characterization of suspended particles using focused-beam, laser reflectance particle sizing." *Sedimentary processes in the intertidal zone*, K. S. Black, D. M. Patterson, and A. Cramp, eds., Geological Society, London, 57–68.
- Lee, H. J. (1985). "State of the art: Laboratory determination of the strength of marine soils." *Strength testing of marine sediments and in-situ measurements*, R. C. Chaney and K. R. Demars, eds., ASTM STP 883, American Society of Testing and Materials, Philadelphia, 181–250.
- Lee, S.-C. (1995). "Response of mud shore profiles to waves." PhD thesis, University of Florida, Gainesville, Fla.
- Lee, S.-C., and Mehta, A. J. (1994). "Cohesive sediment erosion." *Rep. No. DRP-94-6*, U.S. Army Engineer Waterways Experiment Station, Vicksburg, Miss.
- Lee, S-C., and Mehta, A. J. (1997). "Problems in characterizing dynamics of mud shore profiles." *Journal of Hydraulic Engineering*, 123(4), 351–361.
- Le Hir, P., Bassoulet, P., and Jestin, H. (2001). "Application of the continuous modeling concept to simulate high-concentration suspended sediment in a macrotidal estuary." *Coastal and estuarine fine sediment transport processes*, W. H. McAnalley and A. J. Mehta, eds., Elsevier, Amsterdam, 229–247.
- Letter, J. V., and McAnalley, W. H. (1977). "Physical hydraulic models: Assessment of predictive capabilities," Report 2, Galveston entrance movable bed model. *Research Rep. HL-75-3*, U.S. Army Engineer Waterways Experiment Station, Vicksburg, Miss.
- Li, M. Z., and Gust, G. (2000). "Boundary layer dynamics and drag reduction in flows of high cohesive sediment suspensions." *Sedimentology*, 47(1), 71–86.
- Li, Y. (1996). "Sediment-associated constituent release at the mud-water interface due to monochromatic waves." PhD thesis, University of Florida, Gainesville, Fla.
- Li, Y., Mehta, A. J., Hatfield, K., and Dortch, M. S. (1997). "Modulation of constituent release across the mud-water interface by water waves." *Water Resources Research*, 33(6), 1,409–1,418.
- Li, Y., and Parchure, T. M. (1998). "Mudbanks of the southwest coast of India. VI: Suspended sediment profiles." *Journal of Coastal Research*, 14(4), 1363–1372.
- Li, Y., and Mehta, A. J. (2001). "Fluid mud in the wave-dominated environment revisited." *Coastal and estuarine fine sediment transport processes*, W. H. McAnalley and A. J. Mehta, eds., Elsevier, Amsterdam, 79–93.
- Liang, H.-B., and Williams, P. (1993). "An assessment of the impact of the operation of an additional ferry on shoreline erosion in Corte Madera Bay." *Rep. No. 847/877*, Philip Williams, San Francisco.

- Lick, W. (1982). "Entrainment, deposition and transport of fine-grained sediment in lakes." *Hydrobiologia*, 91(2), 31–40.
- Lick, W., Lick, J., and Zeigler, C. K. (1992). "Flocculation and its effect on the vertical transport of fine-grained sediments." *Hydrobiologia*, 235(July), 1–16.
- Lick, W., and Huang, H. (1993). "Flocculation and the physical properties of flocs." *Nearshore and estuarine cohesive sediment transport*, A. J. Mehta, ed., American Geophysical Union, Washington, D.C., 21–39.
- Lin, C.-P. (1986). "Turbidity currents and sedimentation in closed-end channels." PhD thesis, University of Florida, Gainesville, Fla.
- Lin, P. C.-P., and Mehta, A. J. (1997). "A study of fine sedimentation in an elongated laboratory basin." *Journal of Coastal Research*, SI25, 19–30.
- Lindenberg, J., van Rijn, L. C. and Winterwerp, J. C. (1989). "Some experiments on wave-induced liquefaction of soft cohesive soils." *Journal of Coastal Research*, SI 5, 127–137.
- Luettich, R. A., Jr., Wells, J. T., and Kim, S.-Y. (1993). "In situ variability of large aggregates: Preliminary results on the effect of shear." *Nearshore and estuarine cohesive sediment transport*, A. J. Mehta, ed., American Geophysical Union, Washington, D.C., 447–466.
- Maa, P.-Y. (1986). "Erosion of soft mud by waves." PhD thesis, University of Florida, Gainesville, Fla.
- Maa, P.-Y., and Mehta, A. J. (1988). "Soft mud properties: Voigt model." *Journal of Waterway, Port, Coastal and Ocean Engineering*, 114(6), 765–770.
- Maa, J. P.-Y., Wright, L. D., Lee, C.-H., and Shannon, T. W. (1993). "VIMS Sea Carousel: A field instrument for studying sediment transport." *Marine Geology*, 115, 271–287.
- MacPherson, H. (1980). "The attenuation of water waves over a non-rigid bed." *Journal of Fluid Mechanics*, 97(April), 721–742.
- Manning, A. J., and Dyer, K. R. (1999). "A laboratory examination of floc characteristics with regard to turbulent shearing." *Marine Geology*, 160(1/2), 147–170.
- Mantz, P. A. (1977). "Incipient transport of fine grains and flakes by fluids—extended Shields diagram." *Journal of the Hydraulics Division of ASCE*, 103(6), 601–615.
- Marván, F. G. (2001). "A two-dimensional numerical transport model for organic-rich cohesive sediments in estuarine waters." PhD thesis, Heriot-Watt University, Edinburgh, UK.
- Marván, F. G., Wallis, S. G., and Mehta, A. J. (2002). "Episodic transport of organic-rich sediments in a microtidal estuarine systems." *Fine sediment dynamics in the marine environment*, J. C. Winterwerp and C. Kranenburg, eds., Elsevier, Amsterdam, 611–626.
- Mathew, J., and Baba, M. (1995). "Mudbanks of the southwest coast of India. II: Wave mud interactions." *Journal of Coastal Research*, 11(1), 179–187.
- McAnally, W. H. (1989). "Lessons from 10 years experience in 2D sediment modeling." *Proceedings of the International Symposium on Sediment Transport Modeling*, S. S. Y. Wang, ed., ASCE, New York, 350–355.
- McAnally, W. H. (1999). "Aggregation and deposition of estuarial fine sediment." PhD thesis, University of Florida, Gainesville, Fla, 383p.
- McAnally, W. H., and Mehta, A. J. (2000). "Aggregation rate of fine sediment." *Journal of Hydraulic Engineering*, 126(12), 883–892.
- McAnally, W. H., and Mehta, A. J. (2002). "Significance of aggregation of fine sediment particles in their deposition." *Estuarine, Coast and Shelf Science*, 54, 643–653.
- McAnally, W. H. and Thomas, W. A. (1989). "STUDH: A two-dimensional numerical model for sediment transport." *Sediment Transport Modeling*, S. Y. Wang, ed., ASCE, New York, 659–664.
- McCave, I. N. (1984). "Size spectra and aggregation of suspended particles in the deep ocean." *Deep Sea Research*, 31(4), 329–352.
- McDowell, D. M., and O'Connor, B. A. (1977). *Hydraulic behavior of estuaries*. Wiley, New York.
- McLaughlin, R. T. (1959). "The settling properties of suspensions." *Journal of the Hydraulics Division, of ASCE*, 85 (12), 9–41.
- Meakin, P. (1988). "Fractal aggregates." *Advances in Colloid and Interface Science*, 28, 249–331.
- Mehta, A. J. (1991). "Review notes on cohesive sediment erosion." *Proceedings of Coastal Sediments'91*, N. C. Kraus, K. J. Ginerich, and D. L. Kriebel, eds., ASCE, New York, 40–53.
- Mehta, A. J. (1996). "Interaction between fluid mud and water waves." *Environmental hydraulics*, V. P. Singh and W. H. Hager, eds., Kluwer, Dordrecht, The Netherlands, 153–187.
- Mehta, A. J. (2002). "Mudshore dynamics and controls." *Muddy coasts of the world: Processes, deposits and function*, T. Healy, Y. Wang, and J.-A. Healy, eds., Elsevier, Amsterdam, 19–60.
- Mehta, A. J., and Kirby, R. (1996). "Mitigation measures for eroding muddy shores." *Proceedings of North American Water & Environment Congress*, Session W-17, ASCE, New York.
- Mehta, A. J., and Lee, S.-C. (1994). "Problems in linking the threshold condition for the transport of cohesionless and cohesive sediment grains." *Journal of Coastal Research*, 10(1), 170–177.
- Mehta, A. J., and Lott, J. W. (1987). "Sorting of fine sediment during deposition." *Proceedings of Coastal Sediments'87*, N. C. Kraus, ed., ASCE, New York, 348–362.
- Mehta, A. J., and Parchure, T. M. (2000). "Surface erosion of fine-grained sediment revisited." *Muddy coast dynamics and resource management*, B. W. Flemming, M. T. Delafontaine, and G. Liebezeit, eds., Elsevier, Oxford, UK, 55–74.
- Mehta, A. J., Parchure, T. M., Dixit, J. G. and Ariathurai, R. (1982). "Resuspension potential of deposited cohesive sediment beds." *Estuarine comparisons*, V. S. Kennedy, ed., Academic Press, New York, 591–609.
- Mehta, A. J., and Srinivas, R. (1993). "Observations on the entrainment of fluid mud by shear flow." *Nearshore and estuarine cohesive sediment transport*, A. J. Mehta, ed., American Geophysical Union, Washington, D.C., 224–246.
- Mehta, A. J., Williams, D. J. A., Williams, P. R. and Feng, J. (1995). "Tracking dynamic changes in mud bed due to waves." *Journal of Hydraulic Engineering*, 121(5), 504–506.
- Mei, C. C., and Liu, K. F. (1987). "A Bingham-plastic model for a muddy seabed under long waves." *Journal of Geophysical Research*, 92(C13), 14,581–14,594.
- Midun, Z. B., and Lee, S.-C. (1989). "Mud coast protection—The Malaysian experience." *Proceedings of Sixth Symposium on Coastal and Ocean Management*, ASCE, New York, 806–820.
- Migniot, P. C. (1968). "A study of the physical properties of different very fine sediments and their behavior under hydrodynamic

- action." *La Houille Blanche*, 7, 591–620 (in French, with abstract in English).
- Mimura, N. (1993). "Rates of erosion and deposition of cohesive sediments under wave action." *Nearshore and estuarine cohesive sediment transport*, A. J. Mehta, ed., American Geophysical Union, Washington, D.C., 247–264.
- Mitchell, J. K. (1976). *Fundamentals of soil behavior*, Wiley, New York.
- Montague, C. L., Paulic M., and Parchure, T. M. (1993). "The stability of sediments containing microbial communities: Initial experiments with varying light intensity." *Nearshore and estuarine cohesive sediment transport*, A. J. Mehta, ed., American Geophysical Union, Washington, D.C., 348–359.
- Moore, W. L., and Masch, F. D., Jr. (1962). "Experiments on the scour resistance of cohesive sediments." *Journal of Geophysical Research*, 67(4), 1437–1449.
- Moudgil, B. M., and Vasudevan, T. V. (1989). "Evaluation of floc properties for dewatering fine particle suspensions." *Minerals and Metallurgical Processing*, 6(3), 142–145.
- Munk, W. H., and Anderson, E. A. (1948). "Notes on a theory of the thermocline." *Journal of Marine Research*, 7, 276–295.
- Nairn, R. B. (1992). "Erosion processes evaluation paper." *Final Report for International Joint Commission Great Lakes-St. Lawrence River Reference Study Board*, submitted by W. F. Baird and Associates to Water Planning and Management Branch, Environment Canada, Burlington, Ont., Canada.
- Nichols, M. (1984/1985). "Fluid mud accumulation processes in an estuary." *Geo-Marine Letters*, 4–5, 192–198.
- Nunes Vaz, R. A., and Simpson, J. H. (1994). "Turbulence closure modeling of estuarine stratification." *Journal of Geophysical Research*, 99(C8), 16,143–16,160.
- Ockenden, M. C. (1993). "A model for the settling of non-uniform cohesive sediment in a laboratory flume and a field setting." *Journal of Coastal Research*, 9(4), 1,094–1,105.
- Odd, N. M. V., Bentley, M. A., and Waters, C. B. (1993). "Observations and analysis of the movement of fluid mud in an estuary." *Nearshore and estuarine cohesive sediment transport*, A. J. Mehta, ed., American Geophysical Union, Washington, D.C., 430–446.
- Odd, N. M. V., and Cooper, A. J. (1989). "A two-dimensional model of the movement of fluid mud in a high energy turbid estuary." *Journal of Coastal Research*, S15, 185–193.
- Odd, N. V. M., and Rodger, J. G. (1986). "An analysis of the behaviour of fluid mud in estuaries." *Report No. SR 84*, HR Wallingford, Wallingford, UK.
- Oduyemi, K. O. K. (1986). "Turbulent transport of sediment in estuaries." PhD thesis, University of Birmingham, Birmingham, UK.
- Overbeek, J. Th. G. (1952). "Kinetics of flocculation." *Colloid science*, Vol. 1, H. R. Krugt, ed., Elsevier, Amsterdam, 278–301.
- Owen, M. W. (1970). "A detailed study of the settling velocity of an estuary mud." *Rep. No. IT 78*, HR Wallingford, Wallingford, UK.
- Ozturgut, E., and Lavelle, J. W. (1986). "Settling analysis of fine sediment in salt water at concentrations low enough to preclude flocculation." *Marine Geology*, 69(3–4), 353–362.
- Paaswell, R. E. (1973). "Causes and mechanisms of cohesive soil erosion: The state of the art." *Soil erosion: Causes and mechanisms; Prevention and control*, D. H. Gray, ed., Special Report 135, Highway Research Board, Washington, D.C., 52–74.
- Panagiotopoulos, I., Voulgaris, G., and Collins, M. B. (1997). "The influence of clay on the threshold of movement of fine sandy beds." *Coastal Engineering*, 32, 19–43.
- Papanicolaou, A. N., and Diplas, P. (1999). "Numerical solution of a non-linear model for self-weight settlement." *Applied Mathematical Modelling*, 23(5), 345–362.
- Parchure, T. M. (1984). "Erosional behavior of deposited cohesive sediments." PhD thesis, University of Florida, Gainesville, Fla.
- Parker, W. R. (1987). "Observations on fine sediment transport phenomena in turbid coastal environments." *Continental Shelf Research*, 7(11/12), 1,285–1,293.
- Parker, W. R. (1994). "Determining depth and navigability in fine sediment areas." *Coastal, estuarial and harbour engineer's reference book*, M. B. Abbott and W. A. Price, eds., Chapman & Hall, London, 611–614.
- Parker, W. R., and Kirby, R. (1982). "Time dependent properties of cohesive sediment relevant to sedimentation management—European experience." *Estuarine comparisons*, V. S. Kennedy, ed., Academic Press, New York, 573–589.
- Partheniades, E. (1962). "A study of erosion and deposition of cohesive soils in salt water." PhD thesis, University of California, Berkeley, Calif.
- Partheniades, E. (1965). "Erosion and deposition of cohesive soils." *Journal of the Hydraulics Division, ASCE*, 91(1), 105–138.
- Partheniades, E. (1971). "Erosion and deposition of cohesive materials." *River mechanics*, H. W. Shen, ed., H. W. Shen, Fort Collins, Colo., 25–1–25–91.
- Partheniades, E. (1977). "Unified view of wash load and bed material load." *Journal of the Hydraulics Division of ASCE*, 103(9), 1,037–1,057.
- Partheniades, E. (1993). "Turbulence, flocculation and cohesive sediment dynamics." *Nearshore and estuarine cohesive sediment transport*, A. J. Mehta, ed., American Geophysical Union, Washington, D.C., 40–59.
- Patterson, D. M. (1997). "Biological mediation of sediment erodibility: Ecology and physical dynamics." *Cohesive sediments*, N. Burt, R. Parker, and J. Watts, Eds., Wiley, Chichester, UK, 215–229.
- Perlin, M., and Dean, R. G. (1983). "A numerical model to simulate sediment transport in the vicinity of coastal structures." *Miscellaneous Rep. 83-10*, Coastal Engineering Research Center, U.S. Army Corps of Engineers, Fort Belvoir, Va., 117.
- Phan-Thien, N. (1983). "A similarity solution for Rayleigh flow of a Bingham fluid." *Journal of Applied Mechanics*, 50(1), 229.
- Piedra-Cueva, I. (1993). "On the response of muddy bottom to surface water waves." *Journal of Hydraulic Research*, 31(5), 681–696.
- Piedra-Cueva, I., and Mory, M. (2001). "Erosion of a deposited layer of cohesive sediment." *Coastal and estuarine fine sediment transport processes*, W. H. McAnalley and A. J. Mehta, eds., Elsevier, Amsterdam, 41–51.
- Raveendran, P., and Amritharajah, A. (1995). "Role of short-range forces in particle detachment during filter backwashing." *Journal of Environmental Engineering*, 121(13), 860–868.
- Ravisangar, V., Dennett, K. E., Sturm, T. W., and Amritharajah, A. (2001). "Effect of sediment pH on resuspension of kaolinite sediments." *Journal of Environmental Engineering*, 127(6), 531–538.
- Rich, C. I., and Barnhisel, R. I. (1977). "Preparations of clay samples for X-ray diffraction analysis." *Minerals in soil environments*,

- J. B. Dixon and S. B. Weed, eds., Soil Science Society of America, American Society of Agronomy, Madison, Wisc., 797–809.
- Richardson, J. F., and Zaki, W. N. (1954). “The sedimentation of a suspension of uniform spheres under conditions of viscous flow.” *Chemical Engineering Science*, 3, 65–73.
- Roberts, W., Le Hir, P., and Whitehouse, R. J. S. (2000). “Investigation using simple mathematical models of the effects of tidal currents and waves on the profile shape of intertidal mudflats.” *Continental Shelf Research*, 20(11/12), 1079–1097.
- Roberts, W., and Whitehouse, R. J. S. (2001). “Predicting the profile of intertidal mudflats formed by cross-shore tidal currents.” *Coastal and estuarine fine sediment transport processes*, W. H. McAnally and A. J. Mehta, eds., Elsevier, Oxford, UK, 263–285.
- Rodriguez, H. N. (2000). “Mud bottom evolution at open coasts.” PhD thesis, University of Florida, Gainesville, Fla.
- Rodriguez, H. N., and Mehta, A. J. (1998). “Considerations on wave-induced fluid mud streaming at open coasts.” *Sedimentary processes in the intertidal zone*, K. S. Black, D. M. Patterson, and A. Cramp, eds., Geological Society, London, 177–186.
- Rodriguez, H. N., and Mehta, A. J. (2000). “Longshore transport of fine-grained sediment.” *Continental Shelf Research*, 20(11/12), 1–14.
- Rodriguez, H. N., and Mehta, A. J. (2001). “Modeling muddy coast response to waves.” *Journal of Coastal Research*, SI 27, 137–148.
- Ross, M. A. (1988). “Vertical structure of estuarine fine sediment suspensions.” PhD thesis, University of Florida, Gainesville, Fla.
- Rossby, C. G., and Montgomery, R. B. (1935). “The layer of functional influence in wind and ocean currents.” *Papers in Physical Oceanography*, 3(3), 1–101.
- Rouse, H. (1937). “Modern conceptions of the mechanics of fluid turbulence.” *Transactions of the ASCE*, 102, 436–451.
- Sakaiyama, T., and Bijker, E. W. (1989). “Mass transport velocity in mud layer due to progressive waves.” *Journal of the Waterway Port, Coastal and Ocean Engineering*, 115(5), 614–633.
- Sanford, L. P., and Chang, M.-L. (1997). “The bottom boundary condition for suspended sediment deposition.” *Journal of Coastal Research*, SI5, 3–17.
- Sanford, L. P., and Halka, J. P. (1993). “Assessing the paradigm of mutually exclusive erosion and deposition of mud, with examples from upper Chesapeake Bay.” *Marine Geology*, 114(1–2), 35–37.
- Sanford, L. P., Panageotou, W., and Halka, J. P. (1991). “Tidal resuspension of sediments in northern Chesapeake Bay.” *Marine Geology*, 97(1/2), 87–103.
- Scarlato, P. D., and Mehta, A. J. (1993). “Instability and entrainment mechanisms at the stratified fluid mud-water interface.” *Nearshore and estuarine cohesive sediment transport*, A. J. Mehta, ed., American Geophysical Union, Washington, D.C., 205–223.
- Schiffman, R. L., Pane, V., and Sunara, V. (1985). “Sedimentation and consolidation.” *Flocculation, sedimentation and consolidation*, B. M. Moudgil and P. Somasundaran, eds., Engineering Foundation, New York, 57–121.
- Sheng, Y. P. (1986). Modeling bottom boundary layer and cohesive sediment dynamics in estuarine and coastal waters. In: *Estuarine Cohesive Sediment Dynamics*, A. J. Mehta, ed., Springer-Verlag, Berlin, 360–400.
- Sheng, Y. P., and Villaret, C. (1989). “Modeling the effect of suspended sediment stratification on bottom exchange processes.” *Journal of Geophysical Research*, 94(C10), 14,429–14,444.
- Shibayama, T., Takikawa, H., and Horikawa, K. (1986). “Mud mass transport due to waves.” *Coastal Engineering in Japan*, 29, 151–161.
- Shrestha, P. L., and Orlob, G. T. (1996). “Multiphase distribution of cohesive sediments and heavy metals in estuarine systems.” *Journal of Environmental Engineering*, 122(8), 730–740.
- Sills, G. C., and Elder, D. McG. (1986). “The transition from sediment suspension to settling bed.” *Estuarine cohesive sediment dynamics*, A. J. Mehta, ed., Springer-Verlag, Berlin, 192–205.
- Sisko, A. W. (1958). “The flow of lubricating greases.” *Industrial Engineering Chemistry*, 50(1), 1,789–1,792.
- Skafel, M.G., and Bishop, C. T. (1994). “Flume experiments on the erosion of till shores by waves.” *Coastal Engineering*, 23(3–4), 329–348.
- Smith, T. J., and Kirby, R. (1989). “Generation, stabilization and dissipation of layered fine sediment suspensions.” *Journal of Coastal Research*, SI5, 63–73.
- Smith, T. M., McAnally, W. H., and Teeter, A. M. (1987). “Corpus Christi inner harbor shoaling investigation.” *Technical Rep. HL-87-13*, U. S. Army Engineer Waterways Experiment Station, Vicksburg, Miss.
- Soil Conservation Service (SCS). (1992). “Ion exchange analysis.” *Soil survey laboratory methods manual*, U.S. Department of Agriculture, Washington, D.C., 145.
- Stolzenbach, K. D., Newman, K. A., and Wang, C. S. (1992). “Aggregation of fine particles at the sediment-water interface.” *Journal of Geophysical Research*, 97(C11), 17,889–17,898.
- Sutherland, T. F., Grant, J., and Amos, C. L. (1998). “The effect of carbohydrate production by the diatom *Nitzschia curvilineata* on the erodibility of sediment.” *Limnology and Oceanography*, 43(1), 65–72.
- Taki, K. (1990). “Hydraulic study on the rate of resuspension of mud due to free surface water flow.” PhD thesis, Chuo University, Tokyo (in Japanese).
- Taki, K. (2001). “Critical shear stress for cohesive sediment transport.” *Coastal and estuarine fine sediment transport processes*, W. H. McAnally and A. J. Mehta, eds., Elsevier, Amsterdam, 53–61.
- Tambo, N., and Watanabe, Y. (1979). “Physical characteristics of flocs. I: The floc density function and aluminum floc.” *Water Resources Research*, 13(5), 409–419.
- Tarigan, A. P. M. (1996). “An examination of the dependence of mud shore profiles on the nearshore environment.” MS thesis, University of Florida, Gainesville, Fla.
- Tarigan, A. M., Lee, S.-C., and Mehta, A. J. (1996). “Recession of the muddy coast: A departure from the Bruun Rule?” *Proceedings of the 10th Congress of the Asia and Pacific Division of IAHR*, S.-C. Lee, K.-L. Hiew, and S.-H. Ong, eds., National Hydraulics Research Institute of Malaysia, Kuala Lumpur, 468–477.
- Task Committee on Erosion of Cohesive Materials (TCECM). (1968). “Erosion of cohesive sediments.” *Journal of the Hydraulics Division of ASCE*, 94(4), 1017–1049.
- Teeter, A. M. (2001a). “Clay-silt sediment modeling using multiple grain classes. I: Settling and deposition.” *Coastal and estuarine fine sediment transport processes*, W. H. McAnally and A. J. Mehta, eds., Elsevier, Amsterdam, 157–171.

- Teeter, A. M. (2001b). "Clay-silt sediment modeling using multiple grain classes. II: Application to shallow-water resuspension and deposition." In: *Coastal and estuarine fine sediment transport processes*, W. H. McAnally and A. J. Mehta, eds., Elsevier, Amsterdam, 173–187.
- Teeter, A. M., and Callegan, C. (2000). "Effects of channel modifications on currents, salinity, and sedimentation near Daniel Island, Charleston Harbor, SC." *Technical Rep.*, U.S. Army Engineer Waterways Experiment Station, Vicksburg, Miss.
- Teeter, A. M., Letter, J. V., Pratt, T. C., Coleman, C. J., and Boyt, W. L. (1996). "San Francisco Bay long-term management strategy (LTMS) for dredging and dredged material disposal, report 2, baywide suspended sediment transport modeling." *Technical Rep. HL-96-8*. U. S. Army Engineer Waterways Experiment Station, Vicksburg, Miss.
- Teeter, A. M., and Pankow, W. (1989). "Deposition and erosion testing on the composite dredged material sediment sample from New Bedford Harbor, Massachusetts." *Technical Rep. HL-89-11*, U.S. Army Waterways Experiment Station, Vicksburg, Miss.
- Teeter, A. M., Parchure, T. M., and McAnally, Jr. (1997). "Size-dependent erosion of two silty-clay sediment mixtures." *Cohesive sediments*, N. Burt, R. Parker, and J. Watts, eds., Wiley, Chichester, UK, 253–262.
- Tessison, C. (1997). "A review of cohesive sediment transport models." *Cohesive sediments*, N. Burt, R. Parker, and J. Watts, eds., Wiley, Chichester, UK, 367–381.
- Thimakorn, P. (1984). "Resuspension of clays under waves." *Seabed mechanics*, B. Denness, ed., Graham and Trotman, London, 191–196.
- Thomas, W. A., Heath, R. E., Stewart, J. P., and Clark, D. G. (1988). "The Atchafalaya River delta, Report 5: Quasi-two-dimensional model of delta growth and impacts on river stages." *Technical Rep. HL-82-15*, U. S. Army Waterways Experiment Station, Vicksburg, Miss.
- Thorn, M. F. C. (1981). "Physical processes of siltation in tidal channels." *Proceedings of the Conference on Hydraulic Modeling Applied to Maritime Engineering Problems*, Institution of Civil Engineers, London, 47–55.
- Thorn, M. F. C., and Parsons, J. G. (1980). "Erosion of cohesive sediments in estuaries: an engineering guide." *Proceedings of the 3rd International Symposium on Dredging Technology*, British Hydraulics Research Association, Cranfield, UK, 349–358.
- Toorman, E. A. (1995). "Controlled rate concentric cylinder rheometry of estuarine suspensions." *Report HYD148*, Hydraulics Laboratory, Civil Engineering Department, Catholic University of Leuven, Leuven, Belgium.
- Toorman, E. A. (1996). "Sedimentation and self-weight consolidation: general unifying theory." *Geotechnique*, 46(1), 103–133.
- Toorman, E. A. (2001). "Cohesive sediment transport modeling: European perspective." *Coastal and estuarine fine sediment transport processes*, W. H. McAnally and A. J. Mehta, eds., Elsevier, Amsterdam, 1–18.
- Toorman, E. A., and Berlamont, J. E. (1993). "Mathematical modeling of cohesive sediment settling and consolidation." *Nearshore and estuarine cohesive sediment transport*, A. J. Mehta, ed., American Geophysical Union, Washington, D.C., 148–184.
- Torfs, H. (1995). "Erosion of mud/sand mixtures." PhD thesis, Catholic University of Leuven, Leuven, Belgium.
- Torfs, H., Jiang, J., and Mehta, A. J. (2001). "Assessment of erodibility of fine/coarse sediment mixtures." *Coastal and estuarine fine sediment transport processes*, W. H. McAnally and A. J. Mehta, eds., Elsevier, Amsterdam, 109–123.
- Trowbridge, J. H., and Kineke, G. C. (1994). "Structure and dynamics of fluid muds on the Amazon continental shelf." *Journal of Geophysical Research*, 99(C1), 865–874.
- Tsai, C. H., and Hu, J. Q. (1997). "Flocculation of particles by fluid shear in buffered suspensions." *Proceedings of the 7th Symposium on Interactions Between Sediments and Water*, Kluwer, Dordrecht, The Netherlands, 55–62.
- Tsai, C. H., and Lick, W. (1986). "A portable device for measuring sediment resuspension." *Journal of Great Lakes Research*, 12(4), 314–321.
- Tubman, M. W., and Suhayda, J. N. (1976). "Wave action and bottom movements in fine sediments." *Proceedings of the 15th Conference on Coastal Engineering*, ASCE, New York, 1, 168–1,183.
- Uittenbogaard, R. E. (1995). "The importance of internal waves for mixing in a stratified estuarine tidal flow." PhD thesis, Technical University of Delft, Delft, The Netherlands.
- Van Leussen, W. (1994). "Estuarine macroflocs and their role in fine-grained sediment transport." PhD thesis, Utrecht University, Utrecht, The Netherlands.
- Van Olphen, H. (1977). *Clay colloid chemistry*, 2nd Ed., Wiley, New York.
- Villaret, C. and Paulic, M. (1986). "Experiments on the erosion of deposited and placed cohesive sediments in an annular flume and a rocking flume." *Rep. No. UFL/COEL-86/07*, Coastal and Oceanographic Engineering Department, University of Florida, Gainesville, Fla.
- Vinzon, S. B. (1998). "A preliminary examination of Amazon shelf sediment dynamics." Engineer Degree thesis, University of Florida, Gainesville, Fla.
- Vinzon, S. B., and Mehta, A. J. (2001). "Boundary effects due to suspended sediment in the Amazon River estuary." *Coastal and estuarine fine sediment transport processes*, W. H. McAnally and A. J. Mehta, eds., Elsevier, Amsterdam, 359–372.
- Walkley, A. and Black, I. A. (1934). "An examination of the Degtjareff method for determining soil organic matter and a proposed modification of the chromic acid titration method." *Soil Science*, 37, 29–38.
- Wells, J. T. (1983). "Dynamics of coastal fluid muds in low-, moderate-, and high-tide-range environments." *Canadian Journal of Fisheries and Aquatic Sciences*, 40 (Supplement 1), 130–142.
- Wells, M. L., and Goldberg, E. D. (1993). "Colloid aggregation in seawater." *Marine Chemistry*, 41, 353–358.
- Whittig, L. D., and Allardice, W. R. (1986). "X-ray diffraction techniques." *Methods of soil analysis, Part 1*, A. Klute, ed., Soil Science Society of America, American Society of Agronomy, Madison, Wisc., 331–362.
- Wiesner, M. R. (1992). "Kinetics of aggregate formation in rapid mix." *Water Resources Research*, 26(3), 379–387.
- Williams, D. J. A. (1986). "Rheology of cohesive suspensions." *Estuarine cohesive sediment dynamics*, A. J. Mehta, ed., Springer-Verlag, Berlin, 110–125.
- Willis, D. H., and Crookshank, N. L. (1997). "Modelling multi-phase sediment transport in estuaries." *Cohesive sediments*, N. Burt, R. Parker, and J. Watts, eds., Wiley, Chichester, UK, 383–394.

- Winterwerp, J. C. (1998). "A simple model for turbulence induced flocculation of cohesive sediment." *Journal of Hydraulic Research*, 36(3), 309–326.
- Winterwerp, J. C. (1999). "On the dynamics of high-concentrated mud suspensions." PhD thesis, Technical University of Delft, Delft, The Netherlands.
- Winterwerp, J. C., Cornelisse, J. M., and Kuijper, C. (1993). "A laboratory study on the behavior of mud from the Western Scheldt under tidal conditions." *Nearshore and estuarine cohesive sediment transport*, A. J. Mehta, ed., American Geophysical Union, Washington, D.C., 295–313.
- Winterwerp, J. C., and Kranenburg, C. (1997a). "Erosion of fluid mud by entrainment." *Cohesive sediments*, N. Burt, R. Parker, and J. Watts, eds., Wiley, Chichester, UK, 263–277.
- Winterwerp, J. C., and Kranenburg, C. (1997b). "Erosion of fluid mud layers.II: Experiments and model validation." *Journal of Hydraulic Engineering*, 123(6), 512–519.
- Wolanski, E., Asaeda, T., and Imberger, J. (1989). "Mixing across a lutocline." *Limnology and Oceanography*, 34(5), 931–938.
- Wolanski, E., and Gibbs, R. J. (1995). "Flocculation of suspended sediment in the Fly River estuary, Papua New Guinea." *Journal of Coastal Research*, 11(3), 754–762.
- Wolanski, E., Gibbs, R., Ridd, P., King, B., Hwang, K. Y., and Mehta, A. (1991). "Fate of dredge spoil, Cleveland Bay, Townsville." *Proceedings of the 10th Australasian Conference on Coastal and Ocean Engineering*, Institution of Engineers Australia, Canberra, Australia, 63–66.
- Wotherspoon, D. J. J., and Ashley, R. M. (1992). "Rheological measurement of the yield strength of combined sewer deposits." *Water Science & Technology*, 25(8), 165–170.
- Wright, L. D., Wiseman, W. J., Bornhold, B. D., Prior, P. B., Suhayda, J. N., Keller, G. H., Yang, Z. S., and Fan, Y. B. (1988). "Marine dispersal and deposition of Yellow River Silts by gravity driven underflows." *Nature*, 332(6164), 629–632.
- Yamamoto, T., and Takahashi, S. (1985). "Wave damping by soil motion." *Journal of the Waterway, Port, Coastal and Ocean Engineering*, 111(1), 62–77.
- Yamanishi, H., Higashi, O., Kusuda, T., Watanabe, R. (1998). "Scouring of cohesive sediment on a slope under breaking wave action." *Journal of the Waterway, Port, Coastal and Ocean Engineering*, 111(1), 62–77.
- Yeh, H.-Y. (1979). "Resuspension properties of flow deposited cohesive sediment beds." MS thesis, University of Florida, Gainesville, Fla.
- Ziegler, C. K., and Nisbet, B. S. (1994). "Fine-grained sediment transport in Pawtuxet River, Rhode Island." *Journal of Hydraulic Engineering*, 120(5), 561–576.
- Ziegler, C. K., and Nisbet, B. S. (1995). "Long-term simulation of fine-grained sediment transport in large reservoir." *Journal of Hydraulic Engineering*, 121(11), 773–781